CIAMTIS

U.S. DOT Region 3 University Transportation Center

Durability Assessment of Externally Bonded Fiber-Reinforced Polymer (FRP) Composite Repairs in Bridges

November 30, 2022

Prepared by:

Ajay Baniya, Sandra Milev, Rachel Henry, Jovan Tatar

University of Delaware

r3utc.psu.edu

PennState College of Engineering | LARSON TRANSPORTATION INSTITUTE

DISCLAIMER

Technical Report Documentation Page

1. Report No.	2. Government Accession No.	3. Recipient's Catalog No.
CIAM-UTC-REG16		

4. Title and Subtitle	5. Report Date
Durability Assessment of Externally Bonded Fiber-Reinforced Polymer (FRP) Composite Repairs in Bridges	November 30, 2022
	6. Performing Organization Code

7. Author(s)	8. Performing Organization Report No.
Ajay Baniya, PE, SE, https://orcid.org/0000-0003-1626-3617, Sandra Milev, https://orcid.org/0000-0002-0911-0906, Rachel Henry, and Jovan Tatar, PhD, https://orcid.org/0000-0003-4901-4019	

9. Performing Organization Name and Address	10. Work Unit No. (TRAIS)
University of Delaware 127 The Green Newark, DE 19716 The Pennsylvania State University	**11. Contract or Grant No.** 69A3551847103

12. Sponsoring Agency Name and Address	13. Type of Report and Period Covered
U.S. Department of Transportation Research and Innovative Technology Administration 3rd Fl, East Bldg E33-461 1200 New Jersey Ave, SE Washington, DC 20590	Final Report, 02/01/2020 – 07/31/2022
	14. Sponsoring Agency Code

15. Supplementary Notes

Work funded through The Pennsylvania State University through the University Transportation Center Grant Agreement, Grant No. 69A3551847103

16. Abstract

Although carbon fiber-reinforced polymer (CFRP) composite has been extensively used to rehabilitate many deficient bridges, data warranting their long-term performance is lacking. Current durability testing of CFRP composite involves accelerated conditioning as a part of material specification requirements to ensure that they maintain mechanical and physical properties during service life. However, without field data, relating accelerated conditioning test data to real-time outdoor exposure is not reliable. Work conducted at the University of Delaware in the early 1990s resulted in the first full-scale application of externally bonded CFRP on publicly owned bridges in the United States. As such, these bridges offer a unique opportunity to study CFRP durability over a time span of well over two decades. This report provides information on the durability of CFRP composite installed on the Foulk Road concrete bridge in Wilmington, Delaware and Bridge 1-704 in Newark, Delaware. Field evaluation and laboratory testing of CFRP samples collected from several girders were employed to investigate CFRP degradation and bond quality. The results indicate that after more than two decades of service life, the condition of CFRP repairs in the Foulk Road bridge was found to have considerably deteriorated. The condition of CFRP in Bridge 1-704 was found to be functional and performing as expected; however, some evidence of deterioration was noted.

17. Key Words	18. Distribution Statement
Bridge, inspection, evaluation, assessment, CFRP, composite, concrete, steel	No restrictions. This document is available from the National Technical Information Service, Springfield, VA 22161

19. Security Classif. (of this report)	20. Security Classif. (of this page)	21. No. of Pages	22. Price
Unclassified	Unclassified	139	

Table of Contents

List of Tables

List of Figures

List of Abbreviations

AASHTO	American Association of State Highway and Transportation Officials
ACI	American Concrete Institute
ACP	Accelerated Conditioning Protocols
ADT	Average daily traffic
ADTT	Average daily truck traffic
ATR- FTIR	Attenuated Total Reflection- Fourier Transform Infrared Spectroscopy
CAFT	Constant Amplitude Fatigue Threshold
CFRP	Carbon Fiber Reinforced Polymer
DelDOT	Delaware Department of Transportation
DMA	Dynamic Mechanical Analysis
DOT	Department of Transportation
DSC	Differential Scanning Calorimetry
EBFRP	Externally Bonded Fiber Reinforced Polymer
FHWA	Federal Highway Administration
FRP	Fiber Reinforced Polymer
IBRC	Innovative Bridge Research and Construction
IRBD	Innovative Bridge Research and Deployment
ICC-ES	International Code Council Evaluation Service
NIST	National Institute of Standards and Technology
SEM	Scanning Electron Microscopy
USDOT	United States Department of Transportation
UV	Ultraviolet

CHAPTER 1

Introduction

Approximately 1 in 13, or 7.5% of the nation's bridges are structurally deficient or in poor condition, and about 42% of all bridges are at least 50 years old (ASCE Report Card, 2021). The daily number of trips taken across these structurally deficient bridges is about 178 million trips. In Federal Region 3, 13.3% of the bridges are structurally deficient (FHWA, 2017), which is about 77% higher than the national average of 7.5% in 2021. Federal Region 3 includes the District of Columbia and five other states, Delaware, Maryland, Pennsylvania, Virginia, and West Virginia. Pennsylvania and West Virginia are ranked in the bottom five states by percentage of structurally deficient bridges (19.8% and 17.3%, respectively) (ASCE Report Card, 2017). Thus, transportation officials are continuously looking for new and innovative techniques to achieve rapid structural renewal while minimizing expenditures and impacts on traffic.

Among the numerous viable methods to repair structurally deficient bridges, the externally bonded fiber-reinforced polymer (FRP) composite presents numerous advantages in comparison, like favorable strength-to-weight ratio, non-corrosive properties, rapid implementation, and reduced expenditures. The strengthening using FRP composite also helps maintain the overheight clearance requirements, and the original configuration of the structure is not affected significantly (Shin et al., 2003). The application of FRP composite to civil structures began in the 1980s in Switzerland as a viable solution for the strengthening and repair of bridges. Since then, FRP composite has been widely adopted to strengthen and repair deteriorating bridges across the country (National Academies of Sciences, 2017).

Despite the extensive use of FRP composite to strengthen and repair deteriorating bridges across the country, there are no data available that warrant its long-term performance. The need for research on the durability of FRP composite for infrastructure was highlighted in a recent congressional hearing and a NIST report (Dukes et al., 2022).

One of the most important problems that limit the application of CFRP repairs as a reliable solution for bridge rehabilitation in the long term is a lack of understanding of their durability performance under adverse environmental conditions. Considering that simulation of field conditions in laboratory-accelerated durability tests is not a simple task, it is not surprising that failure modes differ between laboratory and field specimens (Tatar and Hamilton, 2016). Several field durability studies (Atadero and Allen, 2013; Al Azzawi et al., 2018; Banthia et al., 2010; Hamilton et al., 2017; Pallempati et al., 2016; Siavashi et al., 2019; Tatar et al., 2021; Tatar and Brenkus, 2021) were performed to-date. Field studies conducted over the last 10 years provided durability data on the FRP performance under natural exposure of up to 15 years in different climates—subtropical (humid and hot), subarctic (extremely low temperatures), dry, and continental. Natural exposure involves synergistic action of several climatic factors (for example, a combination of UV radiation, moisture, and elevated temperature), which leads to faster deterioration (Frigione and Rodríguez-Prieto, 2021) of the material compared to the effect of each environmental factor acting separately. Considering that many FRP strengthening applications are bond-critical, the focus of previous field studies was on the environmental deterioration of the FRP–concrete interface, with limited

usefulness due to missing baseline data in some cases. Atadero and Allen (2013) conducted one of the most thorough assessments of CFRP long-term performance that involved bond evaluation using pull-off tests and IR thermography, tensile testing of aged FRP, and differential scanning calorimetry to measure glass transition temperature (T_g). The decrease in the mean pull-off bond strength from 433 psi to 280 psi from 2003 to 2011 reported in this study indicates durability issues due to environmental exposure. Tensile testing showed that tensile strength and modulus were above the manufacturer's design values. Siavashi et al. (2019) developed a degradation model using field data to describe bond deterioration over long-term CFRP exposure to harsh environmental conditions and estimate the environmental reduction factor (Ce) to be used in the design. Results showed that environmental factors recommended in guidelines overestimate bond strength after 15 years of exposure; the calculated value of C_E in this study was 0.56, which is significantly lower than the value recommended in ACI (0.85 for CFRP).

Significantly less attention was dedicated to polymer or composite chemical degradation after long-term field exposure. Some of the studies that consider chemical degradation after long-term natural exposure of about 20 years are related to aerospace applications (Tian and Hodgkin, 2010). The issue with this type of data is that it involves service conditions different than those typical for bridges/buildings. On the other hand, data related to service conditions relevant to civil engineering structures correspond to a relatively short time span (1-3years) (Belec et al., 2015; Frigione et al., 2006). The most relevant types of environmental exposure in construction are UV radiation, moisture, and elevated temperature. Chemical degradation of DGEBA-amine resins caused by UV light is a complex process that involves UV radiation and oxygen and generally results in the formation of carbonyls and amides. These chemical changes are typically limited to the surface of about a few microns (Frigione, 2006). Synergistic effects of moisture and temperature over a long time have the potential to cause not only reversible changes but also permanent damage in the polymeric network. Epoxy-amine polymer network is formed by reacting difunctional epoxy monomers and tetra-functional hardener (both hydrogens of the amine are reactive). Theoretically, a single molecule can be formed, but this does not happen due to the constraints that limit the polymerization reaction. As a result, due to unreacted secondary amines, 3D macromolecules of different molecular weights form. Reactive centers in this network are secondary hydroxyl groups and tertiary amines that form hydrogen bonding between the macromolecules. Water ingress can disrupt these bonds between the polymer chains (3D macromolecules), causing plasticization and swelling. This process is reversible-hydrogen bonds reform once the water is removed. However, the water can affect the network in more detrimental and permanent ways by hydrolysis of chemical bonds (Powers, 2009; Sukanto et al., 2021).

The objective of this work was to assess the long-term performance and effectiveness of the FRP composite in facilitating rapid structural renewal of deteriorated concrete and steel bridges in Federal Region 3. Delaware has the oldest (1994) FRP repair installed on a publicly owned concrete bridge in its inventory, offering a unique opportunity to study the durability characteristics of these materials over a timespan of over 28 years (Finch, 1997). Similarly, the state also has the oldest (1999) CFRP strengthened, publicly owned steel bridge (Miller, 2000). The overarching objective of the project is to provide data from long-term natural exposure that will contribute to the development of design codes, specifically environmental reduction factors, and construction practices for improved CFRP durability. CFRP material samples were collected from the bridges and characterized at different scales—from macroscopic (tensile testing of CFRP and pull-off tests of the bond to concrete) to microscopic (SEM) to molecular level (FTIR and Raman spectroscopy). Obtained results and observations were analyzed and discussed to better understand how composite properties at different levels correlate and to gain insight into the mechanism of natural aging.

CHAPTER 2

Literature Review

MATERIAL PROPERTIES AND ADVANTAGES

FRP composite consists of thermosetting or thermoplastic polymer matrix and embedded reinforcing fibers, which can be in the form of short, long, continuous, and discontinuous fibers (Agarwal, 2006). The fibers are the load-carrying component of the FRP composite, and the matrix helps the fiber by bonding them together to act compositely, maintaining their orientation, transferring loads to the fibers, and providing protection (Mallick, 2007). The fibers are generally oriented unidirectionally, but they can be oriented in two or more directions depending on the application and desired strength and stiffness of the composite. Figure 1 shows a unidirectional composite made up of long and continuous fibers. The distribution of fibers is homogeneous in the longitudinal direction and random throughout the cross-section.

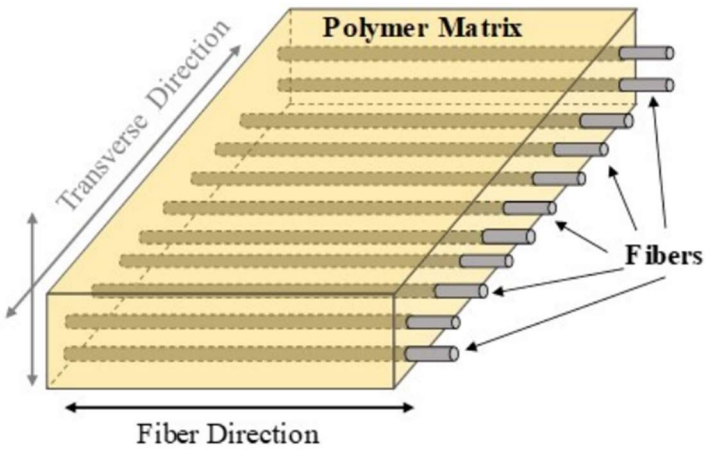

Source: University of Delaware, 2018

Figure 1. Schematic representation of a unidirectional FRP composite.

The most common types of fibers prevalent in the civil engineering industry to repair structures are carbon, glass, and aramid fibers (Garcez et al, 2008). For bridge repair, carbon fibers are best suited, because they are alkaline resistant and non-corrosive (Meier, 2005 and Darby et al. 2004) and they are five times lighter than steel and present 8 to 10 times higher tensile strength. Carbon fibers are synonymously called graphite fibers; typically if the carbon content is about 80 to 95 percent, they are called carbon fibers, but if the carbon content exceeds 95 percent, they are called graphite fibers. The diameter of carbon fiber is extremely small, ranging from 4 to 12 microns (Agarwal, 2006).

There are various methods of application of FRP composite to strengthen the bridge, depending on the nature and requirements of work: (1) externally bonded FRP, (2) near-surface-mounting composite, (3) post-tensioning of FRPs, (4) fiber-reinforced cementitious matrix, (5) spray FRP as a strengthening system,

(6) column retrofitting with composite, and (7) experimental research on emerging applications (Chajes et al., 2019). Externally bonded FRP composite is the simplest and most common method to strengthen bridges which involves applying the composite material to the external face of the structure with a layer of epoxy. Research conducted by Wang (2013) has suggested that the bond strength is not affected by the traffic loads, which will allow the traffic to flow without interruption. Similarly, the time required for implementation is rapid as well, and thus would incur reduced expenditure and reduced effect on the traffic flow. Most importantly, the favorable strength-to-weight ratio and non-corrosive properties of the FRP composite bolster its preference in the bridge repair industry. The strengthening using FRP composite also helps maintain the overheight clearance requirements and the original configuration of the structure need not be changed (Shin, 2003). Vacuum-assisted resin transfer molding (VARTM) is another application method to externally bond FRP composite, which involves creating a vacuum by sealing the FRP material airtight to the structure (Agarwal, 2006). Epoxy is then pulled from one end of the repair to the other by a machine, resulting in a thorough distribution of epoxy, and thus a better and stronger bond can be achieved.

DESIGN GUIDELINES

The absence of prescriptive design codes to specify the design requirements of FRP composite in concrete or steel structures is one of the hindrances to the widespread adoption of FRP composite. However, there are various documents that provide design guidance in the United States.

AASHTO (2012) provides technical guidelines for the repair and strengthening of reinforced concrete (RC) and prestressed highway bridge structures using externally bonded FRP. It requires the glass transition temperature (T_g) of the FRP composite computed using Dynamic Mechanical Analysis according to ASTM E1640 (2018) to be at least 40 °F higher than the maximum design temperature. It recommends tensile tests to be conducted after conditioning FRP composite in various environmental conditions, such as water, alternating UV light, condensation humidity, alkali, and freeze-thaw. FRP composite after exposure to recommended environmental conditions must retain 85% tensile and mechanical properties (i.e., glass transition temperature, T_g). Similarly, after conditioning in the environments discussed earlier, the bond strength of adhesive shall be at least 200 psi or $0.065(f'_c)^{0.5}$, whichever is greater, where f'_c (ksi) is the specified compression strength of the concrete.

ACI 440.2R (2017) explicitly specifies environmental reduction factors for various environmental conditions and different fibers, which are used to reduce the FRP composite rupture strain to account for the effects of environmental degradation. For CFRP composite, the environmental reduction factors are 0.95 for interior exposure and 0.85 for exterior exposure like bridges, piers, unclosed parking garages, and aggressive environments. The glass-transition temperature (T_g) should be adopted such that the anticipated service temperature doesn't exceed T_g -15 °C in a dry environment. It requires the glass transition temperature (T_g) of the FRP composite to be computed using Dynamic Mechanical Analysis according to ASTM E1640. For the application of FRP composite compressive strength f'_c of the concrete has to be a minimum of 2,500 psi and tensile strength needs to be at least 200 psi, determined by using a pull-off type adhesion test per ASTM C1583/C1583M.

ACI 440.9R (2015) discusses accelerated conditioning protocols (ACP) for durability testing of concrete strengthened with externally bonded fiber-reinforced polymer (EBFRP) or reinforced with FRP bars with the objective to encourage researchers to use standard test methods so that a database with consistent test results can be generated. The guideline presents background information in the first four chapters. FRP bar tests are discussed in Chapter 5, while the following three chapters are dedicated to EBFRP tests. In the introductory chapter, it is pointed out that the bond between the EBFRP and concrete is of critical importance for long-term and short-term durability, and moisture has to have a critical effect on the

adhesion. Accordingly, this guideline defines standard testing conditions for continuous immersion in water, continuous exposure to humidity, and immersion in alkaline solution. Procedures for the beam bond test, pull-off bond test, and tensile test are discussed in the following chapters.

Acceptance criteria in the International Code Council Evaluation Service (ICC-ES) AC125 recommend a list of ASTM standards to determine the physical properties of FRP composite systems, like tensile strength, elongation, tensile modulus, coefficient of thermal expansion (CTE), creep, void content, glass transition temperature, and composite interlaminar shear strength (AC125 ICC-ES, 2007). It recommends test conditions for environmental durability tests, such as water resistance, saltwater resistance, alkali resistance, and dry heat resistance. A minimum glass transition temperature (T_g) of 60 °C is required for control and exposed FRP composite and for each environmental durability test, FRP composite must retain 90% tensile strength after 1,000 hours of exposure and 85% after 3,000 hours.

Tatar and Hamilton (2015) identified a bond durability factor (BDF) of 0.60 as an appropriate estimate for wet-layup CFRP composite bonded to concrete based on a database gathered from 25 studies with more than 600 durability test results related to notched-beam three-point bending tests subjected to exposure conditions like hygrothermal, moisture and chemical attack, temperature, cycling, and real-time. A satisfactory fit for the database was found using one-sample Kolmogorov-Smirnov, Anderson-Darling statistical tests, and maximum likelihood estimation, which was then tested against Gaussian, log-normal, generalized extreme value, and Weibull distribution models to find the best fit. Gaussian distribution showed the best fit to the actual data distribution with a mean of 0.85 and a standard deviation of 0.24 (Figure 2). The normalized durability data from the literature were found to be in compliance with a 0.60 BDF for wet-layup CFRP composite bonded to concrete without putty when subjected to exterior exposure. Tatar and Hamilton also observed that an AASHTO FRPS-1 (2012) debonding strain limit of 0.005 was conservative for CFRP with a lower modulus of elasticity, and conservatism diminished as the modulus of elasticity increased. Finally, a procedure that makes a distinction between durability properties associated with CFRP rupture and debonding failure modes was proposed to determine the ultimate design strain primarily in bond-critical applications, which yields up to 15% lower flexural design strength compared to ACI440.2R and AASTHO FRPS-1.

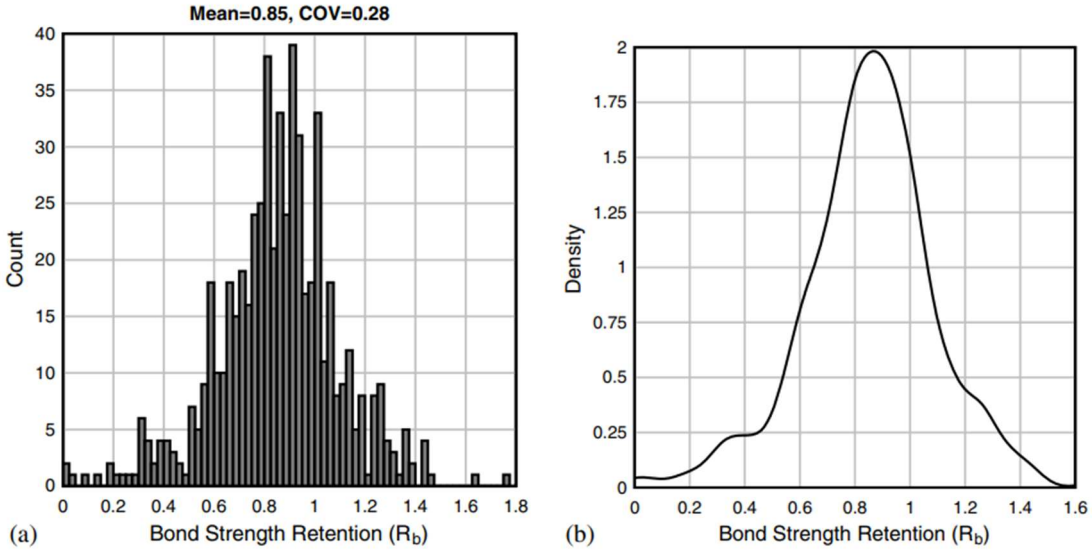

Source: Tatar and Hamilton, 2015

Figure 2. Distribution of literature data: (a) histogram, and (b) kernel distribution estimate.

DURABILITY ASSESSMENT - ENVIRONMENTAL CONDITIONING

The bond strength between the CFRP and concrete at column 1 and column 2 (Figure 3) was evaluated by Siavashi et al. (2019) 15 years after its installation on a highway concrete bridge in Michigan. The research was based on in-situ pull-off bond tests, with an objective to develop a degradation model that will describe bond deterioration over long-term exposure to harsh environmental conditions and estimate the environmental reduction factor (C_e) to be used in the design. Tests were performed on two columns. Recorded bond strength values indicated that degradation was more intense on the side that was exposed to rainwater splashing from the traffic. Due to missing data on the original bond strength, samples were recreated in the laboratory using the same materials that were used onsite. These samples were tested after 0, 9, 14, and 24 months and values served as data points to determine the relationship between bond strength and time. Results from the study showed that environmental factors recommended in guidelines overestimate bond strength after 15 years of exposure; the calculated value of C_e in this study was 0.56, which was significantly lower than the value recommended in ACI (0.85 for CFRP).

Source: Siavashi et al., 2018

Figure 3. Test columns under westbound Interstate 96 over Lansing Road.

Choi et al. (2012) studied the effects of the environment on the durability of the interfacial bonding between concrete and CFRP of different types of commercially available composite systems using the three-point bending test method (Figure 4). Five different CFRP systems made up of varying fiber and matrix properties were used to strengthen the concrete specimens of size 14 × 4 × 4 in., four of which were bonded using the wet-layup method and the remaining one was pre-cured laminate. Each of those CFRP systems was tested after 6, 12, and 18 months after being exposed to various environmental conditions like immersion in chloride and alkali, hygrothermal cycles at different temperatures ranging from 30 to 60 °C, outdoors, and controlled temperatures. It was concluded that the flexural strength of the beam specimens was reduced with environmental exposure and aging. Pre-cured laminate saw the maximum reduction in strength, in the range of 30–60% after 18 months of hygrothermal cycle, which was consistent with the results obtained in previous research by Au and Buyukozturk (2006). The environmental reduction factors (ERF) resulting from exposure to chloride solutions, alkali solutions, and wet-dry cycles for different types of composites were then compared to the 85% ERF, as recommended by ACI 440.3R-04 (ACI 2004).

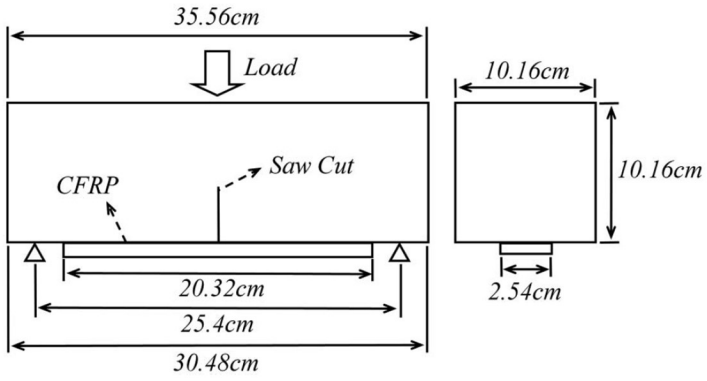

Source: Choi et al., 2012

Figure 4. Schematic of beams for three-point loaded flexural testing.

Tensile tests were carried out by Cruz et al. (2021) to determine the ultimate stress, elastic modulus, and strain of two different laminates (L10 and L50) and epoxy specimens (ADH1 and ADH2) subject to different weather conditions for 0, 1, and 2 years to study the durability of CFRP laminate and epoxy, respectively. Similarly, dynamic mechanical analysis (DMA) was carried out to determine the glass transition temperature of two epoxy specimens. Six different environmental conditions were studied: two control environments and four outdoor environments to simulate various levels of CO_2, freeze and thaw, humidity, chlorides, and temperature exposure. For the epoxy adhesive type ADH1, a 9-21% increase in the glass transition temperature with time was observed for non-immersed specimens after 2 years. However, for the immersed specimen, the glass transition temperature was reduced by about 9%. The glass transition temperature for ADH2 was found to be similar to that of ADH1. The tensile properties of ADH1 decreased by 10–21% after 2 years of exposure; however, the tensile properties of ADH2 increased by 3–34% after 2 years of exposure. The tensile properties of both laminates L10 and L50 increased after 2 years of exposure by 1–10%.

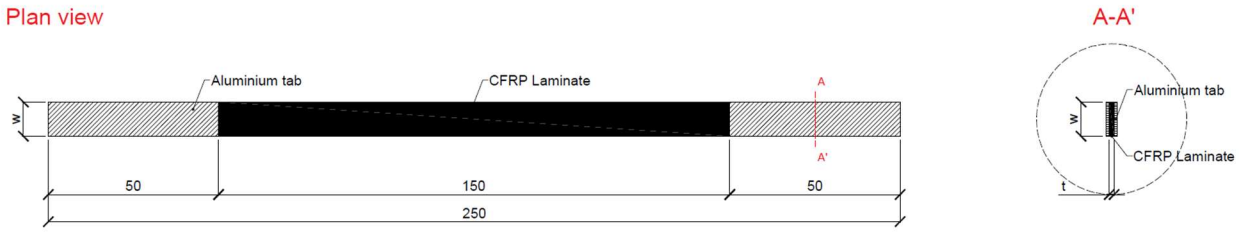

Source: Cruz et al., 2021

Figure 5. Geometry of the CFRP laminate strip specimens used in the tensile tests (units: mm).

The effects of various environmental conditions on the durability of the CFRP-strengthened beams using an epoxy matrix were investigated by Al-Jelawy (2013) using three-point bending tests. Seven different environments were considered to investigate the durability and failure modes of two different wet lay-up CFRP systems applied to the flexural reinforcement of concrete. FRP coupons (12 × 1 in.) and concrete beam specimens (16 × 4 × 4 in.) were prepared. Tensile and three-point bending tests were carried out after 125, 250, and 365 days of exposure to various accelerated conditioning environments and environmental conditioning (Figure 6). Results and failure modes of control and conditioned specimens showed that degradation of CFRP-strengthened beams was controlled by the conditioned concrete tensile strength in the epoxy system. The exposed beams had the same failure mode as the control specimens; that is, flexural IC

induced debonding, all CFRP-strengthened beams debonded in a thin layer of the concrete substrate. The saltwater immersion and ambient environment had a moderate effect on the concrete properties, which caused a 6.5% degradation in tensile strength of the epoxy-based uncoated CFRP-strengthened beams. UV and heat environment didn't have a considerable effect on the beams' bending properties.

Source: Al-Jelawy, 2013

Figure 6. Field conditioning of concrete beam specimens and cylinders.

Long et al. (2012) carried out pull-off tests after 8 months of bonding to assess the effects of tidal and atmospheric exposure on the bond performance of CFRP fabrics and laminates installed on a quay wall in a marine environment (Figure 7) and a bridge abutment in a river environment, both located at Dunkerque Port, in the northern part of France. Six specimens of fabrics and laminates were bonded in each structure in two different zones, tidal and a dry zone. The results presented by the authors were obtained 8 months after the bonding had been completed, and the remaining tests were planned to be conducted in the future. The results of bond strength in the tidal zone were compared to those in the dry zones, which were not subjected to the continuous wet/dry cycles. The residual pull-off strengths of the carbon laminates and fabric in the tidal zone were found to be lower than those in a dry zone by approximately 9–17%. Similarly, the residual pull-off strengths for the marine environment were found to be lower than the river environment by approximately 9–35%. In all cases, the failure mode was observed at dolly/CFRP interface except for the fabric in the marine environment, where the failure mode was cohesive in nature in the concrete substrate.

Source: Long et al., 2012

Figure 7. Bonded CFRP composite on a quay wall in the marine environment.

The arch bridge in Castlewood Canyon State Park was repaired and strengthened to meet increased traffic loads due to widened lanes using externally bonded CFRP. The long-term durability of bond strength between CFRP and concrete/shotcrete with or without corrosion inhibitor was assessed under various accelerated conditions using pull-off tests by Fafach et al. (2004). Seven accelerated environmental parameters were utilized in this study: room temperature, freeze-thaw cycles, wetting in water, wetting/drying cycles in water, deicing chemicals, sodium hydroxide, and high temperature. Based on the observation of test results, no consistent influence of the corrosion inhibitor was found on the bond strength. The difference in the pull-off strength between untreated and treated samples was found to range from -17% to +19% and -17% to +59% for the concrete and shotcrete substrate, respectively, for various environmental exposures. When the specimens were exposed to chloride, shotcrete performed better than concrete: 35% higher pull-off stress for untreated specimens, and 20% higher for the treated specimens, while for other cases concrete performed better than shotcrete. Similarly, the pull-off strengths were found to be lower for all accelerated conditions compared to control specimens at room temperature by approximately 23% to 45% and 10% to 51% for the concrete and shotcrete substrate, respectively (Figure 8a,b).

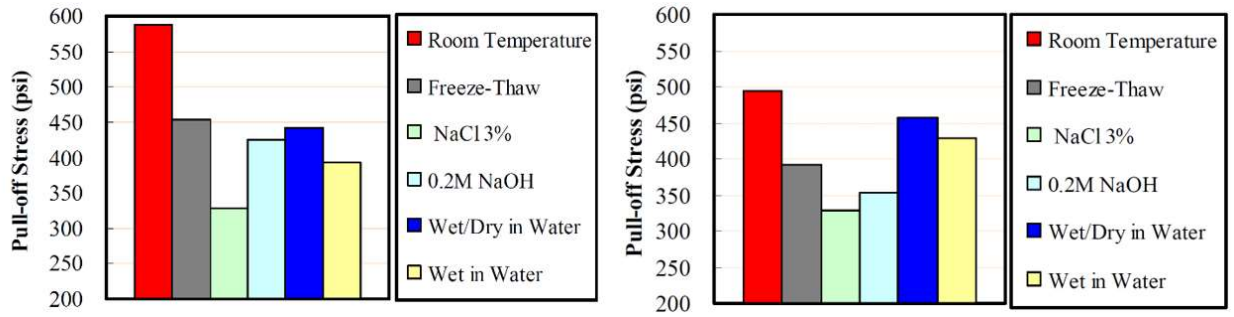

Source: Fafach et at. (2004)

Figure 8. Average pull-off stress after 90 days: (a) concrete substrate untreated with Sica903, and (b) concrete substrate treated with Sica903.

Pull-off tests, tensile tests, DSC tests, and void inspections were carried out on externally bonded FRP installed on the extrados of the concrete arch bridge by Allen et al. (2011) after 8 years of service to study the effect of long-term environmental exposure on bond strength. The Castlewood Canyon Bridge on Colorado SH-83 (Figure 9) was reconstructed using externally bonded FRP and was routinely inspected every 2 years. Voids that were identified after 4 years of service were compared to the voids after 8 years of service, which grew significantly with time by approximately 400%. Similarly, the number of voids identified increased from 3 to 28 over 8 years of service. The DSC tests showed that the glass transition temperature of the composite didn't change and was like the value suggested by the manufacturer. The tensile tests showed that the material has deteriorated over time, and the ultimate tensile strength was found to be lower than the specified design strength. Similarly, pull-off strengths were compared to the pull-off strengths assessed 8 years earlier and it was found that 33% of the pull-off strengths were below 200 psi compared to 2.4% 8 years earlier. The average pull-off strength was found reduced by approximately 30% after 8 years of service.

Source: Allen et al., 2011

Figure 9. Castlewood Canyon Bridge after the 2003 repair where the pull-off tests were conducted.

Al-Tamimi et al. (2015) examined the effect of harsh environmental conditioning on the bond strength between CFRP plates and concrete. A total of 27 concrete specimens (9.5 × 3 × 3 in.) were cast, and a 0.05-in.-thick CFRP layer was applied to each of them. Each concrete specimen was left to cure outside for 2 to 3 days and then in a curing tank for an additional 7 days before CFRP installation. All concrete specimens were subjected to a sustained load of 675 lbf or 1,125 lbf during exposure, which was applied via compression force on springs, which translated to a tensile force on CFRP plates. The samples were divided into two groups, uncured and cured via exposure to 50 °C and exposed to three exposure conditions. One set of specimens was tested under controlled laboratory conditions and the remaining two sets were tested on-site under direct sun exposure with temperature ranging from 38–55 °C and saline tank exposure. The saline-exposed group underwent wet-dry cycles linked to local weather conditions to simulate tidal effects near the shoreline. After exposure for 150 days, the specimens were subjected to the single-lap shear test. The test results were compared based on observed peak loads, maximum slip, load-slip history, shear stresses, strain distribution, and failure modes. Specimens exposed to the sun and saline environment, as well as those that sustained larger loads (1,125 lbf), experienced greater slip and ultimate load. The highest

average peak load was seen in samples exposed to the sun, followed by saline water across all loading conditions. This indicates that the higher temperature experienced in the sun and saline exposure enhanced the bond between CFRP and concrete surfaces. The higher ultimate load and slip seen in sun exposure as compared to saline exposure can be attributed to the strength reduction of the polymer due to wetting and drying cycles. The most common modes of failure seen were minor concrete edge failure with traces of concrete stuck to adhesive, major concrete edge pulled out with main adhesive still attached, debonding near surface adhesive to CFRP plate, and debonding at the adhesive near the concrete surface. Sun-exposed specimens showed a 0.43 retention factor, like the ACI-440 glass retention factor of 0.5, while saline-exposed specimens showed an 85% retention factor. Finally, it was proposed that the environmental reduction factor needs to be directly linked to the reduction in slope of the peak load to the maximum slip or the modulus (Figure 10).

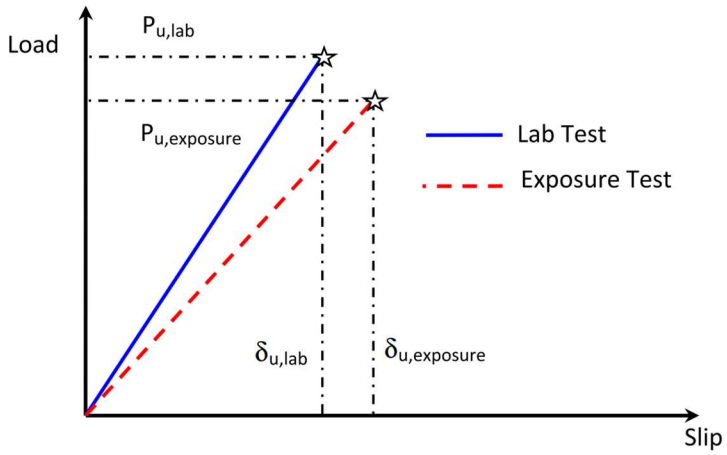

Source: Al-Tamimi et al., 2015

Figure 10. Degradation between lab and environmental exposure.

The reliability of accelerated conditioning protocols to assess FRP bond durability was investigated by comparing the bond strength of specimens aged in the laboratory and specimens aged in the field by Tatar (2016). ACP involved three different exposures: (1) water immersion at 30 °C, (2) water immersion at 60 °C, and (3) 100% RH at 60 °C. Bond strength was evaluated after 8 weeks, using pull-off and three-point bending tests on small beam specimens. Field specimens under consideration included CFRP patches installed on one exterior and one interior girder of Sunshine Skyway Bridge in Florida during its repair in 2014 (Figure 11) and small beam specimens placed on bridge dolphins adjacent to the bridge at the same time. Pull-off bond tests and three-point bending tests were performed on field specimens after six and eighteen months of exposure. Testing of laboratory specimens showed that the highest bond degradation occurred under water immersion at 60 °C. Pull-off bond strength measured on field specimens was higher than 200 psi, indicating good bond performance after 18 months of exposure. Adhesive failure characteristics were more frequently observed in the pull-off test conducted on the exterior girder that was exposed to harsher conditions. A comparison of field conditioning and ACP test results shows that water immersion at 60 °C underestimates bond strength after 18 months of field exposure.

(a) (b) (c)

Source: Hamilton et al., 2017

Figure 11. (a) Repair of Sunshine Skyway Bridge, (b) interior girder test patches, and (c) exterior girder test patches.

Alfar (2006) examined the long-term behavior of CFRP-strengthened concrete slabs subjected to accelerated laboratory testing designed to mimic high saline environments compared with actual saline environmental conditioning. CFRP-bonded concrete slabs (63 × 20 × 4.75 in.) were conditioned under saltwater immersion for 4 months before CFRP application. After the application of CFRP, specimens were conditioned for an additional 12 months. Field specimens were strengthened with the same system as lab specimens and spread among three locations (Dead Sea, Aqaba, and Amman) for 12 months in Jordan, followed by three-point bending tests. Results for the concrete slabs showed midspan debonding of CFRP plates as the dominant failure mode. Most slabs failed initially by flexural or flexural/shear cracks, which induced debonding of CFRP plates. Slabs subjected to harsher conditioning, saltwater immersion, Dead Sea, and Aqaba exposure experienced clean epoxy/concrete separation, while slabs subjected to a control laboratory setting and Amman environment failed within a few inches of the concrete substrate. Specimens subjected to salt immersion experienced higher failure loads compared to control laboratory specimens, while the harsher environmentally conditioned slabs showed a minor difference in failure load compared to the milder Amman environment. Curves of beam deflections showed similar profiles among all conditions (Figure 12). Specimens exposed to saltwater immersion and environmental conditioning showed higher stiffness than control slabs in the range of 2.25% to 3.9% and 0.57% to 6%, respectively, with those exposed to Aqaba conditions having the highest stiffness.

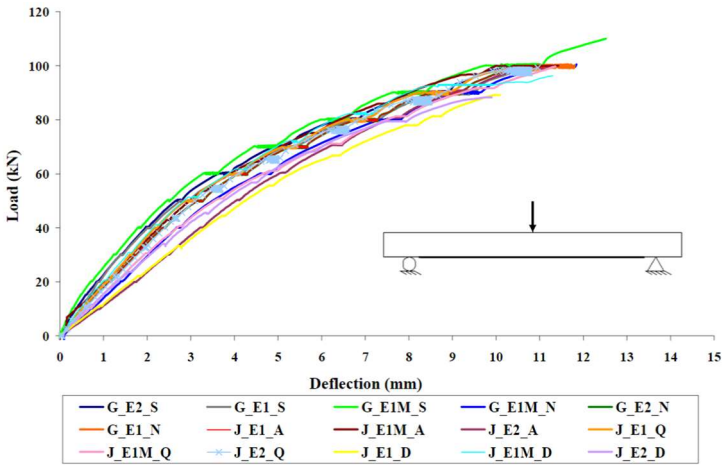

Source: Alfar, 2006

Figure 12. Average measured deflection deflections for all tested slab specimens.

Guo (2020) studied the bond strength degradation between FRP and concrete when subjected to subtropical natural exposure. For this study, 12 × 6 × 4 in. concrete prisms were cast, and six test specimens consisting of two blocks connected by two hot-rolled ribbed bars were prepared. Carbon and basalt FRP sheets were applied to the concrete prisms on the bottom face using an epoxy adhesive. Specimens were exposed to the subtropical environment in Guangdong Province, China for 0, 180, and 360 days. After exposure, specimens were subjected to the four-point bending test. Results from the four-point bending test show a rapid decrease in ultimate loads between 0 and 180 days of exposure. Prisms strengthened with CFRP showed a 13.6% decrease and BFRP showed a 26.9% decrease. After 180 days of exposure, the ultimate load remained more stable up to 360 days. All specimens failed at the FRP–concrete interface (Figure 13). Plots of strain behavior throughout exposure showed a shift in peak strain toward the free FRP end with increased exposure (Figure 14), which indicated the degradation of bond strength with environmental exposure.

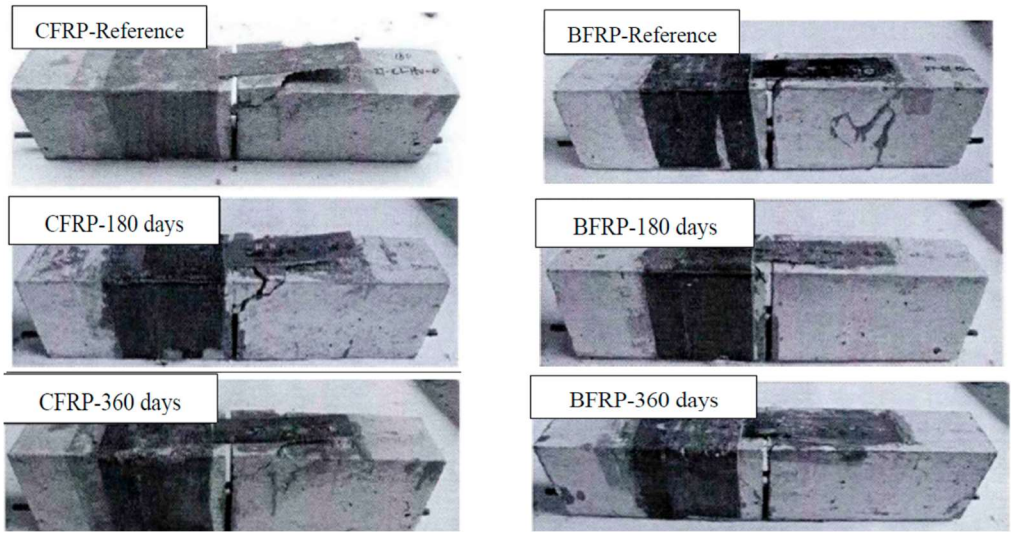

Source: Guo et al. (2020)

Figure 13. Failure mode specimens: (a) specimens with CFRP, and (b) specimens with BFRP.

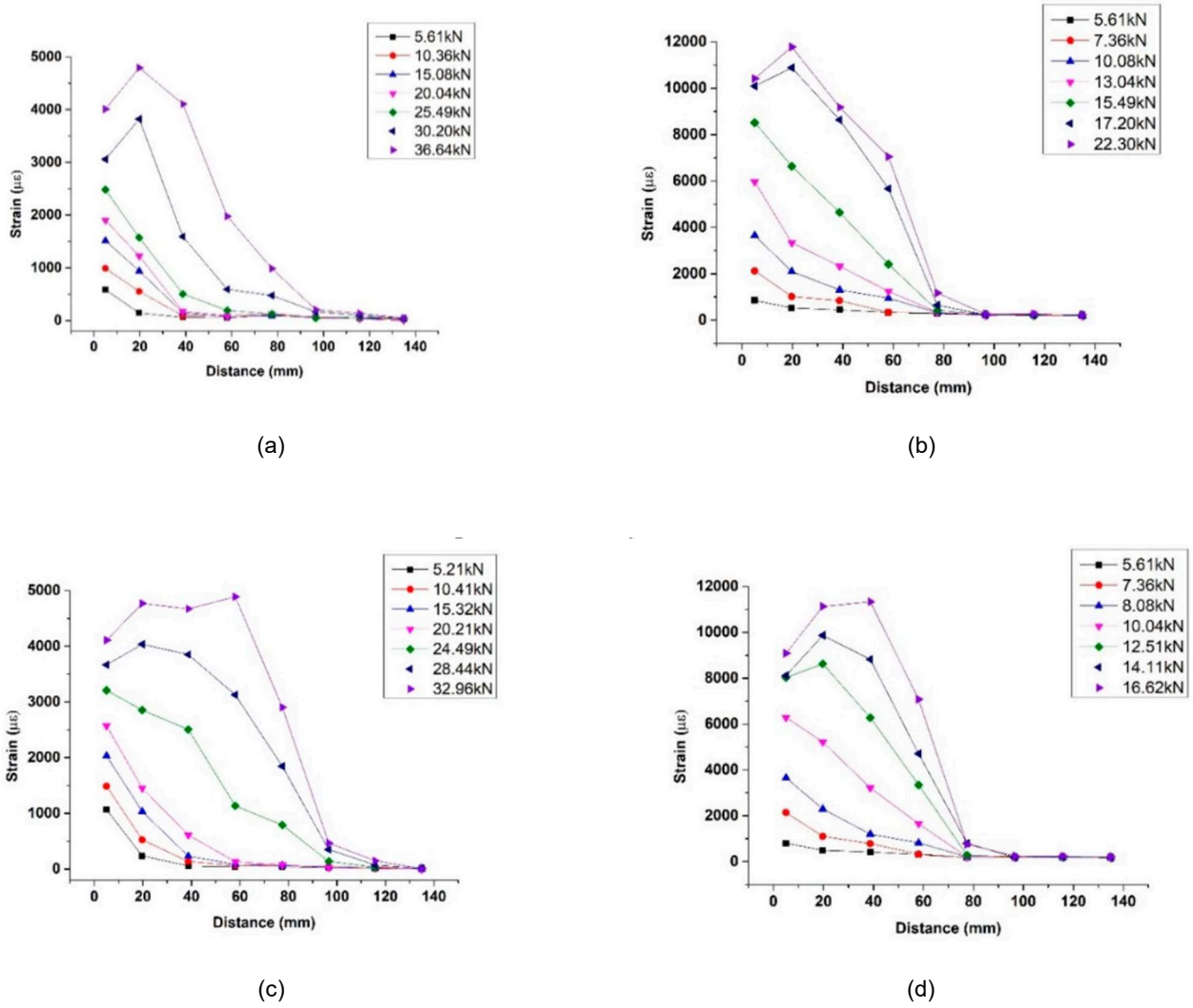

Source: Guo et al., 2020

Figure 14. Strains on FRP: (a and b) Reference beam (R-CFRP-0), and (c and d) Exposure 360 days (NE-CFRP-360).

The long-term effect of tropical environments on the bond strength between CFRP and concrete was studied by Hassan et al. (2015). For this study, 27 concrete prisms (12 × 4 × 4 in.) were cast and strengthened using a pultruded CFRP plate and epoxy adhesive. Specimens were exposed to standard laboratory conditions, wet/dry cycles in plain and saltwater, and the natural tropical environment in Malaysia for 6 months. A few of the specimens were subjected to 40–50% ultimate failure load throughout the exposure. After exposure, specimens underwent the double-lap shear test. The effective bond length for unweathered specimens demonstrated linear characteristics for low load levels and non-uniform non-linear characteristics after 2.25 kips to failure load. For the stressed specimens, non-uniform effective bond lengths were seen for all load levels. It can be concluded that the environmental conditions moderately affected bonding length before the failure load. The average failure load increased after environmental exposure; the greatest increase was seen in wet/dry cycles, which showed a 7–15% increase. However, while the failure load increased, average bond strength slightly reduced. Local bond stress distribution was higher at specimen ends for the unweathered specimens and more uniform along the bond length for conditioned specimens (Figure 15).

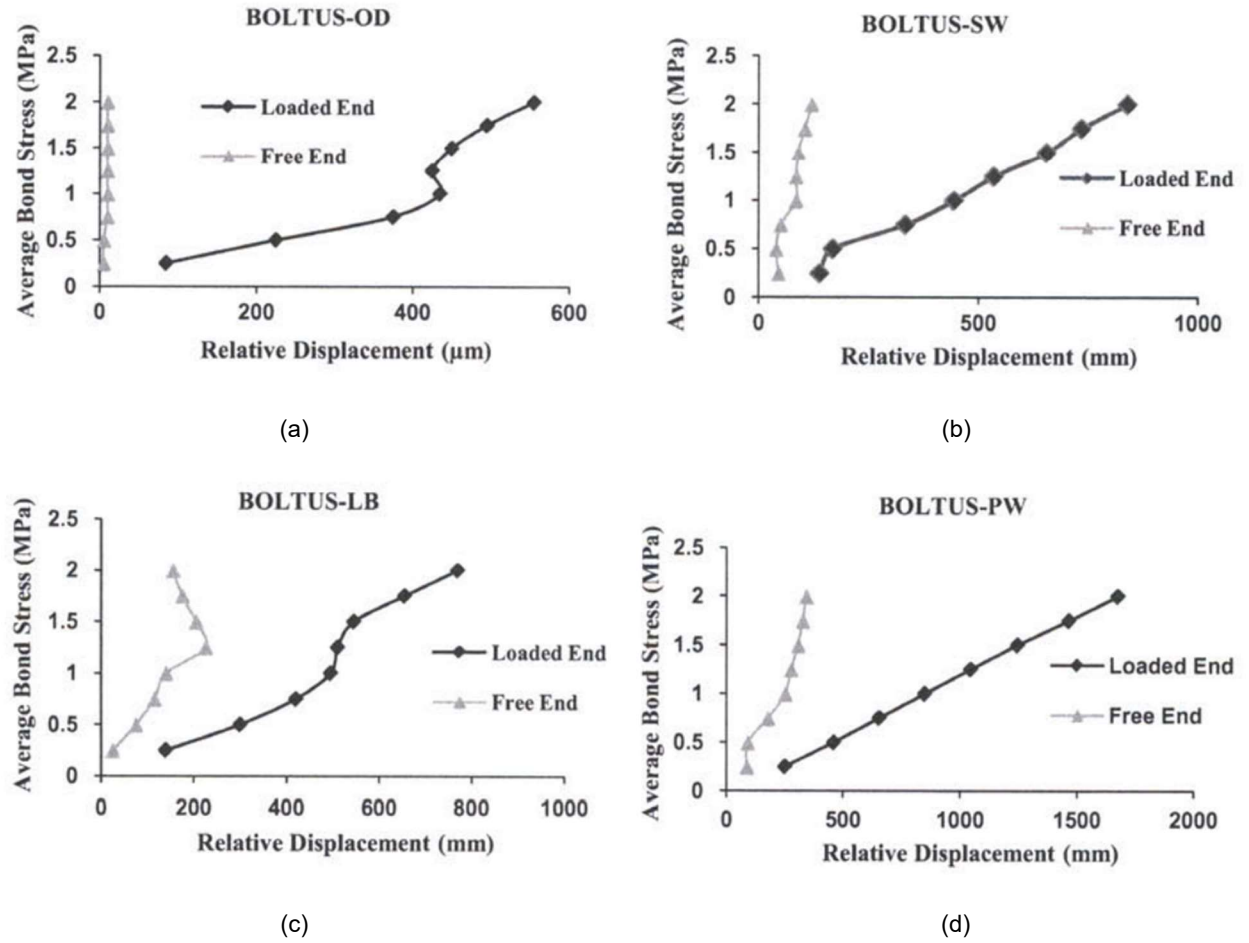

Source: Hassan et al., 2015

Figure 15. Relative displacement at loaded and free ends versus average bond stress for unstressed: (a) outdoor, (b) salt water, (c) laboratory, and (d) plain water.

Sen et al. (1999) examined the effect of marine conditions on the bond strength between CFRP and concrete. For this study, 24 concrete specimens (18 × 18 × 3.35 in.) were cast and strengthened using either bidirectional woven fabric or unidirectional carbon fiber prepreg sheets. Five different epoxy systems were studied, and specimens were strengthened with both one and two plies of carbon fiber. Specimens were exposed to wet/dry cycles and hot/cold cycles in 5% salt water denoted as bond exposure, wet/dry cycles in 15% salt water denoted as durability exposure, and outdoor conditions at the University of South Florida. To mimic tidal conditions, specimens were placed in insulated tanks in an inclined position, and water levels were lowered and raised periodically. During "hightide" water was heated to 60 °C and at "low tide" the tanks were uncovered to allow temperatures and humidity to rapidly reach ambient levels. Specimens were originally intended to be exposed for 2 years; however, bond and durability exposures were terminated after 17 months due to technical issues with cycling. The outdoor and control specimens were tested after 2 years of exposure, after exposure dollies were installed and the pull-off test was conducted. Torsional and tension forces were applied to the dollies to test the specimens; each specimen underwent five tension pull-offs and four torsional tests. Specimens strengthened with the FA2-1 system had a residual strength of 86% in tension. Greater degradation was observed in the specimens exposed to wet/dry conditions by approximately 15% compared to the outdoor (Figure 16). Specimens strengthened with system T2 showed no evidence of bond degradation across all exposure schemes.

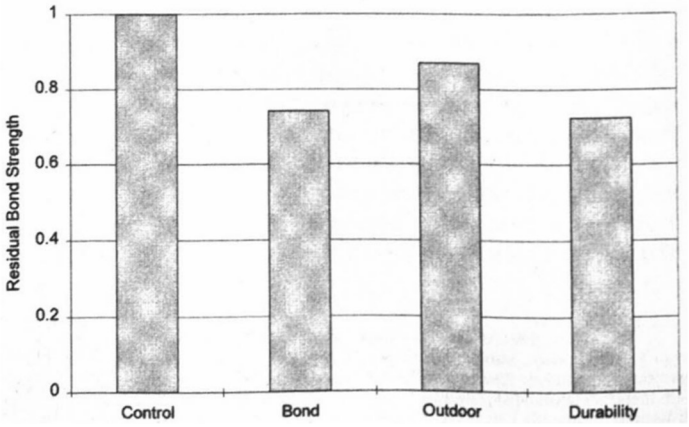

Source: Sen et al., 2019

Figure 16. Summary of residual bond strength.

Hamilton et al. (2017) presented results from the study on the long-term durability of FRP bridge retrofits exposed to real-time environmental conditions typical for the climate in Florida. Assessment of nine bridges repaired with FRP between 2001 and 2014 was conducted through visual inspection, field, and laboratory testing of FRP, concrete, and the bond between them. Detailed evaluation that included concrete compressive tests, chloride content and depth of carbonation in concrete, tensile testing of FRP composite, and pull-off bond strength tests was performed on the Grenada Bridge, Sunshine Skyway Bridge, Indian River Bridge, and University Boulevard Bridge. The other five bridges, all located in Hillsborough County, FL, were only visually inspected. Visual inspection of those bridges revealed that minor debonding due to inadequate surface preparation occurred in some cases. However, no significant deterioration of the repairs was observed. Pull-off bond tests conducted on the other four bridges, in general, satisfied the minimum criterion of 200 psi given in ACI 440.2R. Adhesive failure modes (Figure 17) were recorded (30% of failures at University Boulevard Bridge and 42 % at Chaffee Road), indicating that bond degradation may have occurred. Positive effects of FRP wrapping on the depth of carbonation and chloride content in concrete were observed.

Source: Hamilton et al. (2017)

Figure 17. Adhesive failure mode observed on pull-off test.

An experimental study was conducted by Xie et al. (2018) to investigate the effect of exposure due to a natural hydrothermal environment on CFRP for various exposure durations. A total of 35 CFRP flat coupons were prepared in accordance with ASTM D3039, and 5 each were tested after 0, 6, 12, 18, and 30 months of natural exposure to the subtropical environment in South China. Compared to the CFRP specimen without environmental exposure, the exposed specimen had a tarnished and coarser surface due to solar radiation and precipitation washing. As the exposure duration increased, the specimen had an increased number of smaller fragments at failure, which indicates that environmental exposure could embrittle CFRP. Similarly, as the exposure duration increased, both tensile strength and ultimate strain decreased. After 6, 12, 18, and 30 months, the tensile strength of CFRP coupon decreased by approximately 4.65, 2.78, 6.63, and 9.95%, respectively, and the ultimate strain decreased by 6.7, 3.09, 4.12, and 7.22%, respectively (Figure 18). However, elastic modulus remained consistent at 33,350 ksi for all the exposure duration. The environmental reduction factor was approximately 0.90, which is slightly higher than the environmental reduction coefficient of 0.85 in the American guideline (ACI 440.2R-08).

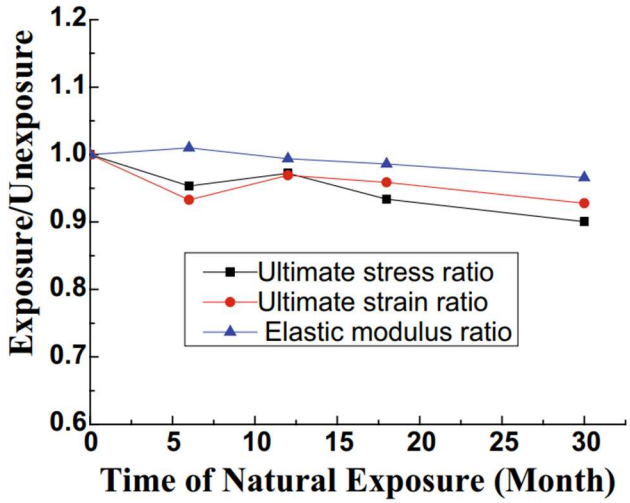

Source: Xie et al., 2016

Figure 18. Effect of natural exposure duration on the tensile properties of CFRP.

The performance of FRP bond to concrete on 8 bridges in Texas was evaluated through visual inspection and pull-off tests by Pallempati (2016). The age of repairs varied between 2 and 8 years. A total of 29 pull-off tests were performed. Visual inspection did not reveal signs of degradation; only minor delamination and air pockets were detected. The majority of failure modes were cohesive failure modes in concrete (58%), which is a type G according to ASTM (Figure 19), followed by mixed failure modes (11%). A correlation between the age of repairs and the percentage of cohesive failures could not be established. Only 5 of 29 pull-off bond strengths were lower than 200 psi, indicating a very good condition of the bond.

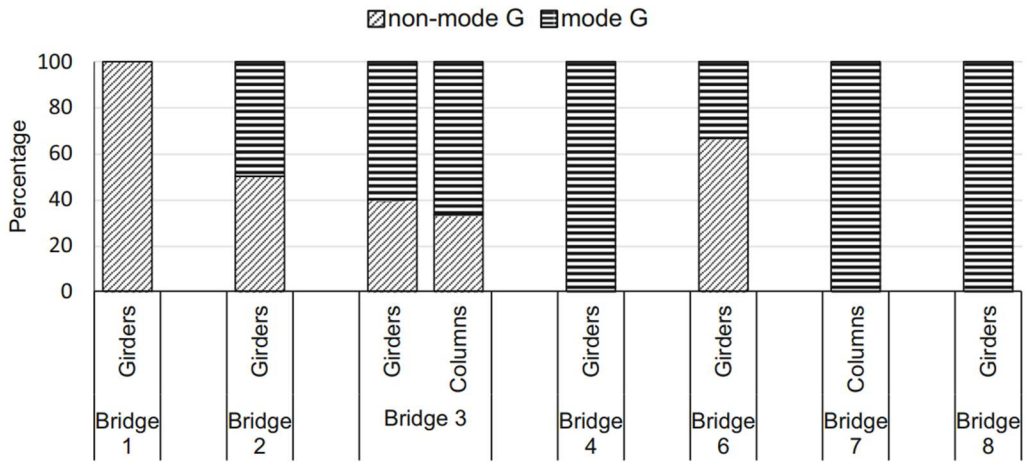

Source: Pallempati et al., 2016

Figure 19. Failure modes for girders and column samples.

Al Azzawi et al. (2018) investigated variability in the performance of FRP bonds to concrete, providing more real-time durability data related to the effect of the marine environment. In particular, the effects of ambient temperature during curing, different installation procedures (conventional and pressure bagging), and strengthening systems (epoxy-based and polyurethane-based) were studied through pull-off testing. CFRP and GFRP composite were installed in 2004, 2006, and 2008 at Friendship Trail Bridge in Tampa Bay, FL, to repair 13 corroded piles. It was found that epoxy-based systems exhibited better long-term performance compared to polyurethane-based, where the higher-bound strength varied from 179 to 357 psi and from 60 to 198 psi for epoxy-based systems and polyurethane-based systems, respectively. The bond strength of the epoxy retrofits was significantly influenced by the curing temperature – application of the resin at low temperatures (12 °C) resulted in lower pull-off test values. Poor performance was observed in the resin applied during hot weather (30 °C) due to a shorter pot life that led to insufficient saturation. Figure 20 shows the residual bond for two piles tested in 2005 and 2016, where no underlying trend could be discerned because of varying test locations.

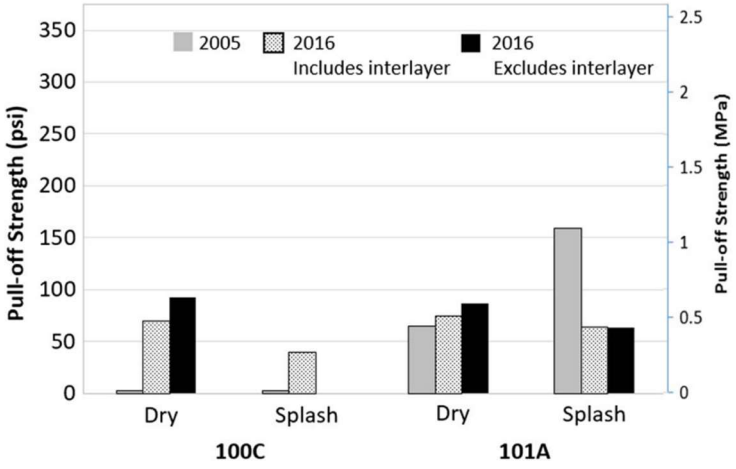

Source: Al-Azzawi et al. (2016)

Figure 20. Pull-off test results at piles tested in 2005 and 2016.

Two CFRP-wrapped bridge girders were taken out of service after 14 years of service post-CFRP strengthening from the Indian River Bridge in Melbourne, FL (Figure 21). To assess the efficacy of CFRP strengthening after 14 years of real-time environmental conditioning in the brackish water environment, Tatar et al. (2016) performed structural tests, dissection, and materials tests at the laboratory and compared the results to the field load test performed on the bridge. A total of 10 tensile tests were performed on CFRP coupons per ASTM D3039 and a total of 6 pull-off tests were conducted on two girders, three per girder. The average ultimate tensile strength and stiffness of the CFRP coupons was 948 kips/in. and 98785 kips/in., respectively. The tensile pull-off strength at all locations failed in a cohesive failure mode with a tensile pull-off strength greater than the minimum recommended by ACI 440.2R (200 psi). From flexural tests, it was observed that CFRP wrap provided 8 and 12% improvement in ultimate strength for girder 1 and girder 2, respectively, determined using the ultimate load to the residual capacity following CFRP rupture. Finally, the usage of CFRP reduced the chloride concentration by 87 and 57% under the CFRP wrap compared to exposed concrete at girders 1 and 2, respectively; thus, CFRP assisted in the control of corrosion in reinforcement.

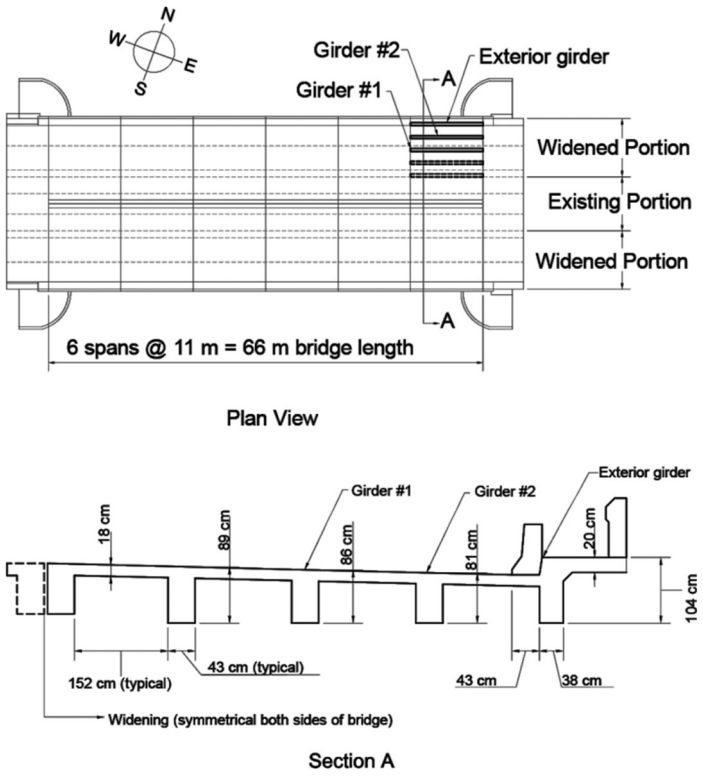

Source: Tatar et al., 2016

Figure 21. Plan and cross-sectional view showing girder 1 and girder 2 at a section of Indian River Bridge in Melbourne, FL.

Another study by Tatar and Brenkus (2021) assessed the performance of FRP-strengthened reinforced concrete bridge T-girders exposed to brackish water after 12 years of service. The subject bridge, University Boulevard Bridge, located in Jacksonville, FL, was strengthened using hybrid FRP system made of CFRP laminates and GFRP spray-up (Figure 22). After 12 years of service, nine girders were extracted by saw cutting the concrete deck from the demolished bridge for laboratory testing. SEM, pull-off test, and tensile tests were conducted and eight girders including two controls were tested in flexure, making use of four-point bending test setup to understand the durability and efficacy of the FRP strengthening system. The

tensile strength and modulus of elasticity of the CFRP coupons were found to be approximately 37% and 5% lower than the manufacturer-specified design value, respectively. In the case of GFRP, there was no difference in modulus of elasticity compared to the manufacturer-specified design value; however, the tensile strength was about 47% lower than the specified value. Similarly, 82% of test locations observed bond strength less than 200 psi (minimum requirement of ACI 440-2R) and potential environmental degradation of GFRP–concrete bond was pointed out, which was in correlation with the bond line defects observed from SEM imaging. From the flexural tests, it was concluded that the FRP reinforcement contributed to the overall girder's flexural strength by up to 12%.

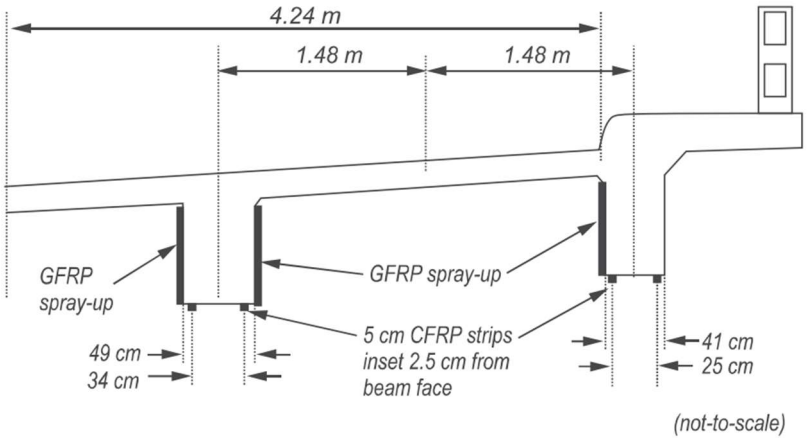

Source: Tatar and Brenkus, 2021

Figure 22. Typical cross-section of the bridge span with FRP reinforcement at University Boulevard Bridge. (Units: cm).

Tatar et al. (2021) evaluated the performance of EBFRP-retrofitted structures in the Cook Inlet earthquake and assessed the condition of FRP retrofits after over a decade of exposure in a subarctic environment. The debonding of EBFRP was documented using infrared thermography and acoustic sounding and pull-off tests (Figure 23) were conducted to assess the bond quality between EBFRP and concrete. IR thermography in combination with acoustic sounding conducted on interior and exterior columns showed severe debonding at exterior columns. The debonded areas on interior columns between 2 $in.^2$ and 24 $in.^2$ could be repaired by resin inspection, while the larger areas (greater than 24 $in.^2$) on exterior columns would require cutting the affected sheet and applying and overlapping CFRP patch at the top of it, per ACI 440.2R. A total of 12 pull-off tests were conducted at Ted Stevens International Airport, where bond strength at 58% of test locations was lesser than ACI 440.2R recommended 200 psi and exhibited complete or partial Mode E failure, which indicates flawed adhesion between CFRP and concrete. Similarly, nine pull-off tests were performed at McKinley Tower, where bond strength at all GFRP locations (66%) was more than the minimum requirement by greater than 110% and bond strength at all CFRP locations (33%) did not meet the minimum requirement by 23%. In conclusion, debonding and pull-off tests showed bond quality deterioration between EBFRP and concrete, likely due to outdoor exposure conditions, installation defects, freeze-thaw expansion, differences in thermal expansion of the materials, or a combination thereof. The CFRP bond to concrete was found to be more susceptible to deterioration due to outdoor conditions compared to GFRP.

Source: Tatar et al., 2021

Figure 23. An example of the bond pull-off test setup.

Material characterization tests were performed by Milev et al. (2022) on CFRP and GFRP samples collected from Ted Stevens International Airport (TSIA) and McKinley Tower (MKT) after 11 and 13 years of service, respectively. A total of 44 DSC tests and 18 TGA tests were run on CFRP and GFRP samples to measure the T_g to assess the physical aging and the fiber content, respectively. Similarly, several microscopy (SEM) and spectroscopy (FTIR and Raman) tests were run on CFRP and GFRP to evaluate the cross-sectional microstructure and potential chemical degradation, respectively. Figure 24 shows the T_g for interior samples were found higher than the minimum recommended by ACI440.2R by more than 30% and 20% at TSIA and MKT, respectively. However, the exterior T_g for both buildings was lower than the minimum recommended temperature per ACI440.2R. Fiber volume contents were found to be below 50% at most of the locations, except on the north wall at MKT where it was up to 71%, which is a concern because the presence of voids allows moisture penetration. Spectroscopy did not reveal any chemical degradation near the exterior surface of FRP. Some inconsistencies were likely present in the FRP installation, as observed from the variability in fiber content at MKT and thermal properties at TSIA, which was found in good correlation with the results from microscopy.

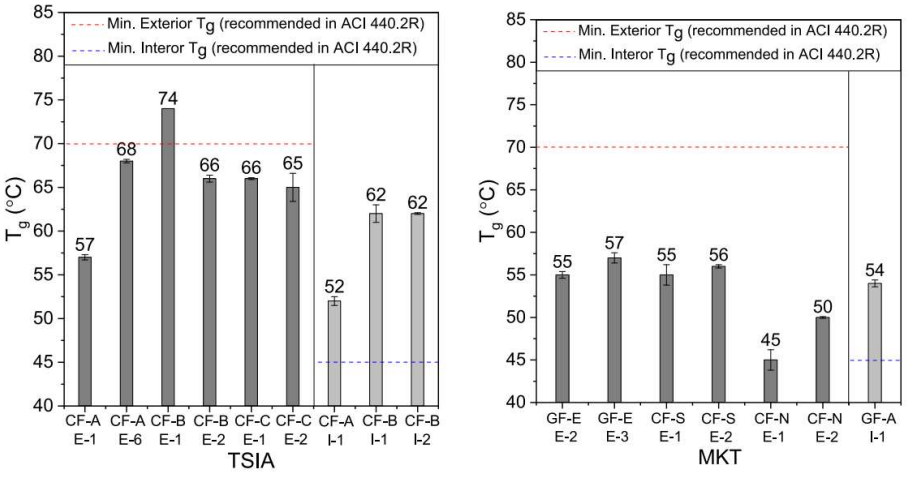

(a) (b)

Source: Milev et al. (2022)

Figure 24. Glass transition temperature of CFRP and GFRP: (a) TSIA and (b) MKT.

DURABILITY ASSESSMENT - LABORATORY ACCELERATED CONDITIONING

Tatar and Hamilton (2015) studied the long-term performance of FRP composite bonded concrete structures when subjected to water immersion and high humidity at elevated temperatures. Several small-beam three-point bending test specimens (12 × 4 × 4 in.) were prepared and conditioned in the accelerated conditioning environment for 1-, 2-, and 8-weeks duration. Five different types of composite systems were selected for strengthening the specimens; four of them were installed using the wet-layup method and the remaining one was composed of precured laminate. Bond retention value (R_b) was determined by dividing the strength of conditioned samples by the average control strength, which was then combined with other test data from a database of over similar 700 test results. Figure 25 shows the reduction in R_b for all exposure conditions after one week of conditioning at 60 °C, which shows the FRP–concrete bond is susceptible to degradation upon exposure to high temperature and humidity or moisture. Based on the laboratory tests and database, the bond durability factor (BOD) of 0.6 was proposed for wet-layup FRP composites without putty.

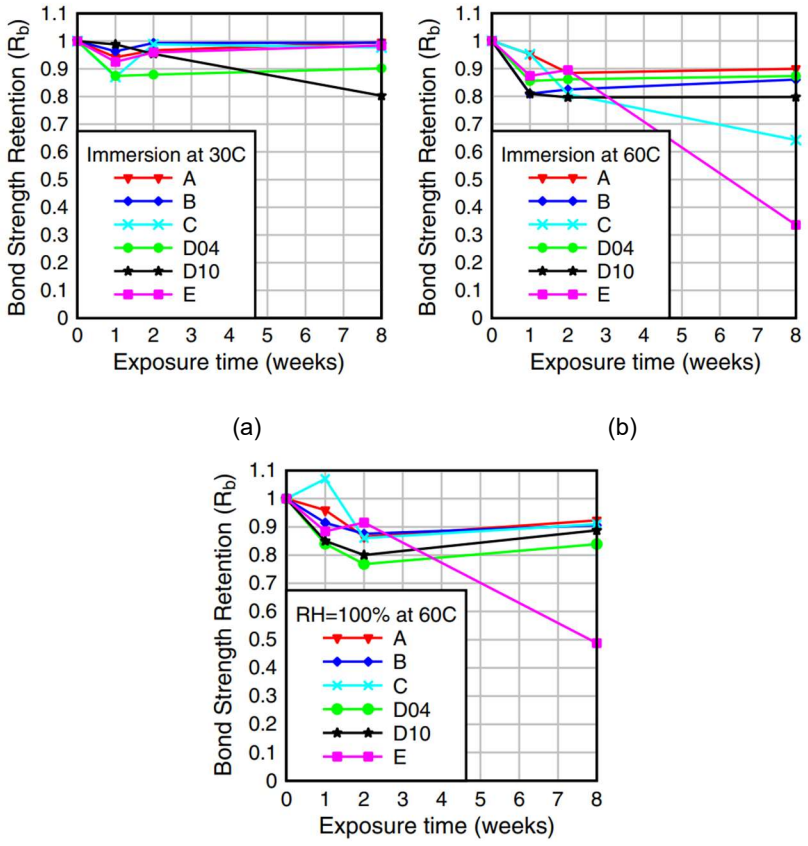

Source: Tatar and Hamilton, 2015

Figure 25. R_b vs. the exposure time in weeks: (a) immersion in water at 30 °C, (b) immersion in water at 60 °C, and (c) RH=100% at 60 °C.

Douglas et al. (2014) investigated the degradation of epoxy properties and the corresponding degradation mechanism upon exposure to various laboratory accelerated conditionings. Two different types of epoxy systems were used to prepare the test specimens sized 2.5 × 0.375 × 0.125 in. and were allowed to cure for a week, followed by accelerated laboratory conditioning (water immersion at 30 to 60 °C, and UV aging)

for up to 8 weeks. DRIFT and ATR IR experiments were then performed on both epoxy systems to determine the mechanism of property loss at after laboratory conditioning. The tensile strength and modulus of both epoxy systems (model epoxy system shown in Figure 26) degraded at higher temperatures after hygrothermal exposure up to 38% and 33%, respectively, after 8 weeks of exposure. The tensile properties after UV exposure degraded as well, but it was not found as detrimental as hygrothermal exposure. Spectroscopy revealed some evidence of oxidative degradation mechanism on samples exposed to UV radiation and hydrolysis was observed on samples exposed to UV and water.

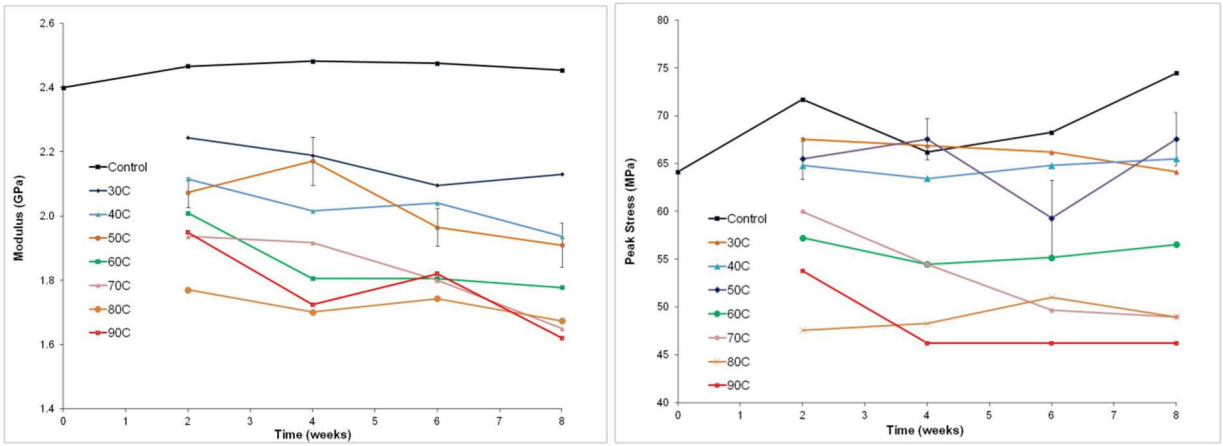

(a) (b)

Source: Douglas et al., 2014

Figure 26. Change in mechanical properties of model epoxy systems with hygrothermal exposure: (a) change in modulus and (b) change in peak stress (units: MPa).

The bond durability of the CFRP under severe environmental and laboratory-accelerated conditions was compared to the durability of different types of recently developed galvanized steel mesh, MSM, and HSM by Sohail et al. (2021). The prism samples (20 × 4 × 4 in.) were made and strengthened using CFRP, HSM, and MSM, and eventually were tested after 180, 360, and 730 days. Three-point bending tests were carried out on six samples after each exposure time at different exposure conditions. The failure mode of CFRP was mostly interfacial and adhesive; four samples failed due to debonding of laminates, and some parts of the failure passed through concrete. The mode of failure changed from interfacial to the adhesive on exposing the specimen to direct sunlight and saline water for 180, 360, and 730 days. The rest of the 16 samples had failure planes on the tension surface at the concrete epoxy interface, thus classified as an adhesive failure. Ultimate load capacity was reduced by 14% in CFRP specimens in comparison to their counterpart laboratory samples after 180 days of saline-water exposure (Figure 27). However, the ultimate load capacity of CFRP was only reduced by 2% after 180 days of direct sunlight exposure (Figure 27). Similarly, after 360 and 730 days of saline-water exposure, CFRP showed a 4% loss and 3% gain in strength compared to the unexposed sample, respectively (Figure 27). Based on all the results, for CFRP it was recommended that 0.85 and 0.9 be used as bond-strength reduction factors under saline–water exposure and direct sunlight exposure, respectively.

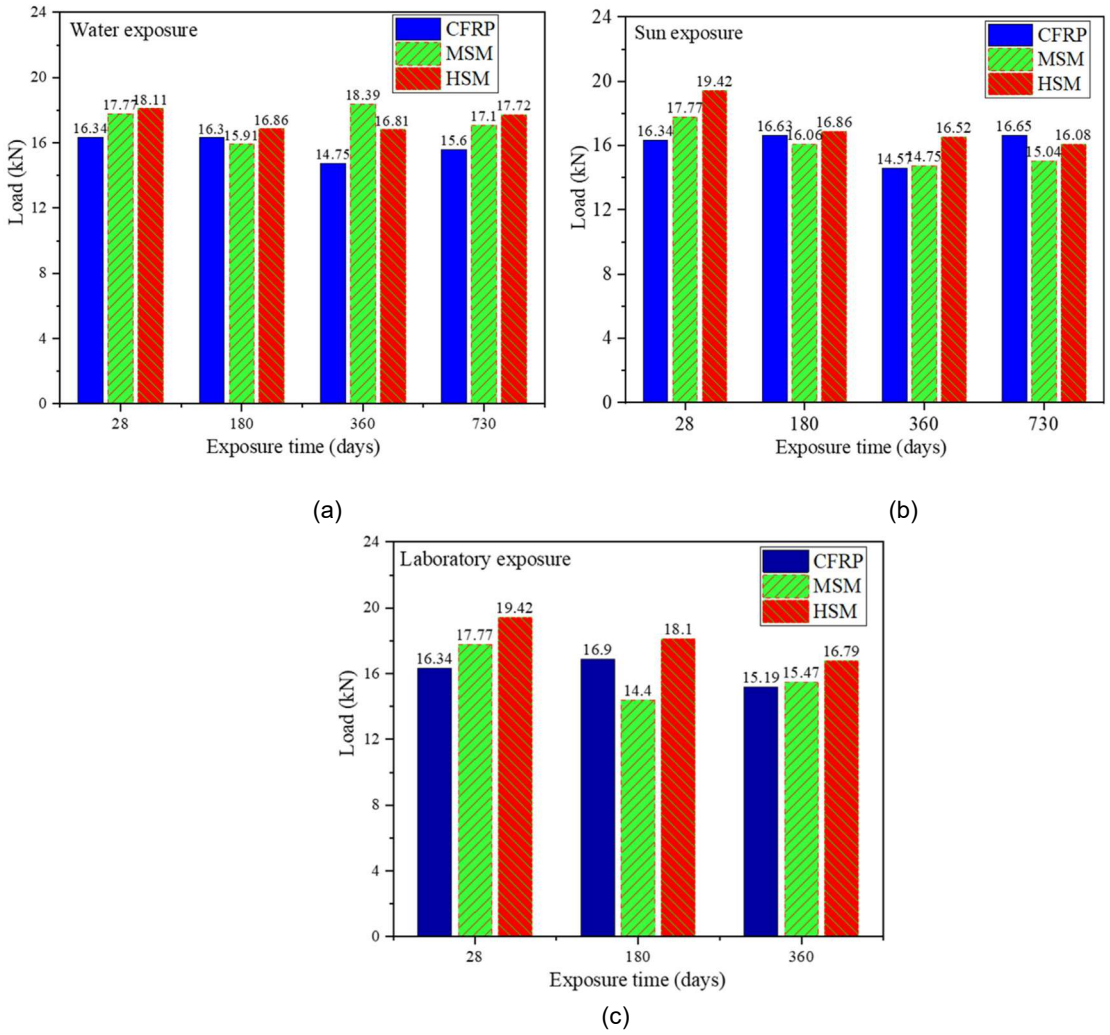

Source: Sohail et al., 2021

Figure 27. Strength of CFRP, MSM, HSM prisms at 28, 180, 360, and 730 days: (a) saline water exposure, (b) sun exposure, and (c) laboratory (units: kN).

Mata and Atadero (2014) studied the bond durability of CFRP-reinforced concrete specimens (14 × 6 × 3.5 in.) after 6 months and 12 months of laboratory-accelerated conditioning by conducting direct tension pull-off tests (Figure 28). The specimens were subjected to various accelerated conditionings at the laboratory such as wet-dry cycles, freeze-thaw cycles, and exposure to deicing agents, and then tested during their respective stages. A total of 100 pull-off tests were conducted at different stages in the laboratory: 10 tests after completion of curing, 45 tests after 6 months, and 45 tests after 1 year, and the laboratory results were compared with the results obtained from the previous field studies. Four structures were selected in the field to represent a range of exposure conditions, lengths of service, and types of FRP reinforcement. To determine the condition of the bond, pull-off tests were conducted on all four structures meeting the requirements of ASTM C1583-04 (2004). The average pull-off bond strength for all four structures ranged from 104 to 522 psi, and the coefficient of variation ranged from 27.7% up to as high as 154.2%. The results obtained by Mata and Atadero (2014) from 10 control specimens also had a high degree of variability, with a coefficient of variation of 17.3%. The results of tests after 6 months and 1 year at identical exposure conditions did not show consistent failure mode as well. The pull-off bond strengths for identical exposure conditions were found in a range of 80 psi to 627 psi. Because of this very large discrepancy in the result,

both in laboratory and field conditions, if pull-off tests are used, the researchers should plan to test a large number of samples to better identify outliers.

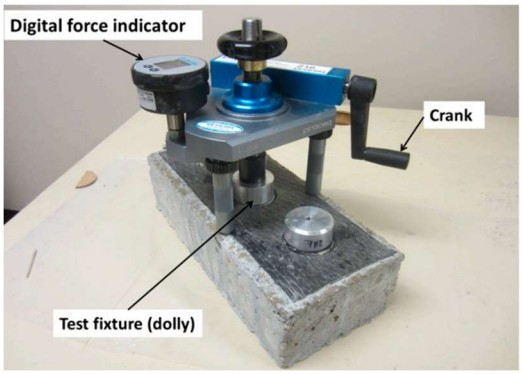

Source: Mata and Atadero, 2014

Figure 28. Pull-off test setup.

Four-point bending tests were carried out by Nuaimi et al. (2021) on beam specimens conditioned under direct sunlight and saline water for 180, 360, and 730 days in the Arabian Gulf to study the durability of reinforced concrete beams strengthened with CFRP. Forty tension-controlled RC beams, sized 140x280x2000 mm, were cast, and 20 among them were reinforced with the CFRP sheet. Two RC beams and two CFRP-strengthened beams were tested after 28 days, followed by tests of six RC beams and six CFRP-strengthened beams on the 180th, 360th, and 730th day. The CFRP-strengthened specimens exhibited 67% higher load capacity than the load capacity of the control beam after 28 days and up to 51% and 71% higher load capacity than control specimens after 730 days of direct sunlight and saline water exposure, respectively (Figure 29). Adhesive, cohesive, and interfacial failure modes were observed overall. All strengthened beams conditioned under direct sunlight saw cohesive failure like the control beam on the 28th day except for the ones tested after 180 days. However, all the beams conditioned in saline water observed adhesive failure. Because the failure modes changed from cohesive to adhesive after conditioning in saline water for 180 days, the epoxy bonds seemed to be a critical aspect of hygrothermal exposure. The ductility of RC beams and CFRP-strengthened beams were compared under all exposure conditions and testing durations, where RC beams were found to be more ductile. The exposure to saline water or direct sunlight did not significantly affect the beam stiffness in the strengthened beams. The author suggested a bond reduction factor equal to 0.6 and a flexural strength reduction factor equal to 0.85 for saline conditioning, which is less than the recommended reduction factor by ACI 440.2R-17 (2017).

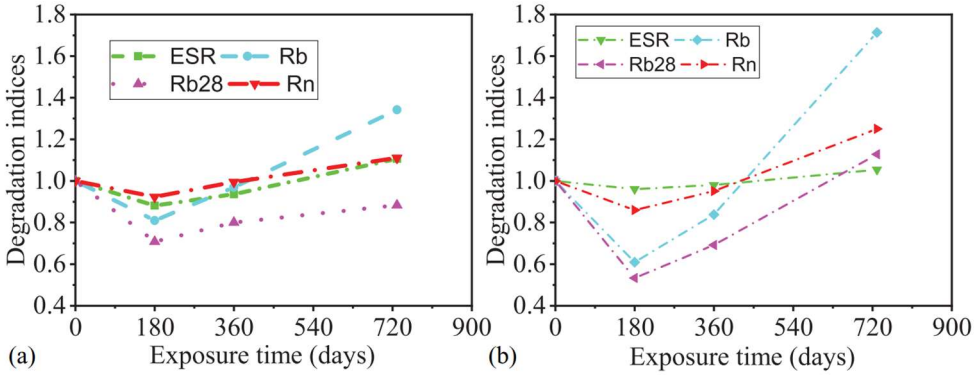

Source: Nuaimi et al., 2021

Figure 29. Degradation indices for the CFRP under: (a) sunlight, and (b) saline water after exposure for 180, 360, and 730 days.

Three-point bending tests were carried out by Zhang et al. (2021) on beam specimens immersed in fresh water at temperatures between 18 to 22 ℃ for 1, 3, and 6 months to study the durability of concrete beams strengthened with Carbon Fiber-Reinforced Polymer (CFRP). Thirty-six CFRP-strengthened concrete beam specimens sized 26 × 6 × 6 in. were cast from the same batch of concrete and cured in the environmental chamber with a temperature of 20 ℃ and 95% relative humidity for 28 days. Three CFRP-strengthened beams were tested after 28 days of curing, followed by tests of three CFRP-strengthened beams each after 1 month, 3 months, and 6 months of water immersion. The flexural tests before and after immersion were conducted using the servo-electric universal testing machine. All the strengthened beams failed by debonding in concrete adjacent to the concrete-adhesive interface accompanied by the substrate diagonal cracking near the notch. The failure load was highest after 1 month of immersion followed by 3 months and 6 months, where the failure load was found lower by 4% and 10%, respectively. However, compared to the control specimens the failure loads at 1 month, 3 months, and 6 months immersion were found higher by about 13%, 8%, and 2%, respectively.

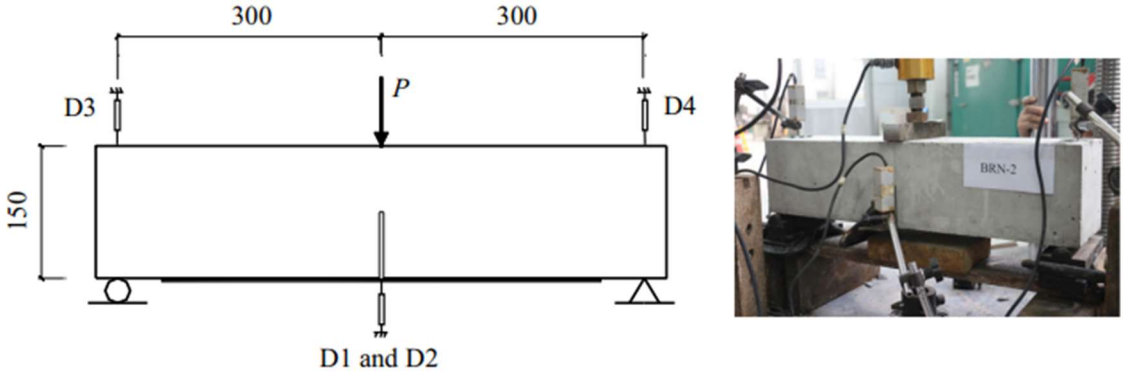

Source: Zhang et al., 2021

Figure 30. Three-point bending test setup (units: mm).

The effects of various hygrothermal conditions on the durability of the interfacial bonding between concrete and carbon fiber laminate (CFL) were investigated using the double shear test method by Zheng et al. (2016). A total of twenty 28 × 4 × 4 in. specimens were prepared and divided into six groups based on temperature and humidity to simulate the climatic condition of South China. Group B specimens were subjected to constant humidity of 95% and different temperatures (5 ℃, 25 ℃, and 60 ℃). Similarly, group C specimens were subjected to a constant temperature of 60 ℃ and different humidity (60%, 75%, and 95%). Strain gages bonded along the CFL surface and linear variation displacement transducers (LVDTs) were used to measure longitudinal strains. Upon testing, all the specimens observed cohesive failure in the concrete substrate. It was concluded that the hygrothermal environment had adverse effects on the CFL-concrete interface. Compared to the reference specimen, the ultimate load at failure decreased as much as 27.9% when the temperature was 60 ℃ and relative humidity was 95%. The maximum strains of the specimens decreased by about 17% to 37% compared to the reference specimen, which implies decay of bond behavior after exposure to the hygrothermal environment.

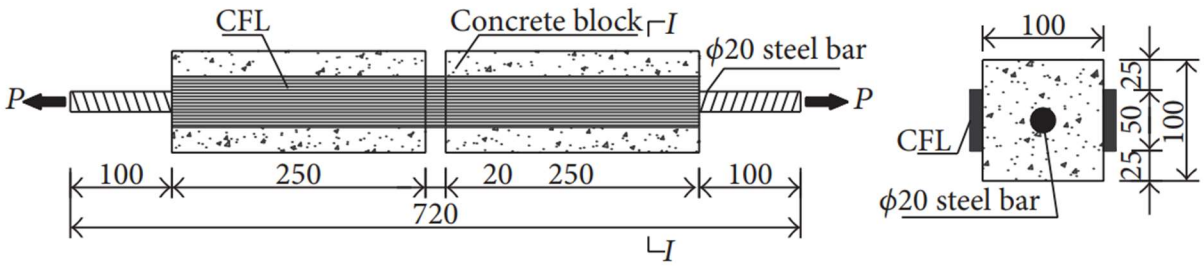

Source: Zheng et al., 2016

Figure 31. Schematic diagram of a double shear specimen (units: mm).

Pull-off tests were carried out by Fazli et al. (2018) to assess the effects on the bond performance of CFRP-strengthened concrete slabs (12 × 12 × 2 in.) after 12 months of exposure in a marine environment. The concrete slab specimens were strengthened using CFRP fabric on the top surface of the slab (Figure 32a) and left bare on the bottom surface of the slab (Figure 32b). To accelerate the degradation of the specimens subjected to marine exposure conditions, test specimens were subjected to wet/dry cyclic conditioning over periods of 3, 6, 9, and 12 months, and full immersion in the salt-water solution at 60 °C for periods of 3, 6, 9, and 12 months. The test results confirmed two dominant modes of failure, cohesive failure in the concrete substrate, and mixed cohesive failure in substrate and epoxy failure at the epoxy/substrate interface. The 12-month marine environmental conditioning resulted in a reduction of pull-off strength by approximately 6–35% for wet/dry cyclic conditioning and 11–37% for full immersion in the saltwater at 60 °C.

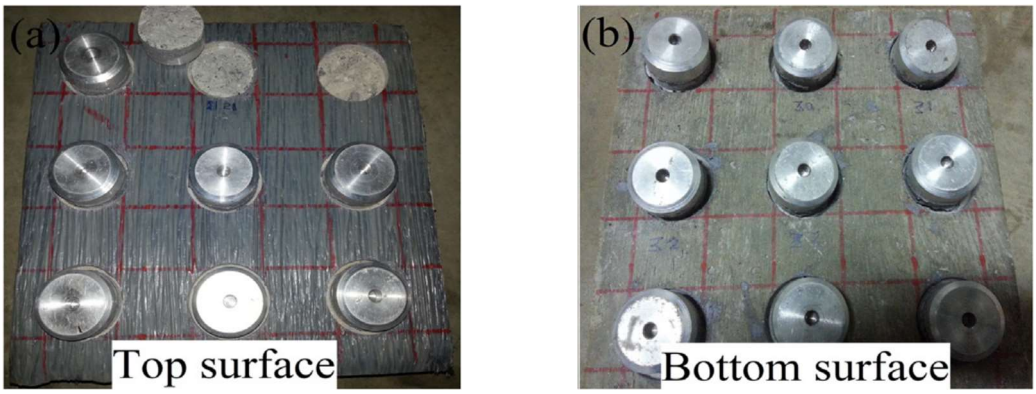

Source: Fazli et al., 2018

Figure 32. Concrete slab: (a) CFRP installed on top surface, and (b) bare surface.

Pull-off tests were carried out by Mikami (2012) after 40, 100, and 250 hygrothermal cycles to study the effect of long-term environmental exposure on bond strength (Figure 33). A total of 30 concrete beam specimens (12 × 2.5 × 1.25 in.) were strengthened with a single-ply CFRP and were exposed to accelerated conditioning in the laboratory, such as cyclic hygrothermal conditions, and immersion in distilled or salt water. Each hygrothermal cycle consisted of a 15-minute ramp time from 25 °C to either 100 or 180 °C, followed by 70 minutes of isothermal condition and a 30-minute ramp down back to 25 °C. A total of 150 tests were performed, 5 tests per concrete beam specimen. The concrete failure modes were found primarily cohesive in nature at room temperature, but for hygrothermal cycles to 100 °C and 180 °C, cohesive/mixed failure and adhesive failure were observed, respectively. The effect of high temperature at 0% relative humidity was found to be most damaging in nature. At 0% relative humidity (RH), after 250 cycles of conditioning when the temperature increased from 100 to 180 °C, the average adhesive strength

dropped from 567 psi to 73 psi. The mode of failure changed from mixed/cohesive to adhesive as the temperature increased. Immersion in distilled water caused more degradation in bond strength compared to the exposure to 100% RH, especially at 100 ˚C after 250 cycles, where the average adhesive strength decreased to 299 psi compared to 647 psi for 100% RH.

(a)

(b)

(c)

Source: Mikami, 2012

Figure 33. Beam conditioned at various cycles room temperature and distilled water: (a) 40 cycles, (b) 100 cycles, and (c) 250 cycles.

The effects of thermal cycles in air or water were examined by Liu et al. (2019) on the bond performance between CFRP and concrete using the single-lap shear test. Concrete specimens (16 × 4 × 4 in.) were prepared and cured at 95% RH for 3 months, followed by the installation of CFRP using the wet lay-up method. The specimens were then held at -18 and 30 ˚C for 2 hours, followed by 2 hours of ramping of the specimens to 30 and -18˚C, respectively (Figure 34). Two conditionings were adopted: first, the specimens were immersed in water and second, the specimens were exposed to thermal cycles in air; 270 thermal cycles in the air increased the interfacial fracture energy of the CFRP plate-concrete and CFRP sheet-concrete by 35% and 20%, respectively, while 270 thermal cycles in water reduced the interfacial fracture energy of the CFRP plate and CFRP sheet-concrete by 9% and 46%, respectively. Based on the thermal cycles in water, a reduction factor of 0.7 was proposed for the CFRP–concrete structure. The failure modes of both CFRP sheet-concrete and CFRP plate-concrete were found cohesive in nature. However, the thermal cycles in water changed the failure mode to interfacial debonding between the adhesive layer and concrete.

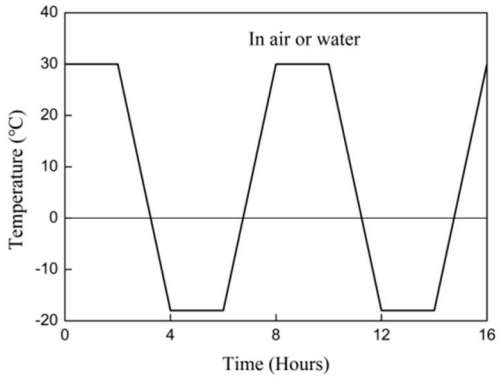

Source: Liu et al., 2019

Figure 34. Freeze-thaw cycle parameter.

Chotickai and Somana (2018) presented a study on the degradation of CFRP–concrete interphase under wet-dry cycles (in fresh and saltwater) at 25 ℃. The influence of the concrete strength and number of CFRP layers on the ultimate load and failure modes was assessed using small beam specimens subjected to three-point bending after 3, 8 and 12 months of exposure. It was found that several CFRP layers have more influence on bond strength, as observed in the CFRP strain profile after 12 months of exposure (Figure 35). The ultimate load retention for normal-strength concrete specimens and high-strength concrete specimens varied in the range of 95% to 115% and 94% to 128%, respectively. Failure modes were affected by the exposure to wet-dry cycles, changing from concrete to bond slippage failure in normal-strength concrete. In high-strength concrete specimens shift in failure modes due to exposure was not obvious.

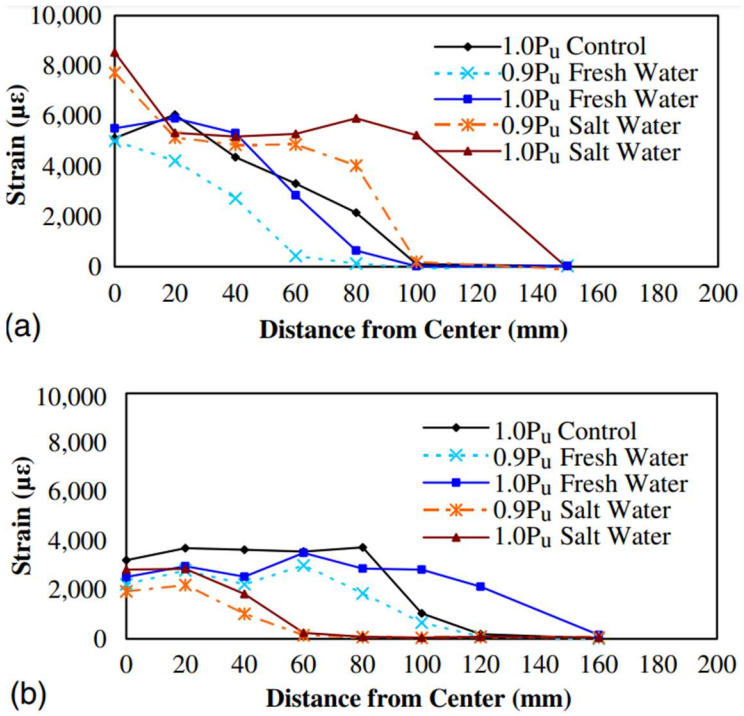

Source: Chotickai and Somana, 2018

Figure 35. CFRP strain profiles for normal strength concrete specimens after 12-month exposure: (a) specimens with one CFRP layer, and (b) specimens with two CFRP layers (units: mm).

Dai et al. (2010) conducted experiments to understand how moisture affects the initial and long-term bonding strength of FRP sheets to concrete interfaces. The study tested a total of 56 specimens: 48 underwent the three-point bending test and 8 underwent the pull-off test. For the three-point bending test, 16 specimen combinations were used with three beams cast for each condition. Each of the eight beams designated for the pull-off test was tested four times and the results were averaged for each specimen. The testing schemes varied concrete moisture content, primer, adhesive, relative humidity, and exposure length. Moisture content was varied to test two extreme conditions seen in practical settings during FRP installation. Concrete with a moisture content of 4.2% was used to simulate a dry surface during installation, and concrete that had been soaked in seawater for three days, moisture content of 9.0%, was used to simulate a wet surface during installation. Carbon strand sheet (CSS) was applied to each of the 56 specimens. After FRP installation, the specimens were placed in an exposure pool and underwent wet/dry cycles for 0, 8, 14, and 24 months. The cycles consisted of a 4-day immersion in 60 °C salt water and 3-day dry laboratory air. The pull-off test conducted on unweathered specimens showed similar interfacial tensile bond strength for dry and wet specimens. The hydrophobic primer was effective on wet specimens before exposure, but after wet/dry cycling for 8 months, both wet and dry specimens were not able to prevent interfacial tensile bond strength loss in the range of 70 to 80% (Figure 36). After various exposure lengths, the normal bonding adhesive increased flexural capacity and ductility (Figure 37a,b), while the low elastic modulus adhesive decreased flexural capacity (Figure 37c).

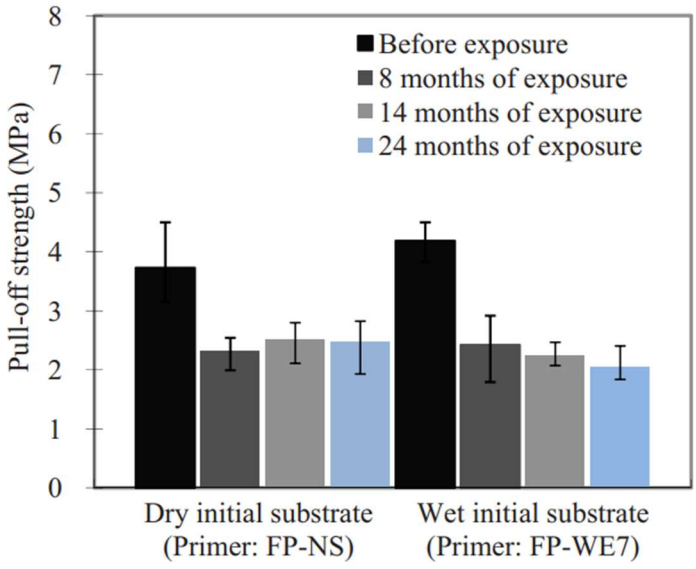

Source: Dai et al., 2010

Figure 36. Degradation of interfacial tensile strength.

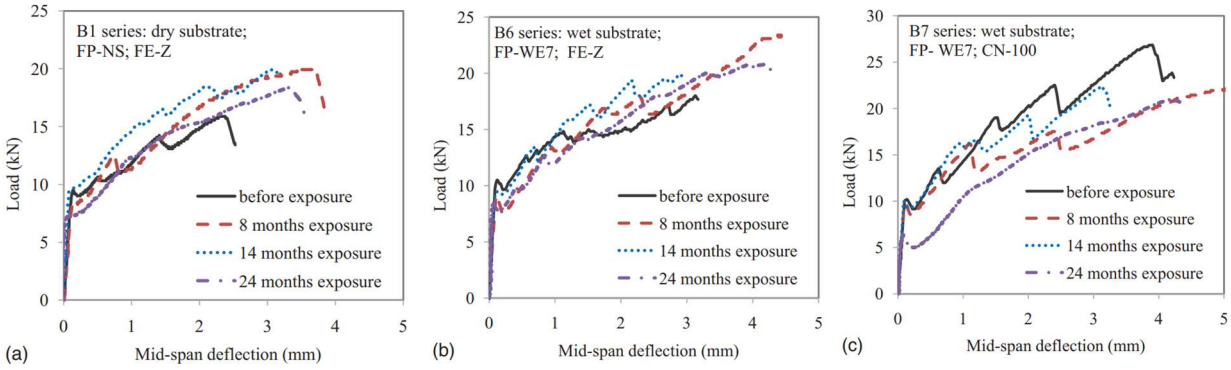

Source: Dai et al., 2010

Figure 37. Effects of moisture on the long-term performance of FRP bonded concrete beams: (a) dry substrate with normal adhesive, (b) wet substrate with normal adhesive, and (c) wet substrate with low elastic modulus adhesive.

The durability of concrete beams strengthened with either CFRP sheets or plates and exposed to freeze-thaw cycles or salt water was assessed using small beam specimens by Al-Mahmoud (2014). A total of 36 specimens were prepared using two independent prismatic concrete blocks with 6 × 6 in. cross-sections, connected through steel hinges as shown in Figure 38. During 300 freeze-thaw (FT) cycles specimens were exposed to temperatures that varied from -18 to 15 °C, followed by four-point bending tests. In the case of saltwater immersion, specimens were kept in the 3.5% salted tap water at 20 °C. Failure modes, ultimate load, and bond strength were evaluated and compared with the values corresponding to the control specimens, which were kept in standard laboratory conditions. The ultimate load of CFRP plates decreased by 25% after 300 FT cycles, while only a negligible decrement was observed in specimens immersed in salt water. CFRP sheet specimens' ultimate load decreased by 25% after 300 FT cycles and 48% after 120 days of immersion in salted water.

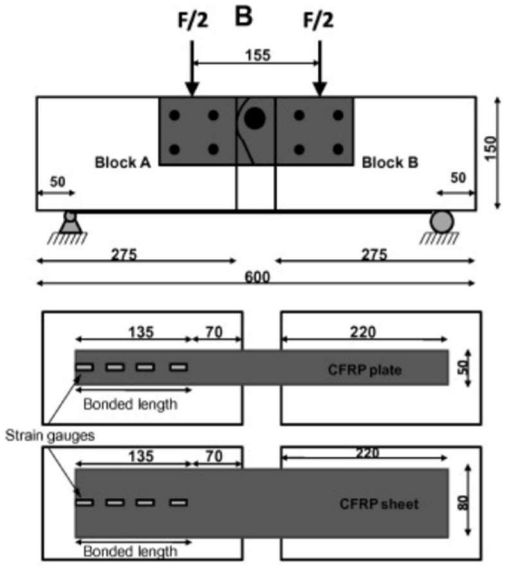

Source: Al-Mahmoud, 2014

Figure 38. Four-point bending test detail and setup (units: mm).

The long-term bond performance of CFRP-strengthened concrete members after varying cyclic temperatures, humidity, and sustained loading was studied by Gamage et al. (2009). For this study, a total of thirty-one 10 × 3 × 3 in. concrete blocks were cast and left to cure for 28 days before installation of CFRP. A primer layer was first applied to the surface and left to cure for 30–60 minutes. After the primer was dry, a two-part epoxy adhesive and carbon sheet were applied using the wet-layup method and left to cure for 7 days. Specimens were placed in an environmental chamber where a spring system applied a constant load in which 4-mm displacement is equivalent to 225 lbf. All specimens, aside from two controls, were subjected to temperature cycles between 20 and 50°C for 4.5 hours and 1.25-hour soaking time and minimum and maximum temperatures. The specimens varied in their exposure time, between 100 and 2,400 hours, and the percentage of sustained loading they experienced, between 0 and 50%. After exposure, specimens were subjected to the single lap shear test, aside from those that experienced greater than 35% of sustained loading which failed during exposure. Members that were conditioned for 400–450 temperature cycles showed a 28%, 25%, and 30% reduction in strength after 0%, 15%, and 25% sustained loading, respectively (Figure 39). The primary failure mode of specimens under cyclic temperature, 90% humidity, and high sustained loads were at the CFRP and concrete interface after a short number of cycles. Specimens that experience conditioning and low sustained loads failed by concrete fracture after low cycle numbers and at the CFRP and concrete interface after high cycle numbers.

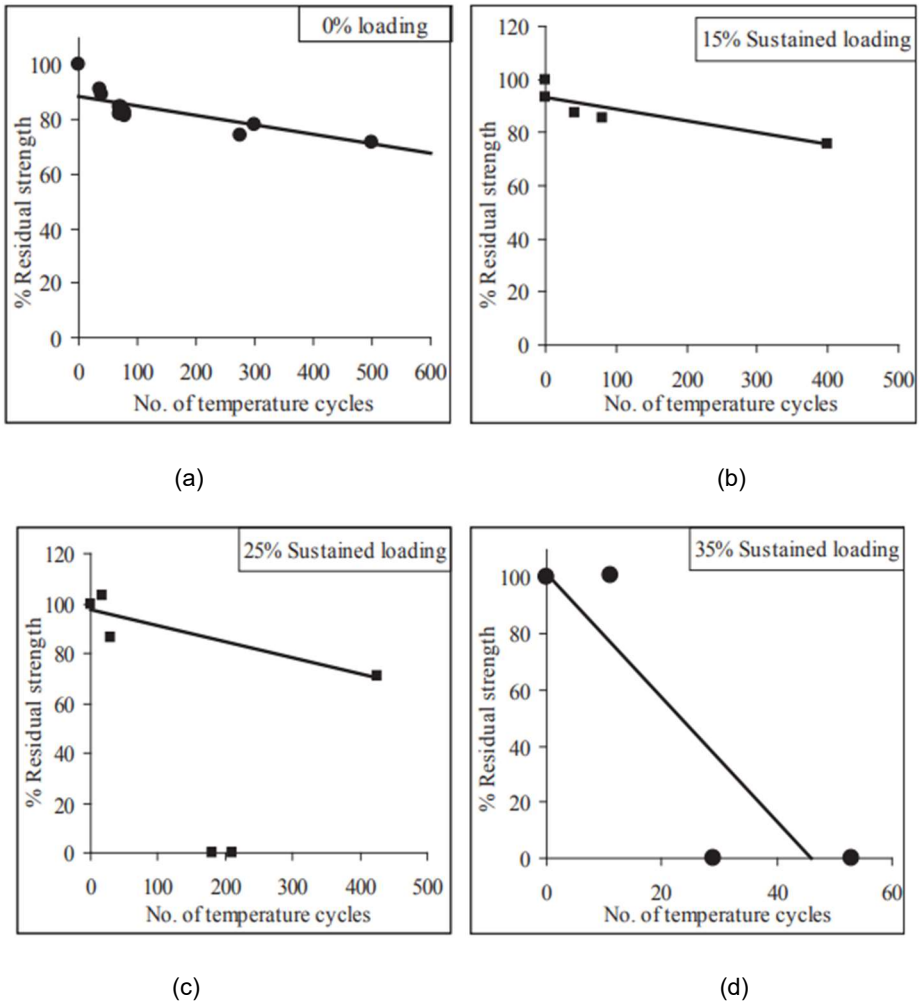

Source: Gamage et al., 2009

Figure 39. Residual strength variation with exposure cycle: (a) no sustained load, (b) 15% sustained loading, (c) 25% sustained loading, and (d) 35% sustained loading.

Al-Lami et al. (2020) assessed the long-term behavior of the bond between CFRP and concrete using single-lap shear test (Figure 40) and pull-off tests. Specimens were immersed in water at 38±2 °C degrees and tested after 500, 100, and 1,500 hours. In addition to bond tests, tensile testing of CFRP coupons and epoxy specimens was performed. The average tensile strength of the epoxy resin increased between 0 and 1,000 hours of exposure and slightly decreased up to 1,500 hours. Hygrothermal aging did not significantly impact the tensile strength or elastic modulus of the CFRP coupons. The ultimate strain of specimens exposed for 500 hours was 107% higher than the unweathered specimens, those exposed for 1,000 and 1,500 hours decreased by 4% and 15%. The results from the pull-off test showed minor change after 500 hours and an increase of 17.7% and 46.9% after 1,000 and 1,500 hours, respectively. All pull-off test specimens failed within the concrete substrate. The predominant failure mode for the direct shear test was a cohesive failure within the concrete substrate, with a few specimens failing by mixed adhesive failure at the interface. The critical load, defined as the mean load within the global slip range, increased by 16.3% after 500 hours and then decreased with increasing exposure time. The specimen's fracture energy followed the same trend as the critical load, with a 28.5% increase after 500 hours and a slight decrease after 1,000 and 1,500 hours.

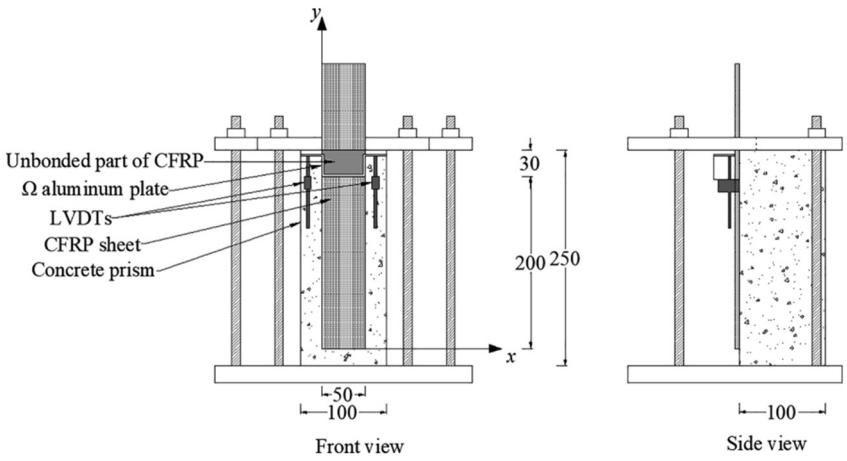

Source: Al-Lami et al., 2020

Figure 40. Single-lap direct-shear test setup (units: mm).

Pan et al. (2018) also conducted a research study to correlate the degradation of FRP-concrete bond strength with the number of freeze-thaw effective cycles. Experimental testing and data found in the literature were used to develop a freeze-thaw degradation model, which later served to predict the service life of CFRP and GFRP bond to concrete in the field. Experimental testing that was part of this study included single-lap shear tests on prismatic concrete specimens exposed to two different conditions: (1) freeze-thaw cycles and immersion in water and (2) freeze-thaw cycles at RH 90%. Freeze-thaw cycling procedure consisted of 10 hours at -20 ℃ and 30 ℃. Freezing from 30 to −20 ℃ and thawing from −20 to 30 ℃ were achieved in 2 h. Specimens were tested after 30, 60, and 90 cycles. It was found that five cycles of accelerated conditioning (according to ASTM C666) are equivalent to one year of exposure in the field (climate data from a cold region in China were used as a reference). The environmental coefficient decreased with the increasing number of equivalent freeze-thaw cycles; it took 60 cycles for CFRP and 256 cycles for GFRP to reach the 0.85 and 0.5 environmental reduction factor, respectively (Figure 41). Based on temperature data and the number of freeze-thaw cycles, the service lives of CFRP and GFRP were predicted to be 12 and 51 years, respectively.

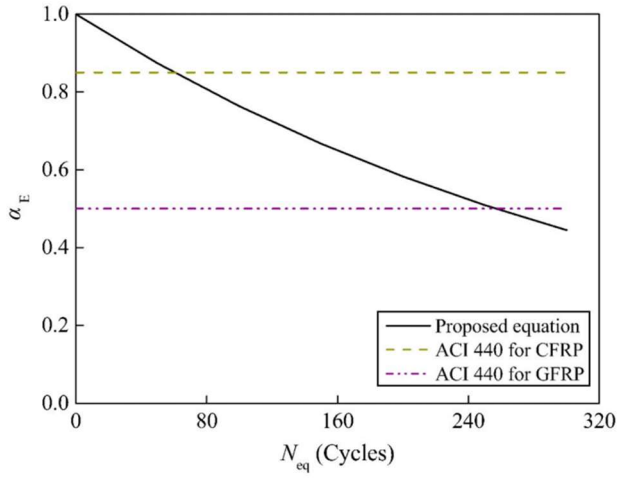

Source: Pan et al., 2018

Figure 41. Comparison of the proposed and ACI 440 recommendation's environmental coefficient.

Mohammadi et al. (2017) examined the effect of alkaline conditioning on concrete strengthened with CFRP applied via EBR and EBROG methods. Most previous studies involved the application of FRP using the EBR method, in which concrete was sandblasted and cleaned. The EBROG method was adopted to delay or eliminate debonding of FRP sheets from concrete. In this method, grooves were made into concrete surfaces and filled with epoxy. After cleaning the concrete surface, FRP sheets were applied using the wet-layup method. For this study, 24 concrete prisms (14 × 6 × 6 in.) were cast and cured for 28 days, then strengthened using the CFRP system using EBR and EBROG methods. Specimens were then subjected to four types of conditioning, controlled laboratory conditions, and immersion in alkaline media at 23, 40, and 60 °C. Specimens were then exposed for 3,000 hours before being subjected to the single-lap shear test. Results showed that specimens subjected to a 60 °C alkaline solution had a reduction in maximum bond strength of 23.3% with the EBR method and only 4.7% with the EBROG method. EBR specimens showed a sudden drop in strength and bond stiffness with increasing temperature. EBROG specimens saw no significant change in debonding load with increasing exposure temperature. The strain curves for specimens strengthened with the EBR method showed two stages, an initial exponential trend followed by a second, more irregular behavior with loads greater than 77% of the maximum load. Specimens strengthened using the EBROG method showed one exponential trend of strain, relating to a more typical strain profile. Specimens prepared with the EBR method had stress shifts toward the middle of the bond before debonding, while in the EBROG method stresses shifted over a limited length before FRP rupture (Figure 42). The results of this study indicate that the EBROG method is a more effective method for FRP installation for specimens exposed to harsh environments.

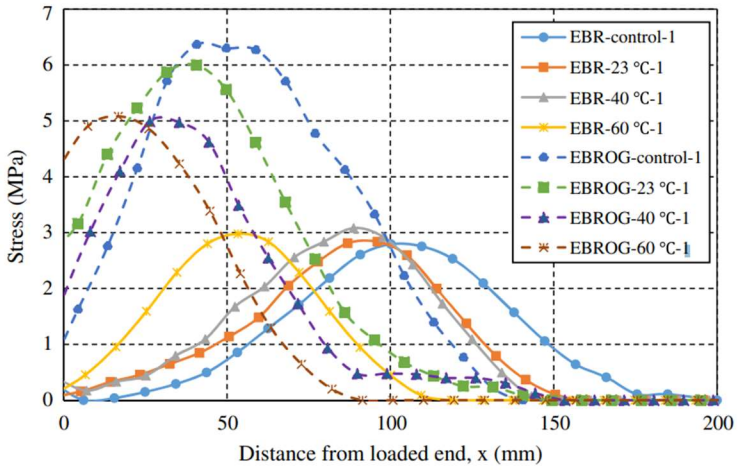

Source: Mohammadi et al., 2017

Figure 42. Comparison of stress measurements along the CFRP-concrete bond increasing temperature in the EBR and EBROG methods.

Shrestha et al. (2016) evaluated the effects of moisture exposure on the bond between CFRP and concrete using a single-lap shear test and pull-off bond tests with the objective of predicting the durability of the FRP. The testing program involved six different, commercially available composite systems immersed in water under 20 °C for up to 18 months in the laboratory. In addition to bond tests, water absorption of epoxy was monitored during the exposure, and material testing was conducted to evaluate concrete compressive strength and epoxy tensile strength. Results show that moisture absorption rate and absorption capacity varied significantly between different types of epoxies, from 0.71% to 2.65% by weight. Furthermore, it was concluded that water absorption cannot be an indicator of epoxy tensile strength prediction. For example, epoxy with 0.72% absorption had 32% reduced tensile strength, whereas epoxy with more than 2% moisture content showed a reduction in tensile strength between 11% and 22%. Shear bond strength

was significantly reduced in the first 3 months for the two epoxy systems, but for the other four, it either decreased slightly or increased. The reduction of pull-off bond strength varied from 19% to 41%. An interesting observation was that the pull-off failure mode was unaffected by the length of exposure and was governed by failure in concrete.

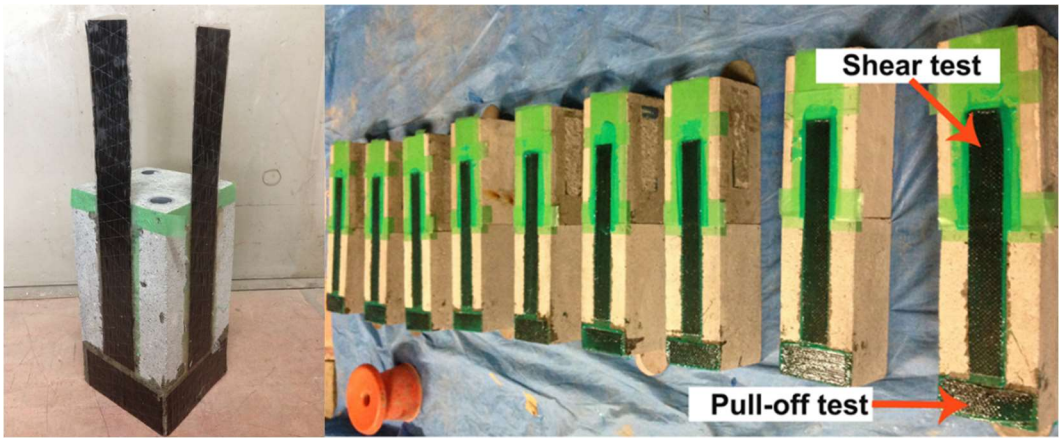

(a) (b)

Source: Shrestha et al. (2016)

Figure 43. (a) Sample specimen for FRP system and (b) preparation of the bond specimen.

Another study was conducted by Shrestha et al. (2014) to understand how moisture affects the bond strength between CFRP and concrete. Concrete specimens of normal and high strength were cast and strengthened with a carbon fiber sheet and epoxy resin. Two separate epoxy primers and saturants were used and were referred to as Epoxy-E, Epoxy-F, and Epoxy-R. While the properties of the resin were not provided, Epoxy E is described as bisphenol-A and bisphenol-F base and the hardener as polythiol and polyamines. Epoxy-F and Epoxy-R are described as bisphenol-A-type bases and a hardener of polyamines. Epoxy-F was used as a primer and Epoxy-R was used as a saturant. After allowing specimens to cure for one month, they were subjected to various weathering conditions. Specimens were immersed in tap water at 20 °C and wet-dry cycles at 20 °C for various exposure times, followed by single-lap shear tests. Specimens cast with normal-strength concrete and subjected to constant immersion experienced a 5–12% reduction in bond strength for Type-E and Type-F saw a 1–12% reduction throughout the various exposure times (Figure 44a). Wet-dry cycles on normal-strength concrete showed similar results, with a 7–12% reduction for Type-E and a 1–3% reduction for Type-F (Figure 44b). While the normal-strength specimens did not show significant change under weathering, high-strength specimens saw significant loss under immersion. High-strength specimens subjected to constant immersion saw a 32 and 30% reduction in bond strength for Type E and F, respectively (Figure 44c). The greater reduction for high-strength concrete could be attributed to fewer pores in high-strength concrete, which did not allow as strong of a bond to form between FRP and concrete. For normal-strength concrete, the failure mode shifted from within the concrete substrate to the primer-concrete interface after immersion. For high-strength concrete, the failure mode shifted from mixed failure at the primer-concrete interface to complete adhesive failure after immersion.

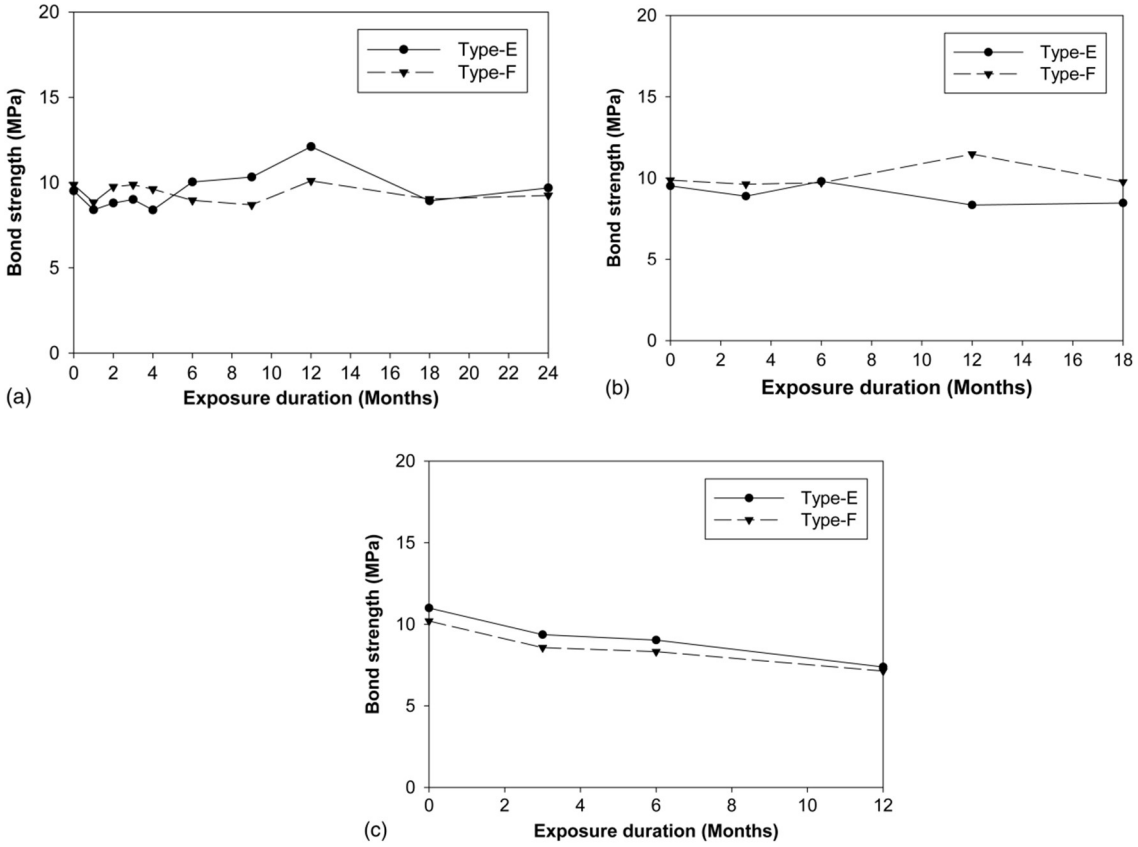

Source: Shrestha et al., 2014

Figure 44. Effect of different exposures on bond strength: (a) continuous immersion and normal strength, (b) wet-dry cycles and normal strength, and (c) continuous immersion and high strength.

Cromwell et al. (2011) assessed the effect of a series of environmental conditions on the bond strength between CFRP and concrete. A total of 64 CFRP plate and CFRP fabric tensile test specimens were prepared per ASTM D3039 and then subjected to various exposure conditions like 100% humidity and 38 °C, immersion in 22 °C salt water, immersion in 22 °C calcium carbonate for 1,000, 3,000, and 10,000 hours, dry heat at 60 °C for 1,000 and 3,000 hours, diesel fuel immersion for 4 hours, UV exposure for 2,000 hours, and freeze-heat and freeze-thaw cycles. Similarly, a total of four concrete beams (96 × 8 × 6 in.) were cast and bonded using CFRP plate and CFRP fabric, which underwent freeze-thaw cycles and UV conditioning before three-point bending testing. Specimens were bonded with 5 × 3/4 in. FRP strips using the wet-layup method and CFRP plates. The flexural strength of CFRP plate-strengthened beams that underwent 360 freeze-thaw cycles and 420 hours of UV conditioning was reduced by 6% compared to the control beams. However, the tensile strength of CFRP plates increased in the range of 2% to 13% (Figure 45), and the tensile strength of CFRP fabrics increased by up to 21% after various environmental exposures compared to control specimens.

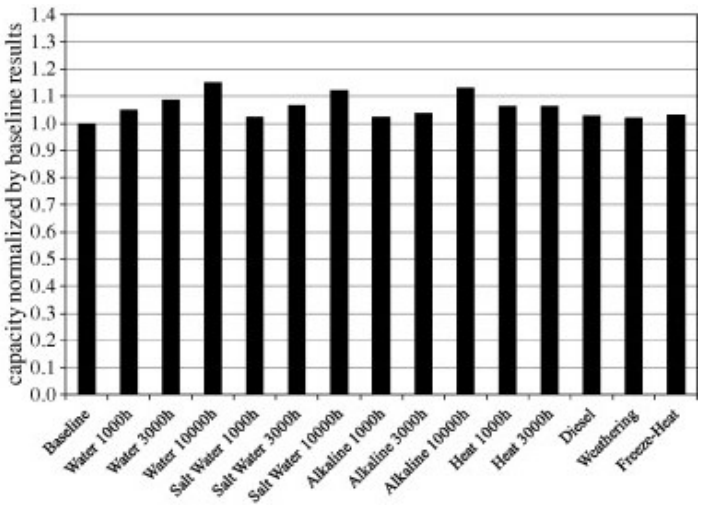

Source: Cromwell et al., 2011

Figure 45. CFRP plates tension test results normalized by baseline control data.

The influence of water immersion on bond strength, maximum slip, and effective bond length was studied using single-lap shear tests by Pan et al. (2015). CFRP plates were attached to prismatic concrete specimens, immersed in distilled water at 20 ℃ and 50 ℃, and tested after 2, 4, and 6 weeks. The effect of adhesive thickness on moisture uptake was also considered by testing specimens prepared with 0.2 mm and 1-mm-thick layers of adhesive at different temperatures (Figure 46). The moisture content was higher in 0.2-mm-thick adhesive. After two weeks of immersion in water, ultimate load decreased by 21.6% and 32.9% at 20 ℃ and 50 ℃, respectively. Based on test results, it seems that ultimate load strength is affected by adhesive thickness. However, the effective bond length of specimens with 1-mm-thick adhesive decreased with immersion time, whereas in specimens with 0.2 mm it was unchanged with an increase of immersion time.

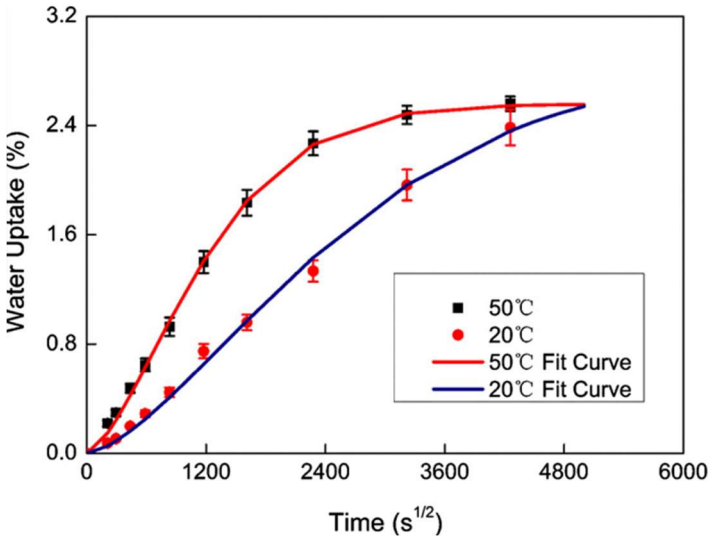

Source: Pan et al., 2015

Figure 46. Water uptake curves of the adhesive samples immersed in water at 20 ℃ and 50 ℃.

Two 12 × 6 × 4 in. concrete blocks were connected using two hot-rolled ribbed bars (HRBs) with a 0.4-in. gap between the blocks (Figure 47) and were subjected to tidal-like conditions to evaluate the bond strength between FRP and concrete in research conducted by Wang et al. (2020). CFRP sheets were applied to the bottom of the specimens. Specimens were subjected to wet-dry cycles designed to simulate tidal conditions. Specimens were placed in an environmental chamber in which 20 °C saltwater was pumped in during the wet stage. During the dry stage, the water was pumped out of the chamber and a fan and heating wire dried the specimens at 40 °C. Each cycle consisted of 10 hours of wetting and 14 hours of drying, specimens underwent 90, 180, 270, and 360 cycles. After conditioning, specimens underwent the four-point bending test. The results showed a decrease in the debonding load for specimens with increasing exposure cycles, with a total reduction of 29.3%. Plots of strain distribution indicate that increasing exposure cycles created a shift in peak strain from the middle to the end of the specimen, indicating degradation in bond behavior. Bond shear stress decreased by 15.5% and stiffness decreased by 25.9% in the ascending stage and 18.4% in the descending stage. Most specimens failed within the concrete substrate, with varying thicknesses of concrete attached to FRP. Increasing exposure cycles decreased the amount of concrete remaining on the FRP interface.

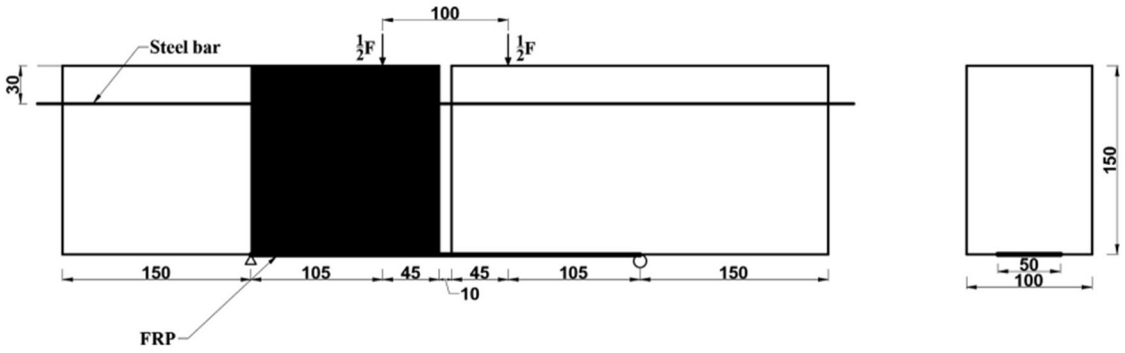

Source: Wang et al., 2020

Figure 47. Geometric dimensions of the specimens (units: mm).

Grace et al. (2005) studied the bond behavior between CFRP and concrete under a variety of different environmental conditions and repeated loading cycles. Pre-cured laminate plates, installed by the supplier, and CFRP fabric sheets were applied to 108 × 10 × 6 in. concrete beams (Figure 48). The plates were applied using a structural epoxy, and two plies of the carbon fiber fabric were applied using the wet-layup method. After the concrete beams were strengthened, they were subjected to different environmental conditions and loading cycles. Stainless steel tanks were used to expose specimens to 100% humidity at 38±2 °C, alkaline at 23±2 °C, and saltwater at 23±2 °C for 1,000, 3,000, and 10,000 hours. A dry-heat chamber was used to expose specimens to 60 °C for 1,000, 3,000, and 10,000 hours. Specimens were also exposed to 350 and 700 freeze-thaw cycles consisting of 4 hours of 4 °C and –17.8 °C and 35 thermal expansion cycles consisting of 5 hours of 48.9±1.5 °C and 26.7±1.5 °C. After conditioning, beams were loaded in two stages. Beams were first loaded to 12 kips and then unloaded to zero; after this, beams were loaded to failure using the four-point bending test. Plate beams that were subjected to 10,000 hours of 100% humidity demonstrated the largest change in load response, with a 33% reduction. All beams, both strengthened with plates and fabrics, failed at the concrete-adhesive interface. The results showed CFRP plates and fabrics increased beam strength by 59% and 55%, respectively, compared to beams that were unstrengthened. Dry heat, as opposed to 100% humidity, did not have a significant effect on CFRP plate beams but increased failure loads of CFRP fabric beams. Both saltwater and alkaline immersion improved the load-carrying capacity of CFRP plate beams for short-term exposure and decreased load-carrying

capacity for CFRP fabric beams. Thermal expansion cycles reduced failure loads of CFRP plate beams by 15% and had minimal effect on CFRP fabric beams. After 750 freeze-thaw cycles, beams saw a 9.5 and 13% reduction for plates and fabrics, respectively.

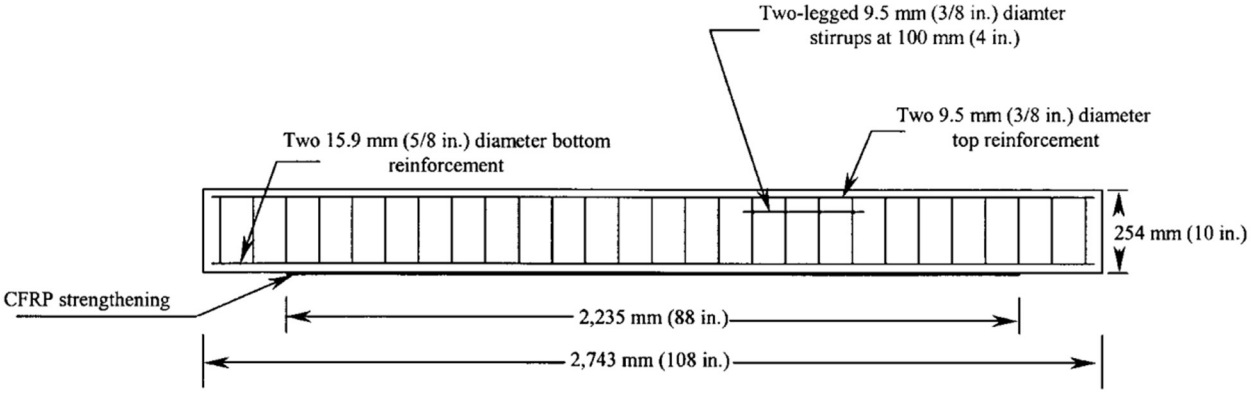

Source: Grace et al., 2005

Figure 48. Longitudinal detail of test beam strengthened with CFRP.

Lai et al. (2012) assessed the effect of elevated immersion temperatures on the bond strength between CFRP and concrete. For this study, a total of 36 concrete beams (14 × 6 × 6 in.) were cast and strengthened with CFRP strips applied using the wet-layup method. After strengthening, beams were immersed in 25 °C, 40 °C, and 60 °C water for 5, 15, and 30 weeks. After exposure, beams were left to dry before undergoing the single-lap shear test. The paper describes the ruptured ratio, which compares the area of rupture to the total area of the specimen. Specimens immersed at 25 °C showed similar rupture ratios to the control specimens; specimens immersed at 40 °C and 60 °C showed an increase. The results showed little variation between the various exposure times, meaning the water temperature played a larger role in bond degradation than the exposure time. From this, it can be concluded that most of the bond deterioration occurred within the first few weeks of exposure.

Pull-off tests and four-point bending tests (Figure 49) were performed by Sopal (2008) on six reinforced concrete deck girders to assess the environmental durability of girders strengthened with surface-bonded CFRP. Each girder was either a T-beam or an inverted T-beam with an overall length of 22 ft. The width of the flange and depth of the web were equal to 3.5 ft and 3 ft, respectively, and the flange and the web thickness of the deck were equal to 14 in. and 6 in., respectively. The wet-layup method was used to install the CFRP to the deck girder using a combination of various CFRP systems like MBrace, Sika, Fyfe, and Edge CFRP system. Out of 6 girders, two of them were control specimens, two of them were exposed to hygrothermal conditions for 34 weeks at 15 °C, and the remaining two were exposed to 300 freeze-thaw cycles. Each freeze-thaw cycle was equal to 3 hours in total with temperatures varying from -16 °C to 16 °C. The two specimens did not exhibit strength reductions due to the hygrothermal exposure per the results from the pull-off tests; the strength was in fact found to improve by 25% and 6% as compared to the control specimen. However, the results of the four-point bending tests were contrasting where after 34 weeks of hygrothermal exposure, the strength was reduced by 6% and 11% on two specimens. The remaining two specimens did not exhibit significant strength reductions on exposure to freeze-thaw cycles; the average reduction in strength was approximately 2.5% for pull-off tests, and the average increment in strength was 6% for four-point bending tests.

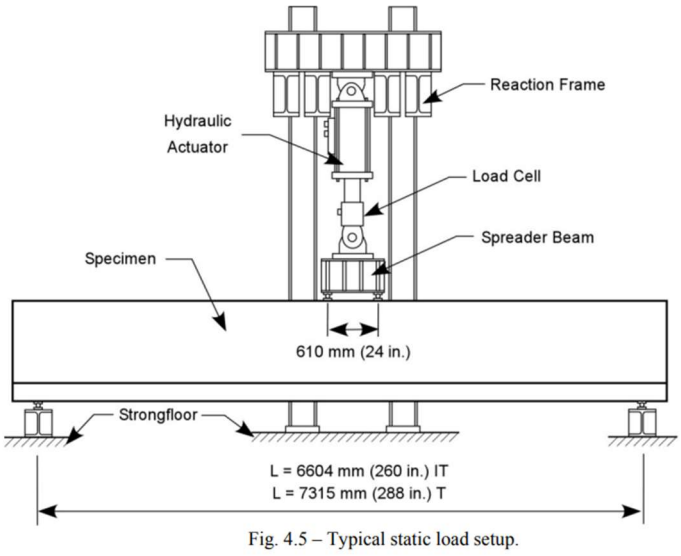

Source: Sopal, 2008, and Mitchell, 2008

Figure 49. Typical static load setup for four-point bending test of concrete deck.

Pull-off tests and four-point bending tests (Figure 49) were performed by Mitchell (2008) on six reinforced concrete deck girders to assess the environmental durability of girders strengthened with surface-bonded CFRP. The specimen consisted of a T-beam or inverted T-beam with an overall length of 22 ft designed to fail in shear. The width of the flange and depth of the web were equal to 3.5 ft and 3 ft, respectively, and the flange and the web thickness of the deck were equal to 14 in. and 6 in., respectively. The wet-layup method was used to install the CFRP to the deck girder using a combination of various CFRP systems like MBrace, Sika, Fyfe, and Edge CFRP system. Out of six girders, two of them were control specimens, two of them were exposed to the 550 freeze-thaw cycles, and the remaining two were exposed to the 300 freeze-thaw cycles. Each freeze-thaw cycle was equal to 3 hours in total with temperatures varying from -16 ℃ to 16 ℃. All the specimens exhibited strength reductions due to the freeze-thaw cycle. Per the results from the four-point bending tests, the strength was found reduced by 2% on the inverted T-beams subjected to 550 cycles and about 14.5% on the T-beams subjected to 300 cycles as compared to the control specimen. According to the pull-off test results, two T-beam specimens also exhibited strength reductions on exposure to 300 freeze-thaw cycles, where the strength was reduced by 20% and 14% as compared to the control specimen. However, the results of the pull-off tests were contrasting on the remaining two inverted T-beam specimens where, after 550 freeze-thaw cycles, the strength was increased by 9% and 12%.

Pack (2003) used CFRP plates and CFRP fabrics to strengthen concrete specimens that were exposed to 100% humidity, alkalinity, salt water, dry heat, freeze-thaw cycling, vehicle fuel, and UV radiations for various durations to simulate various environmental factors. Tensile tests of CFRP coupons, single-lap shear strength tests, and three-point bending tests were conducted to assess the environmental durability of CFRP. The CFRP plate tensile test specimens experienced an increase in tensile strength after 10,000 hours of immersion in water, salt water, and alkaline water by 13% (Figure 50). The CFRP plate bond specimens that were exposed to 1,000 hr in saltwater and dry heat, 3,000 hr in alkaline, and 20 cycles of freeze/thaw failed primarily due to bond failure. Similarly, the primary mode of failure of the unweathered and conditioned flexural specimen was interfacial debonding. For CFRP fabrics, the ultimate load increased by 20% after 1,000 hours of exposure to 100% humidity, alkaline medium, salt water, dry heat, 20 cycles of freeze/thaw, and 2,000 hours of UV exposure. Approximately 83% of the specimens exposed to salt water failed in the interfacial concrete layer and the remaining 17% experienced bond failure. Specimens exposed

to freeze/thaw cycles, 100% humidity for 1,000 and 3,000 hours, and dry heat for 1,000 and 3,000 hours experienced bond failure.

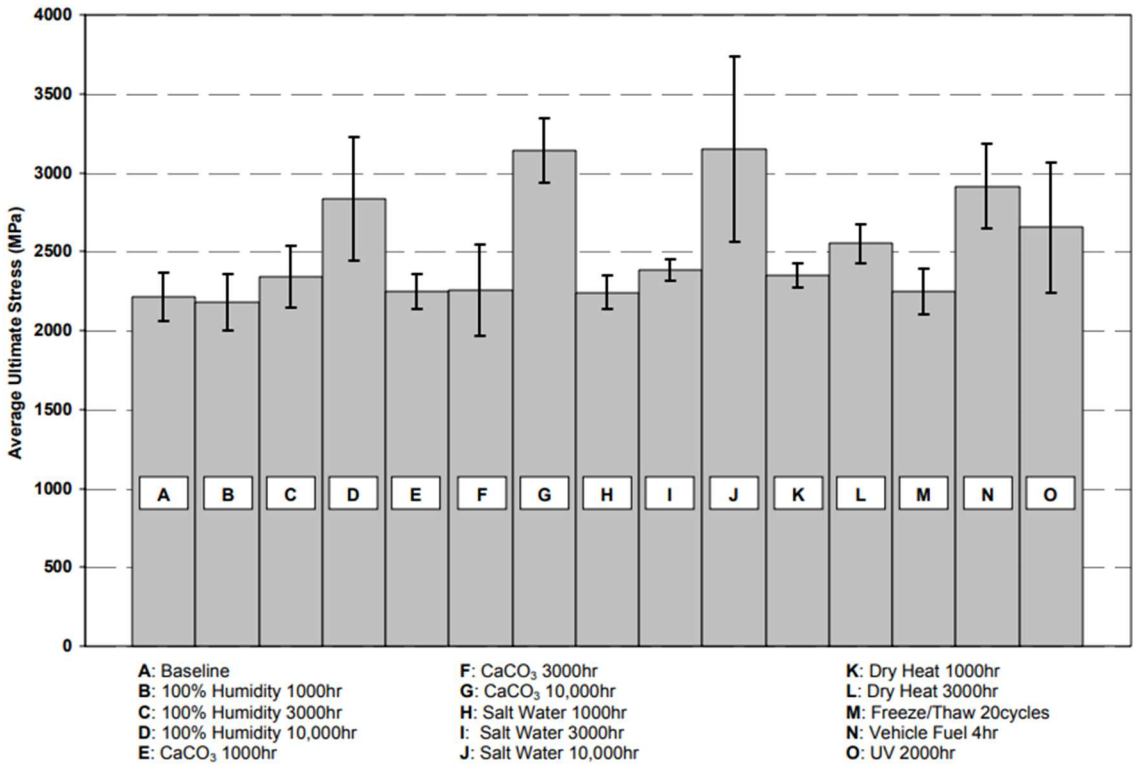

Source: Pack, 2003

Figure 50. Average CFRP plate ultimate tensile stress.

Single-lap shear tests were performed by Yun and Wu (2011) on CFRP bonded to 4.35 ksi or 6.5 ksi concrete specimens to assess the durability of CFRP–concrete joints under the freeze-thaw cycle. Twenty-six total specimens were tested in total, out of which four were unweathered and the remainder were exposed to the freeze-thaw cycle in fresh water and saltwater medium (Figure 51), distributed equally. The length of the cycle was 4 hours in total and the temperature range was from 4 ℃ to -18 ℃. Two layers of Carbon fabric were bonded to concrete specimens using Sikadur-300 epoxy using the wet-layup method. When 4.35 ksi concrete specimens were subjected to 17, 33, and 50 freeze-thaw cycles in saltwater, the strength was reduced by 5%, 22%, and 31% compared to the unweathered specimens. Similarly, when 4.25 ksi concrete specimens were subjected to 17, 33, and 50 freeze-thaw cycles in freshwater, the strength was reduced by 9%, 22%, and 31%. A major reduction in strength was seen after 67 cycles, which was approximately 45% for 4.25 ksi concrete specimens exposed to fresh water and 87% for 6.5 ksi concrete specimens exposed to saltwater.

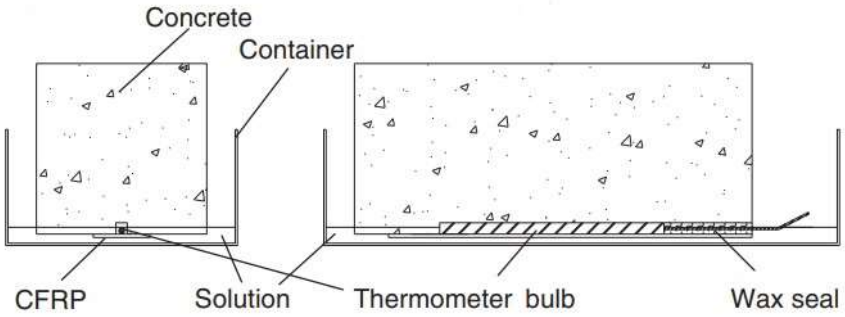

Source: Yun and Wu, 2011

Figure 51. Freeze-thaw test setup.

EXISTING STUDIES AT THE UNIVERSITY OF DELAWARE

Experimental tests were conducted by West (2001) to investigate the potential for and the elimination of galvanic corrosion on a steel substrate when attached to a CFRP composite. A three-ounce fiberglass scrim was bonded to the surface of the composite samples using vinyl ester resin and the SCRIMP manufacturing process. The addition of scrim was found effective in eliminating the current flow, thus making CFRP composite less prone to galvanic reaction. A set of three samples were tested to investigate the performance of the rehabilitation at the edges of the CFRP composite attached to the steel. The penetration of moisture to the interface was observed along some of the edges of the samples, causing discoloration and some minor surface corrosion. The application of a heavy fillet of adhesive at all edges was recommended to effectively isolate the interface and eliminate moisture penetration.

The bond strength of Ciba AV8113 to steel substrate was assessed by Mertz and Gillespie (1996). After 8 months of water exposure at the temperature of 65 °C, followed by 720 hours of fatigue cycles, the lap-shear strength was found to be 1,800 psi (corresponding to 67% shear strength). Mertz and Gillespie observed that the greatest concern with the bonded CFRP composite is the failure of the adhesive bond at the termination of the composite patch due to the concentration of shear and peeling stresses. Such failure mode can be controlled by tapering the composite over the length at the termination of the composite. Similar studies to determine the bond strength of MA555 adhesive subject to laboratory-accelerated conditioning were not available; however, Miller (2000) established that MA555 performed better than Ciba AV8113. Miller tested 36 steel specimens doubly reinforced with CFRP composite to analyze the force transfer length using both Ciba AV8113 and Plexus MA555 structural adhesives. When tested to yield the steel bar, debonding was only observed on one Ciba specimen, while no debonding was observed on Plexus specimens, even though the Plexus adhesive had lower shear strength. The potential reason behind no debonding on Plexus specimens was the larger elongation to failure (140–160%) compared to 25% for Ciba adhesive.

Laboratory tests were conducted by Finch (1997) to assess the bonding of composite materials to concrete, and details of a full-scale implementation on a prestressed concrete box-beam girders bridge were presented. A series of single-lap shear tests were conducted to assess the force transfer from the CFRP composite into the concrete and to evaluate the effect of surface preparation, type of adhesive, and concrete strength on average bond strength. A total of fifteen adhesively bonded, double-lap shear specimens were made from 30 concrete blocks by sandwiching two CFRP composite between two concrete blocks; each of the blocks was sized 6 × 6 × 9 in. The average bond strength of the CFRP composite to concrete was found

to be 798 psi using static tests. A total of 13 test specimens were subject to fatigue stresses as well. Upon testing, the fatigue resistance of the bond was found to be dependent on the stress range and the maximum level of stress. Approximately 80% of the specimens subjected to cyclic loads at a 25% stress range reached 2 million cycles without failing. All of the specimens that did not fail were followed by static tests and were proven undamaged. All of the specimens subjected to higher stress ranges (45% and 70%) failed before 2 million cycles. Upon evaluation of the bond strength of the CFRP composite, full-scale field implementation was performed. It was concluded that the use of the CFRP composite in such a type of rehabilitation can be performed for approximately 10% of the cost of the bridge replacement.

CHAPTER 3

Bridge BR 1-704

METHODOLOGY

This study involved visual inspection, field evaluation, and experimental investigations of FRP composite samples extracted from two subject bridges: (1) Foulk Road bridge, and (2) Bridge 1-704 over Christiana River, both located in the State of Delaware, which is then followed by the baseline analysis of data collected from previous research studies related to the long-term performance of FRP composite in concrete structures subjected to laboratory-accelerated conditioning. Bridges considered for assessment were chosen from the Delaware Department of Transportation (DelDOT) bridge inventory.

Description of the Bridge

Bridge 1-704 carries southbound Interstate I-95 traffic over the Christina River near the intersection to State Route 896 in Delaware, just outside of Newark, Delaware (Figure 52). The bridge is simply supported with steel girders and a concrete deck. The overall length of the bridge is 114 ft, comprising three simple spans with a skew angle of 13º (Figure 55). The spacing of the girders varies along the cross-section of the bridge, as shown in Figure 54. The main span is 63 ft long with composite concrete decks and the two approach spans are 24 ft long and designed non-compositely.

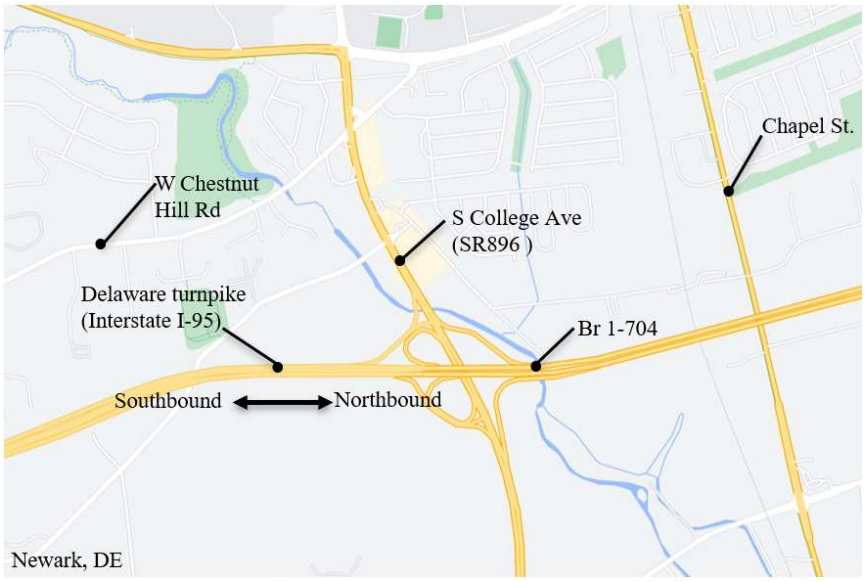

Source: Google (2022)

Figure 52. Location of Bridge 1-704.

The bridge was selected for strengthening using CFRP composite because it had reasonably high ADTT—5,920, as estimated by DelDOT—and the lack of traffic under the bridge provided a relatively safe work environment (Miller, 2000). Bridge girder G5 was chosen to demonstrate the strengthening technique by Miller (2000) because it was found subjected to the largest live-load stress range among girders G1 through G12. The purpose of strengthening was not to strengthen the girder; it was solely intended to demonstrate the strengthening technique, so the failure of the system wouldn't compromise the overall integrity of the structure.

Figure 53. Bridge 1-704 over I-95.

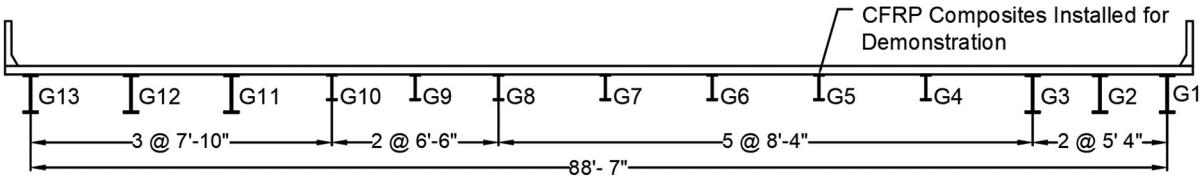

Notes:
1. The dimensions of the structural members are not to scale.
2. Cross-section view doesn't show the skew of 13°.

Source: Miller, 2000

Figure 54. Bridge 1-704 cross section A-A; see along with the framing plan (Figure 55).

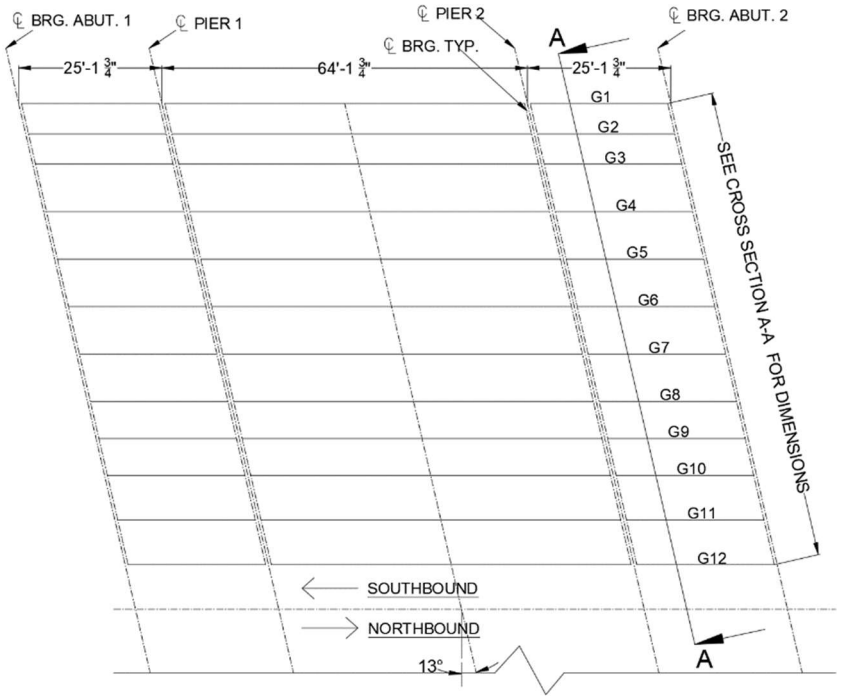

Source: Miller et al., 2001

Figure 55. Bridge 1-704 framing plan (southbound).

Girder Strengthening

The strengthening system consisted of bonding CFRP composite to the bottom face of the tension flange of the steel girder using structural adhesives. The FRP laminates consisted of T-300 unidirectional carbon fibers embedded in a vinyl-ester resin matrix produced using pultrusion process. At the beginning of 2000, CFRP laminates measuring 60 in. (length) ×1.46 in. (width) × 0.2 in. (thickness) were bonded to the soffit of the girder using either a two-part high-strength epoxy (Araldite AV8113/HV8113) or a methacrylate adhesive (Plexus MA555), as shown in Figure 56. The use of two adhesives provided the opportunity to examine the in-field application and long-term durability of both adhesives. The properties of CFRP composite and adhesives are shown in Table 1 and Table 2, respectively. The CFRP samples were collected from the bridge after 22-year-long service life to investigate CFRP degradation and bond strength.

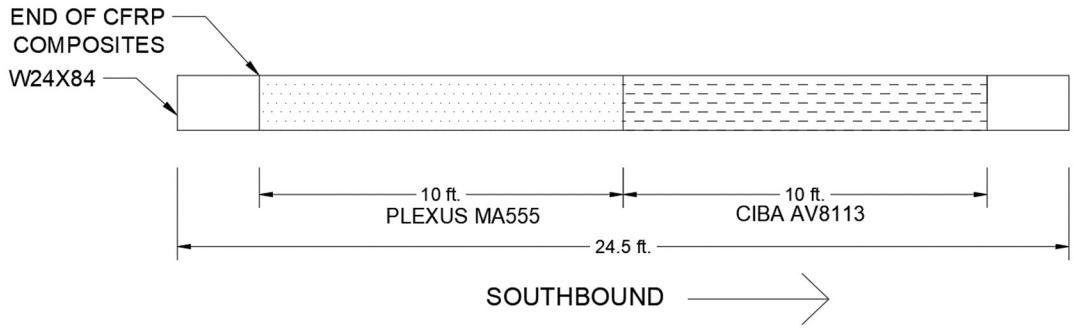

Source: Miller, 2000

Figure 56. CFRP Retrofit scheme.

Table 1. CFRP composite properties.

FRP Composite	T-300 Carbon and Vinyl Ester Resin
Fiber Orientation	Unidirectional (0º) [3]
Nominal Fiber Volume Fraction	51% [3]
E_{11}	16,300 ksi [2]
υ_{12}	0.37 [2]
$\sigma_{failure}$	135 ksi [1]
$\varepsilon_{failure}$	9,000 με [1]
Weight	0.057 lb/in^3 [3]

Source: Miller (2000), Ammar (1996)

Notes: 1. Data obtained by Ammar (1996) from a three-point bending test.

2. Data obtained by Ammar (1996) from simple tensile tests.

3. Information provided by the manufacturer (DFI Pultruded Composite, Inc., Kentucky).

Table 2. Structural adhesive properties.

Criteria	Ciba-Geigy AV8113	Plexus MA555
Shear Strength ASTM D-1002	2,660 psi [a]	1,250–1,495 psi [d]
Tensile strength ASTM D-638	2,280 psi [a]	Information not available
Tensile Modulus	15.6 ksi [a]	Information not available
Tensile Elongation	25% [a]	Information not available
Glass Transition Temp. (T_g)	90 °C [a]	103 °C [a]
Glass Transition Temp. (T_g)	88 °C [b]	103 °C [a]
Shear Modulus	43 ksi [b]	Information not available
Manufacturer	Ciba-Geigy Corp, Madison Heights, MI [d]	ITW, Danvers, MA [d]

Source: West (2001)[a] , Rajagopalan (1996)[b], Ammar (1996)[c], and Miller (2001) [d]

The surface of the girder was sandblasted to remove all primer, paint, and corrosion on the underside of the tension flange on the same day as strengthening. The steel surface was pretreated using Plexus PC120 primer (ITW, Danvers, MA) on the northern half of the span where Plexus MA555 was used. Plexus PC120 primer is a coupling agent to be used in conjunction with Plexus MA555 adhesive (West, 2001). Similarly, the bare surface was pretreated using Z-6040 silane (Dow Corning, Midland, MI) on the southern half of the span where Ciba AV8113 was used. Z-6040 silane is a coupling agent typically used to promote the adhesion of organic resins to inorganic surfaces (West, 2001). The structural adhesives were then applied to the CFRP laminates and steel surface in a thin layer, approximately 1/16 in. thick on both surfaces, making total thickness equal to approximately 1/8 in. A glass-fiber fabric (3 oz, 120-fiberglass scrim) was then evenly pressed into the adhesive applied to the steel surface to make sure no air pockets were present. Glass-fiber fabric was used to act as a barrier between steel substrate and CFRP composite to prevent the steel substrate from galvanic corrosion. Finally, the CFRP laminates were attached to the steel girder. Additional details regarding installation procedures can be reviewed at Miller (2000).

Existing Study at the University of Delaware

An in-service strain monitoring system consisting of a strain transducer, data acquisition system, and power supply (Figure 57) was deployed by Miller et al. (2001) to measure the live-load strain. The strain transducer was attached to the bottom flange of the girder G5 at the midpoint of the span. Before installation of the FRP composite, an in-service system was deployed for two weeks to measure the live-load strain peak events. Only the peak events larger than 75 με were recorded. The typical stress range was observed between 2 and 3 ksi for the trucks, with the overall average being 2.4 ksi. To demonstrate the fatigue durability of CFRP composite/steel bond, small-scale and large-scale fatigue tests were conducted at the laboratory. For small-scale tests, seven double-reinforcement specimens were loaded at a stress range of 12 ksi for 2.55 million cycles, where no indications of debonding were observed after the end of 2.55 million cycles. Similarly, for large-scale tests, two 20-ft-long steel bridge girders rehabilitated by bonding FRP composite to the top and bottom of the tension flange were used. Both girders were tested in three-point bending for 10 million cycles at a calculated load of 13.8 kips such that the maximum tensile stress would be 5 ksi at the tension flange. Static tests were run before and after 10 million cycles. There were no stiffness changes in the girders after 10 million fatigue cycles, indicating no debonding in the FRP composite/steel interface.

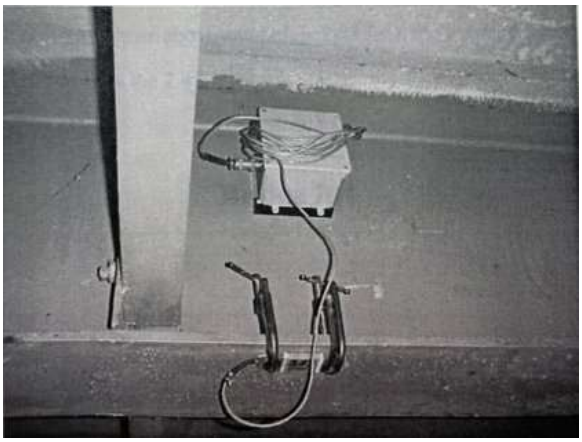

Source: Miller, 2000

Figure 57. In-service system to measure the live-load strain peaks before installation of FRP composite.

Structural Health Monitoring of Bridge Br 1-704

General Overview

Structural health monitoring of bridge 1-704 was performed for 15 days, between January 11 and January 27, 2022 (except for January 17 due to power supply interruption). The in-service monitoring system was comprised of a digital data acquisition system, three strain transducers, a 100-Ah battery, and enclosure, as shown in Figure 58. ST355 (Figure 58b) was installed on the bottom face of the girder, at the same location where Miller (2000, Figure 57) collected data. Additional strain transducers, ST356 and ST348, were also installed to complement ST355 measurements.

(a) (b)

Figure 58. Strain monitoring system: (a) data acquisition system inside enclosure, (b) strain transducers.

A Campbell Scientific, Inc. data acquisition system, consisting of CR5000 data logger and Loggernet software, was used to collect and process strain transducer data. CR5000 datalogger allows 20 differential analog input channels at the execution rate ranging from 500 microseconds to 8 milliseconds, depending on the number of channels being executed (Campbell Scientific, 2001). Two CompactFlash (CF) cards with a capacity of 2 GB storage were used for data storage. Strain transducers ST350 (Figure 58b) were manufactured by Bridge Diagnostics, Inc. ST350 transducers has the effective gage length of 3 inches and its internal circuitry consists of full Wheatstone Bridge with four fully active 350Ω foil gages with capability to measure strain ranging from +4,000 με to -4000 με (Bridge Diagnostic, 2019). Each ST350 strain gage was calibrated in the Structural Engineering Laboratory at the University of Delaware by running a multitude of three-point bending tests along with recalibration done by Bridge Diagnostic, Inc.

For the in-service monitoring of the bridge 1-704, six individual channels were used in the datalogger, associated with three strain transducers. The datalogger was powered using a 100-Ah rechargeable battery with an output of 12V. The transducers were attached to the bottom flange of the steel girder G5 using steel clamps, as shown in Figure 58b. The datalogger provided an excitation voltage of 5 volts to the transducers. It measured the voltage drop, which was then multiplied by the calibration factor provided by the manufacturer to obtain live-load strain, expressed in terms of microstrain (με). Data were recorded at the sampling rate of 100 Hz, which would allow the datalogger to record 25 data points per truck crossing, which is equal to at least one datapoint for each foot along the length of the girder. The peak strain thus recorded represents truck live load at 1-ft distance away from the strain transducer. Loggernet was used to monitor the real-time strain measurement and store the data in a tabular format; each table contained a record date and time stamp, three strain transducers' output and the battery voltage. The CompactFlash card was replaced every 48 hours for storing the data. The in-service monitoring was halted for 10 minutes every 48 hours during the CompactFlash card replacement process.

Baseline Correction of Data

Typical strain data have five strain components: (1) creep- and shrinkage-induced strain response, (2) temperature-induced deformations, (3) noise, (4) quasi-static strain response due to ambient traffic or live load, and (5) dynamic strain response due to the ambient traffic and other dynamic loads such as wind (Jayathilaka et al., 2020). For this study, the peak strain due to live load was evaluated, which is a fourth strain component. To evaluate the peak strain due to live load, the other four strain components were excluded from the strain data collected. The effect of noise and wind (third and fifth strain components) on

the live-load strain on the interior girder was negligible as compared to the effect of live load related to truck events, and thus can be neglected. Strain response due to creep, shrinkage, and temperature variation (first and second strain components) was considered constant for a 10-minute period, which was then eliminated by determining a baseline strain for each strain transducer for the 10-minute period (Wipf et al. 2007).

For the elimination of the first and second strain components, the data file was divided into multiple 10-minute subsets, and a baseline strain was determined for each subset. Nearly 132 million rows of data were processed using Python 3.10 to create approximately 13 million 10-minute subsets and baseline strain for each of them, as shown in Figure 59. The baseline strain for each 10-minute subset was determined by computing the mode of the 10-minute strain data rounded up to the nearest whole number (Lu et al. 2010). Mode represents the value most frequently repeated during the 10-minute subset. The baseline strain was then subtracted from the strain data to eliminate the effects due to creep, shrinkage, and temperature.

Baseline correction of data is demonstrated using an example event (a) shown in the 4-hour time history versus strain plot as shown in Figure 59. The baseline strain value of 939 με is the mode of 60,000 data points, collected within 10-minute intervals immediately before an example event (a) as shown in Figure 59. For the given example event (a), the baseline corrected strain is equal to 107 με, which is obtained by subtracting the baseline strain value (939 με) from the unprocessed strain collected by ST355 (1046 με). Thus, obtained baseline corrected strain is the peak strain due to live load only.

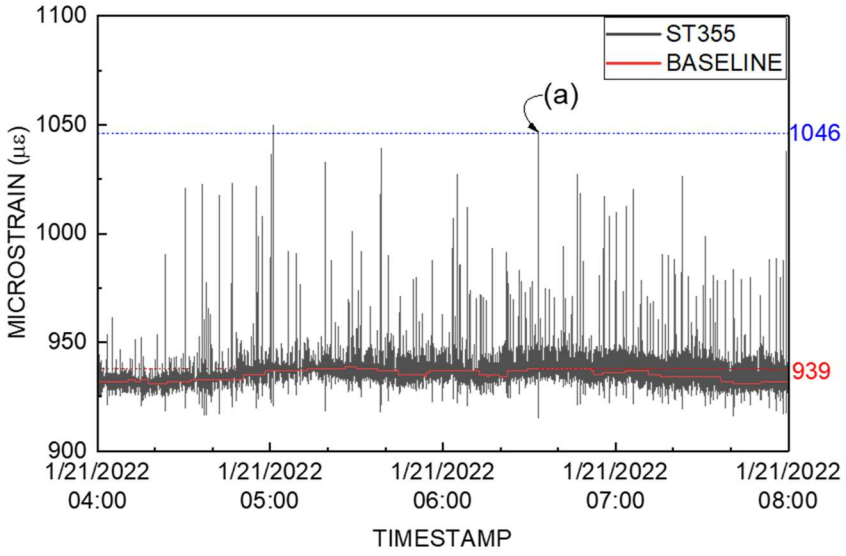

Figure 59. Girder G5 strain 4-hours' time history.

Visual Inspection and Sample Collection

The primary focus of this study was to characterize the condition of CFRP composite after a 22-year-long service life. The locations exhibiting delamination or other deterioration of CFRP composite were documented by photographic evidence. Control samples measuring 36 in. (length) ×1.46 in. (width) × 0.2 in. (thickness) and 30 in. (length) ×1.46 in. (width) × 0.2 in. (thickness) were preserved in the Structural Engineering Laboratory located at the University of Delaware since 1999.

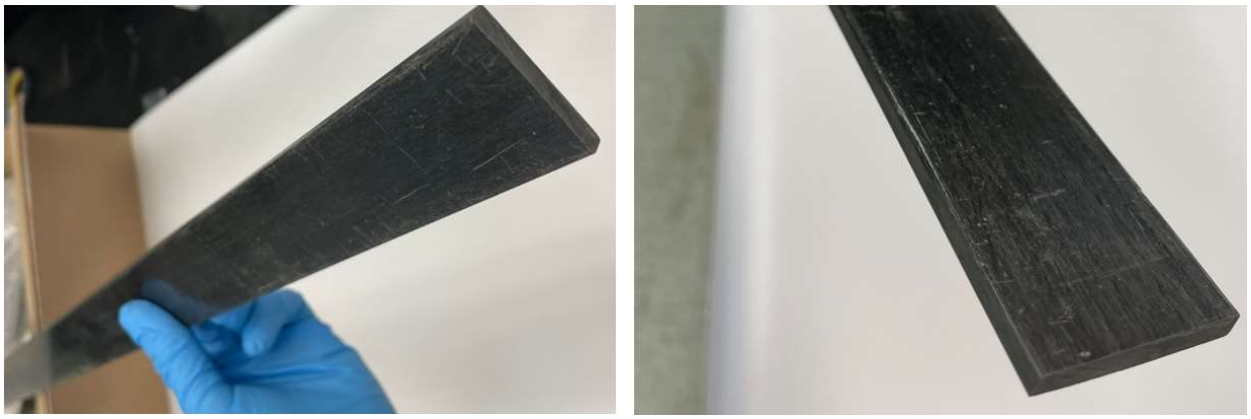

Figure 60. Control CFRP composite preserved for 22 years in the Structural Engineering Laboratory at the University of Delaware.

Girder G5 was selected for sample collection, as it was the only girder rehabilitated using CFRP composite. Prior to the collection of samples, structural health monitoring of the girder was conducted as described in Chapter 2, and the preliminary results were assessed. The sample collection work took place during the summer of 2022. Two types of samples were collected from the girder for laboratory tests: (1) 1-in.-diameter circular sample of CFRP composite, approximately 0.26-in. thick (S1 through S40), and (2) 36 in. (length) × 1.46 in. (width) CFRP composite with varying thickness along the length of the CFRP. S1 through S40 were collected by drilling a 1-1/8-in. diamond-coated core saw through the CFRP and glass fabric. A plywood rig was built at the Structural Engineering Laboratory with 1-1/8-in. holes to stabilize and guide the core saw during drilling. Similarly, for 36-in.-long samples, an oscillating multi-tool and demolition screwdriver along with hammer were used. Collected samples were stored sealed under standard laboratory conditions (22 ℃ and relative humidity of 50%). According to the Delaware Environmental Observing System (2022), the recorded weekly average of minimum and maximum daily temperature at "I-95 @ DE 896" station (about one-quarter mile from the location of the bridge) varied between -10 ℃ and 35 ℃ from 2013 to 2022. The recorded average monthly relative humidity at the same location was between 61% and 72%.

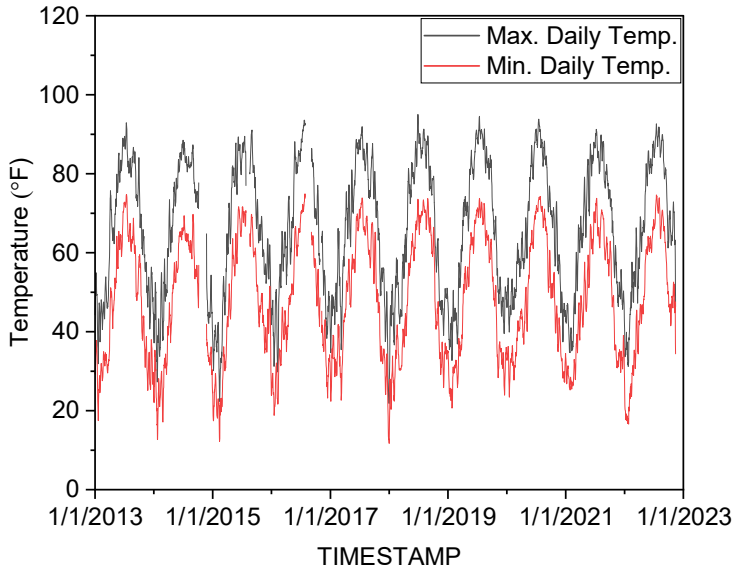

Source: Delaware Environmental Observing System, 2022

Figure 61. Weekly average of maximum and minimum daily temperature at Br 1-704 from 2013 through 2022.

The circular CFRP samples (F1 through F40) were spread out evenly along the length of the girder, not further than 2 in. from the edge of the girder, as shown in Figure 62 and Figure 65. The longer CFRP samples (36-in. long) were collected for tensile tests, three-point bending tests, and DMA tests, so it was necessary for the specimen to have at least 10 in. (length) × 1.0 in. (width) × 0.16 in. (thickness) to meet the requirements for all the tests (ASTM D3039, 2017; ASTM D7264, 2015). After multiple attempts at different locations of the girder, the samples meeting minimum requirements could only be collected from two locations, shown in Figure 62.

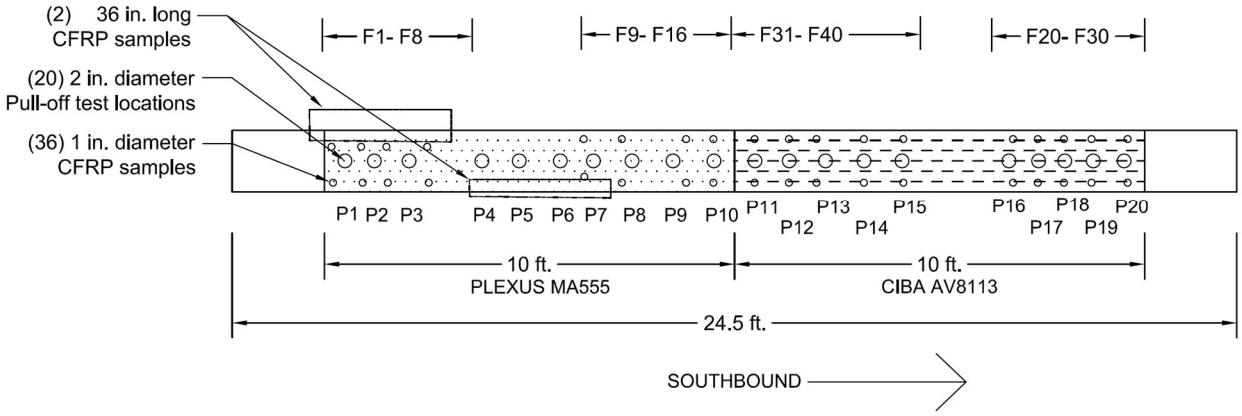

Notes: 1. Tentative location of pull-off tests, P1 through P20 (Figure 64). A minimum clear spacing of 6 in. between each test location and a minimum clear distance of 3 in. from the edge is maintained at all test locations.

2. Tentative location of 1-in.-diameter CFRP samples, F1 through F40 (Figure 63). Minimum clear spacing of 3 in. between each location is maintained at all test locations.

3. Figure not drawn to scale.

Figure 62. Bottom view of the girder G5 showing the tentative location of sample collected and pull-off tests.

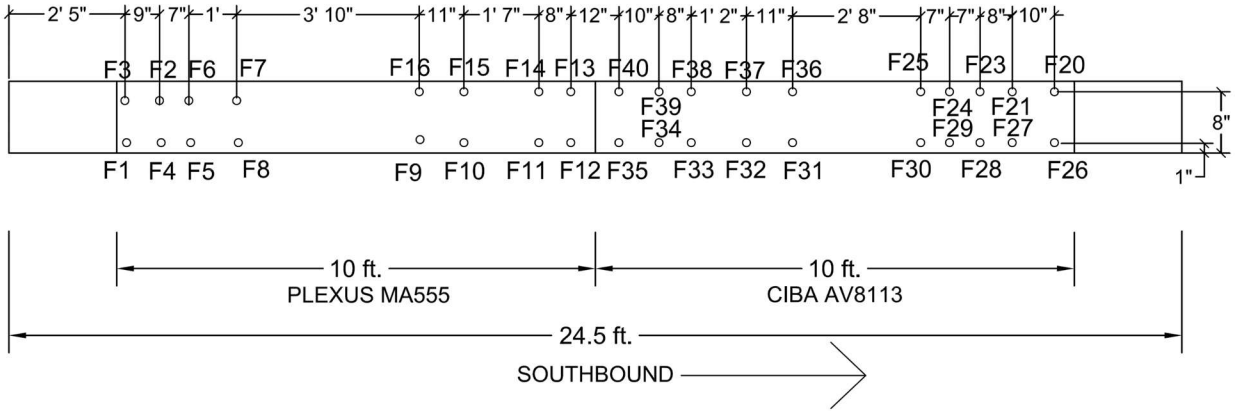

Figure 63. Location of F1 through F40 samples.

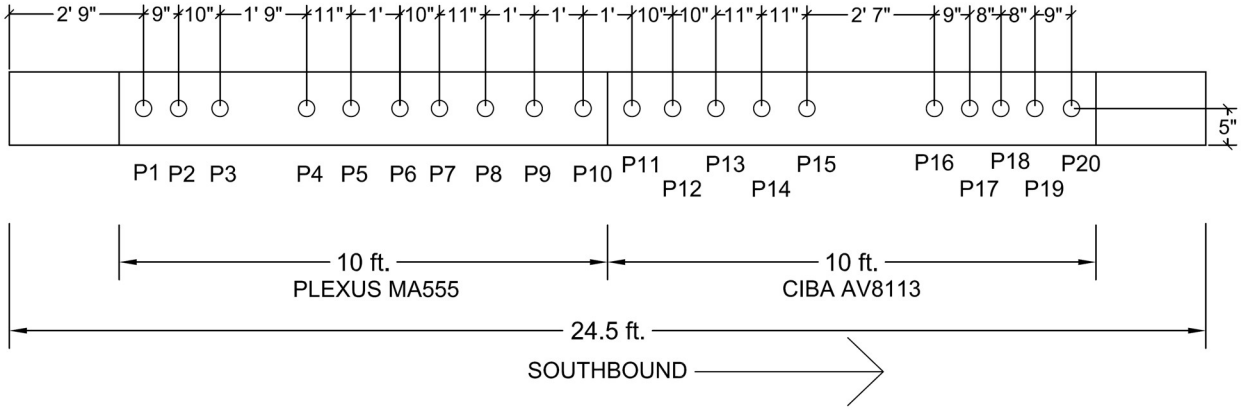

Figure 64. Location of P1 through P20 samples.

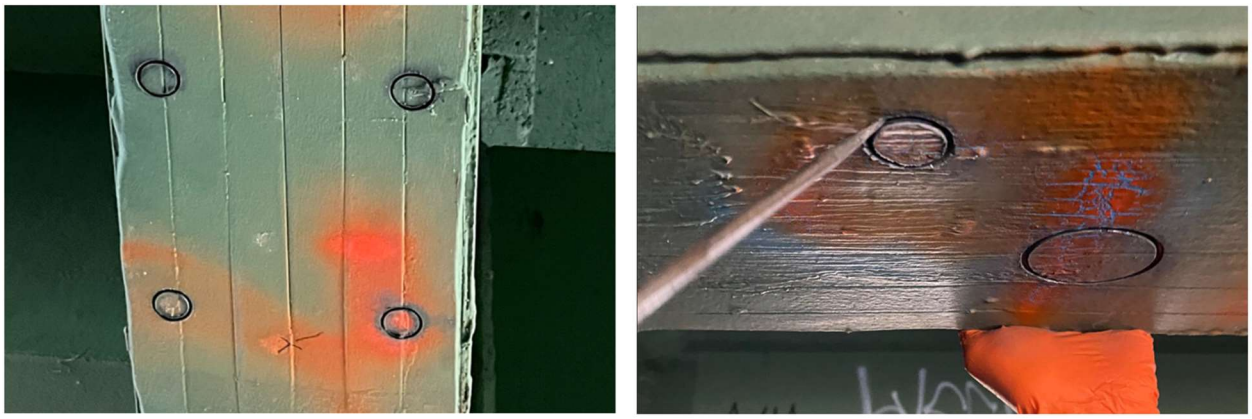

(a) (b)

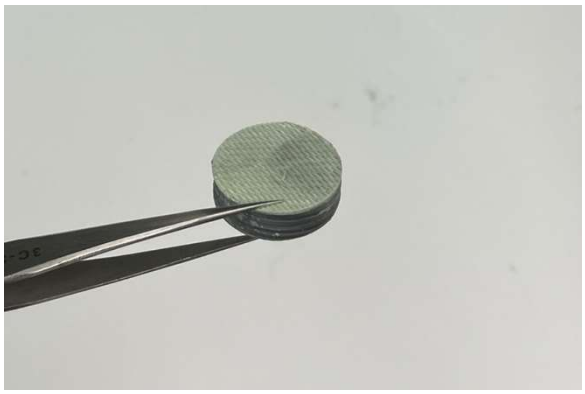

(c)

Figure 65. CFRP sample collection at Br 1-704: (a) CFRP composite drilled using a 1-1/8-in. diamond-coated core saw, (b) sample collection under progress using flat-head screwdriver, and (c) 1-in.-diameter CFRP sample.

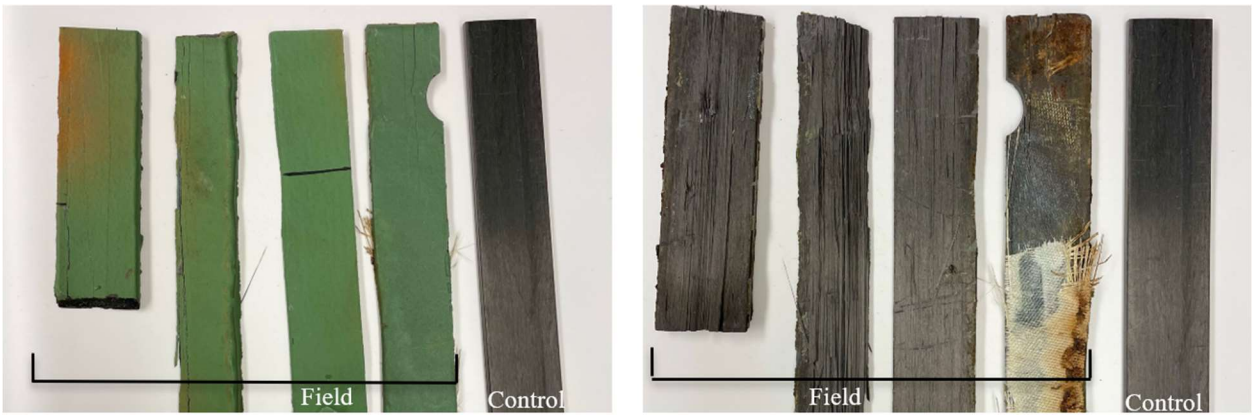

(a) (b)

Figure 66. Field samples from Br 1-704 and control sample : (a) paint side of composite samples shown, and (b) other side of the samples.

Materials Characterization Experiments

Attenuated Total Reflectance - Fourier Transform Infrared (ATR-FTIR)

FTIR spectroscopy was used for the chemical characterization of CFRP composite control samples and field samples collected from Bridge 1-704. Both control and field samples were sanded consistently using 100-grit sandpaper on all sides to make the surface even and remove paint or adhesive from the surface, and then cut into approximately 5-mm (width) × 2-mm (thickness) × 5-mm (length) dimensions, as shown in Figure 67. The samples were cleaned with acetone to remove surface contaminants and then dried prior to taking an FTIR spectrum.

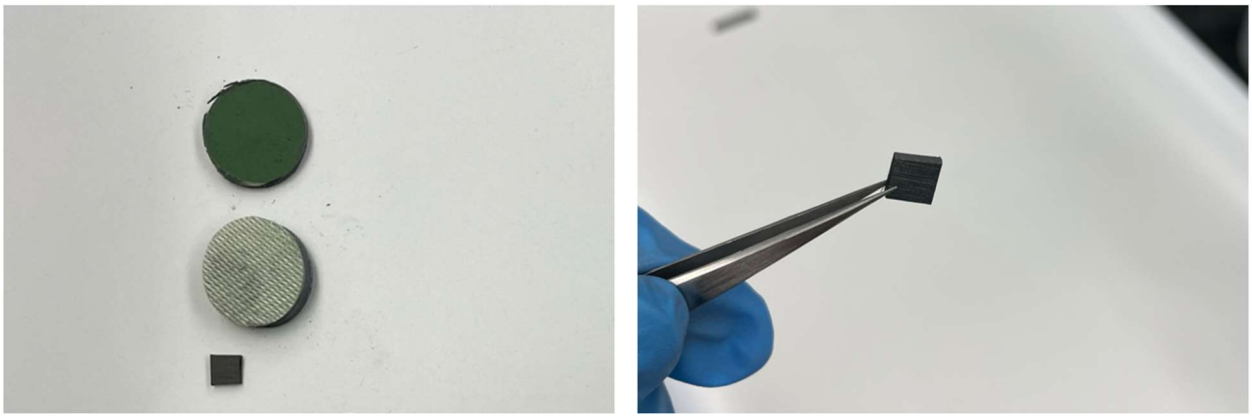

(a) (b)

Figure 67. Preparation of FTIR and Raman test specimen using the CFRP composite samples collected from the field: (a) 1 in. diameter control samples front and back view, and (b) Final look of the sample ready for spectroscopy.

FTIR experiments were carried out on a Nicolet Nexus 870 ESP spectrometer controlled by the OMNIC ESP 5.2 software in attenuated total reflection mode (ART-FTIR) using a diamond crystal. Each spectrum was the accumulation of 64 scans with a resolution of 4 cm^{-1}, from 400 to 4,000 cm^{-1}. Background spectra were collected within 60 minutes of sample spectra collection. Origin software was later used for baseline correction and analysis.

Dynamic Mechanical Analysis (DMA)

Dynamic Mechanical Analysis (DMA) was used to obtain the glass transition temperature (T_g) of unidirectional CFRP composite control samples and field samples collected from Bridge 1-704. Both control and field samples were sanded consistently using 100-grit sandpaper on all sides to make the surface even and remove paint or adhesive from the surface, and then cut into approximate dimension of 0.8 in. (length) × 0.2 in. (width) × 0.08 in. (thickness), as shown in Figure 68.

The Perkin Elmer DMA8000 dynamic mechanical analyzer (DMA) was used with a single cantilever fixture, where one clamp is fixed and the other oscillates sinusoidally. The 0.8-in.-long samples were subjected to a controlled sinusoidal displacement of 0.002 in. at the frequency of 1 Hz in a single cantilever bending fixture, resulting in peak static stress (corrected) on the sample ranging from 44 psi to 116 psi. The test samples were oriented such that the principal stress was perpendicular to the fiber direction. The dynamic analysis was performed from 0 ℃ to 250 ℃ with a heating ramp of 5 ℃/min in nitrogen

atmosphere. Storage modulus (E'), loss modulus (E''), and damping factor ($tan\,\delta$) were monitored as a function of temperature.

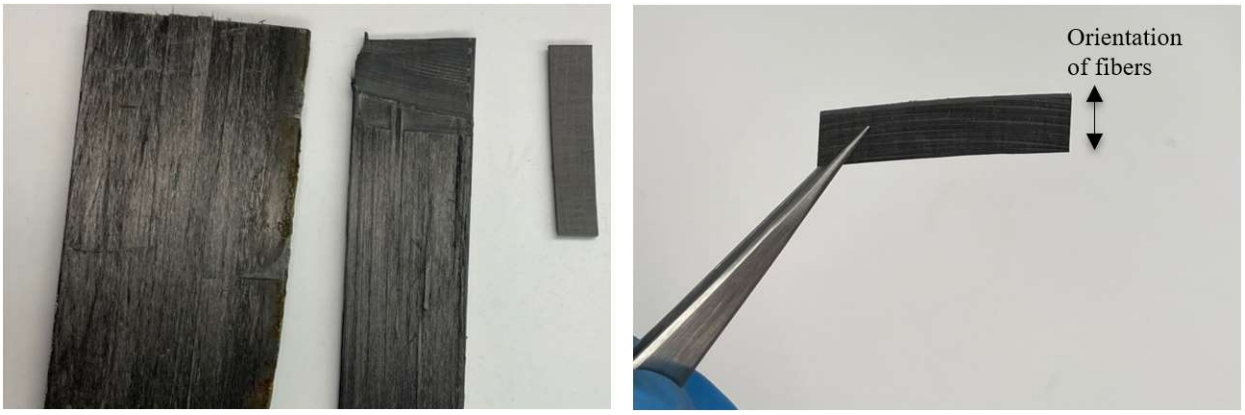

(a) (b)

Figure 68. Preparation of DMA test specimen using the CFRP composite samples collected from the field: (a) loose fibers were sanded to make the surface even, and (b) final look of the sample ready for DMA testing.

Data were analyzed in Origin. T_g of each CFRP composite sample was taken as the extrapolated onset to the sigmoidal change in the storage modulus (E') observed at which the matrix changes from a glassy to a rubbery state, as recommended by ASTM (2018). Two tangents were constructed to the storage modulus curve, one below the transition temperature and another at the inflection point. The temperature at which the tangent lines meet was reported as the T_g of the sample. Above T_g, the composite softens and loses its mechanical properties like flexural and tensile modulus, and flexural strength.

Differential Scanning Calorimetry (DSC)

DSC was used to obtain the glass transition temperature (T_g) of structural adhesives. The powdered test samples were prepared by scrapping the structural adhesive from beneath the glass fabric from the 1-in. CFRP composite samples (Figure 65c).

TA instruments DSC 2500 was used for calorimetric measurements. Three replicate samples were taken from 1-in. circular CFRP composite samples (Figure 65) that were previously extracted from the bridges using a saw with a diamond drill bit. The samples (10 mg–20 mg) were placed inside aluminum pans, sealed, and then heated between -20 °C and 240 °C at a heating rate of 10 °C/min under a nitrogen atmosphere. Aluminum crucibles were pierced to prevent pressure from building up during the experiment. Mineral oil (Krytox GPL 107 fluorinated synthetic oil, the Chemours Company FC, LLC, Wilmington, DE) was applied to the bottom of the pans to improve heat transfer between the sample and the pan. An empty sealed aluminum crucible was used as a reference inside the furnace. Results were analyzed in Origin to determine the T_g by constructing the slope of the heat flow/temperature curve before and after the transition; the T_g was then manually calculated according to the ASTM E1356-08 (2014) procedure.

Pull-Off Tests

Pull-off tests were conducted on the field to evaluate the pull-off strength of pultruded CFRP composite systems adhesively bonded to a steel substrate. The purpose of the test was to determine the greatest

perpendicular (tension) force that the CFRP composite system can bear before the plug of material is detached. The test locations, P1 through P20, were evenly spaced along the length of the girder, as shown in Figure 62. A minimum clear spacing of 6 in. between each test location and a minimum clear distance of 3 in. from the edge of the girder was maintained at all test locations.

The surface preparation involved drilling a hole through the CFRP composite system that includes 0.2-in.-thick CFRP laminate, a 1/16-in.-thick layer of adhesive, glass fabric, and another layer of 1/16-in.-thick layer of adhesive followed by removal of paint from the CFRP, and roughening and removal of dust from the CFRP and the testing puck (Figure 70 a,b). A 57-mm diamond-coated core saw was used to drill the CFRP composite system (Figure 69). A wooden template was built at the Structural Engineering Laboratory with 2-1/8 in. holes on it to hold the core saw in the predetermined location. The grinding and surface conditioning disc was used to remove the paint and roughen the CFRP surface. Testing pucks were roughened by hand using sandpaper and cleaned with acetone-rinsed paper towel to completely remove the dust remnants.

Figure 69. Diamond-coated core saw used to drill the CFRP composite system.

Two-part epoxy adhesive (Sikadur-30) was then applied to the testing pucks after mixing part A and part B in the ratio of 3:1 by volume. The pucks were then attached to the girder within 15 minutes from the end of mixing, centered at the core previously prepared. Duct tape was used to keep the pucks in place while they were cured, as shown in Figure 70(c). Tests were conducted the following week according to ASTM D7522 (2021) using a Proceq DY-216 adhesion tester. The load was applied to the puck at a constant rate of 1 MPa/min (150 psi/min) until failure. Maximum failure load, failure mode, and photographs of all the pucks after the tests were recorded. Failure modes identified based on the location of the failure interface, as shown in Figure 71, were evaluated according to ASTM D7522 (2021).

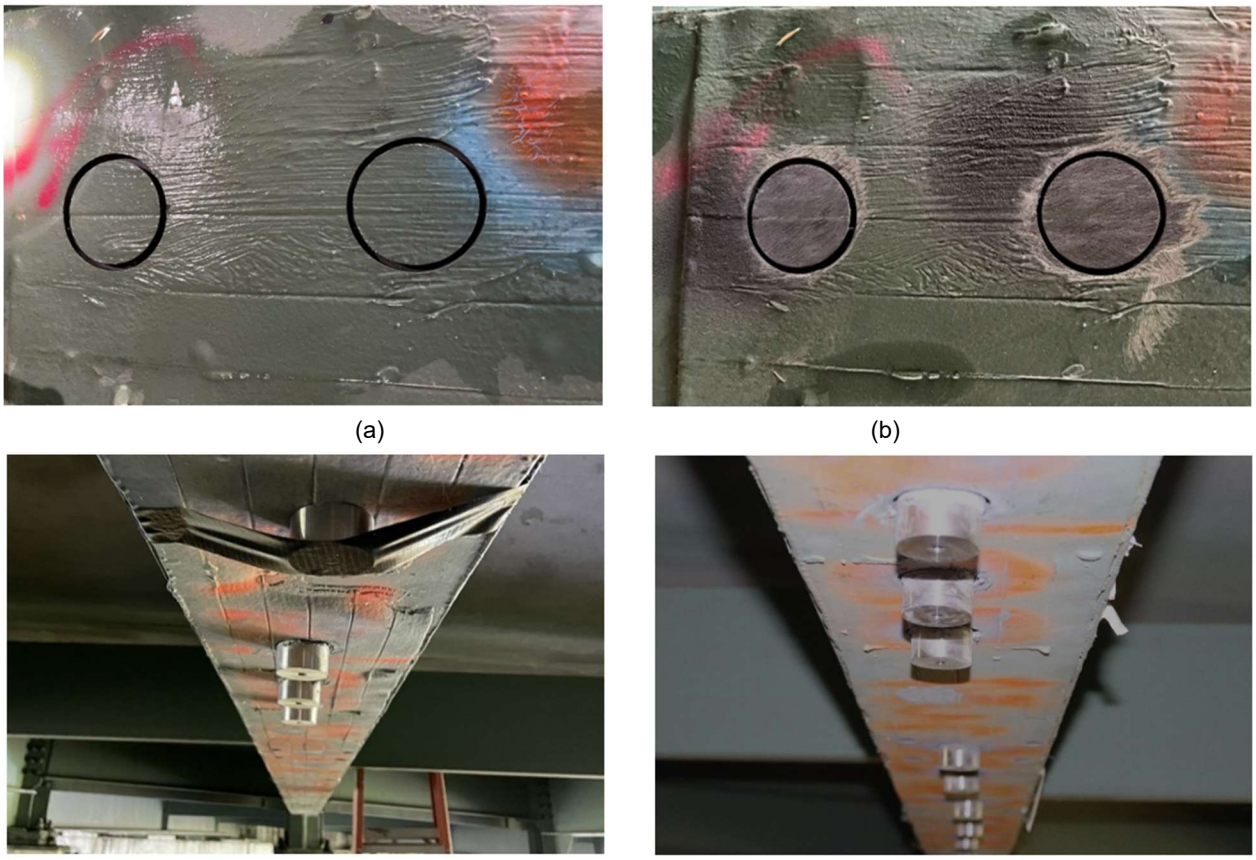

(a) (b)

(c) (d)

Figure 70. Preparation for pull-off tests at Br 1-704: (a) hole drilled through CFRP composite system, (b) removal of paint and roughening of CFRP composite, (c) puck taped to the steel girder while epoxy is being cured , and (d) after epoxy was cured.

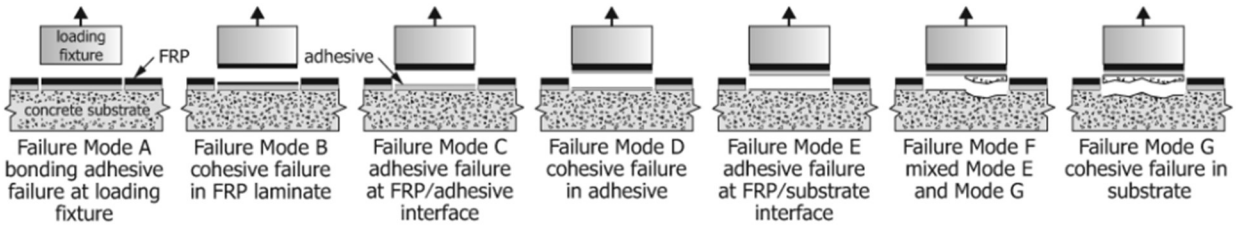

Source: ASTM D7522 (2021)

Figure 71. Failure modes for pull-off test (reprinted, with permission, from ASTM D7522/D7522M-21 Standard Test Method for Pull-Off Strength for FRP Laminate Systems Bonded to Concrete or Masonry Substrates, copyright ASTM International. A copy of the complete standard may be obtained from www.astm.org).

Tensile Tests

Tensile tests were performed on field and control samples according to the procedures specified in ASTM D3039 (2014) to determine Young's modulus (E) and Poisson's ratio (υ) of the samples. Tensile test samples measuring approximately 10 in. (length) × 0.5 in. (width) were cut from control samples (Figure 60) and field samples (Figure 66) and then sanded with a 100-grit sandpaper on all sides to make the surface even and remove paint or adhesive from the surface. The thickness of control CFRP coupons and field

CFRP coupons were approximately 0.21 in. and 0.16 in., respectively. The field CFRP coupons were sanded on the front and back sides to remove the paint and remnants of glass-fiber fabric or adhesives, respectively, which resulted in the reduction in thickness of the field coupons by approximately 0.05 in. compared to control coupons. ASTM D3039 recommends the usage of gripping tabs when testing unidirectional materials to the failure in the fiber direction. The coupons were tested to approximately 33 ksi, which is equal to approximately 24% of the specified flexural strength, so the gripping tabs were not used. To prevent the coupon from gripping damage, the coupons were wrapped with sandpaper at the end such that the coupons were not in direct contact with the lower and upper grip fixture of the testing equipment.

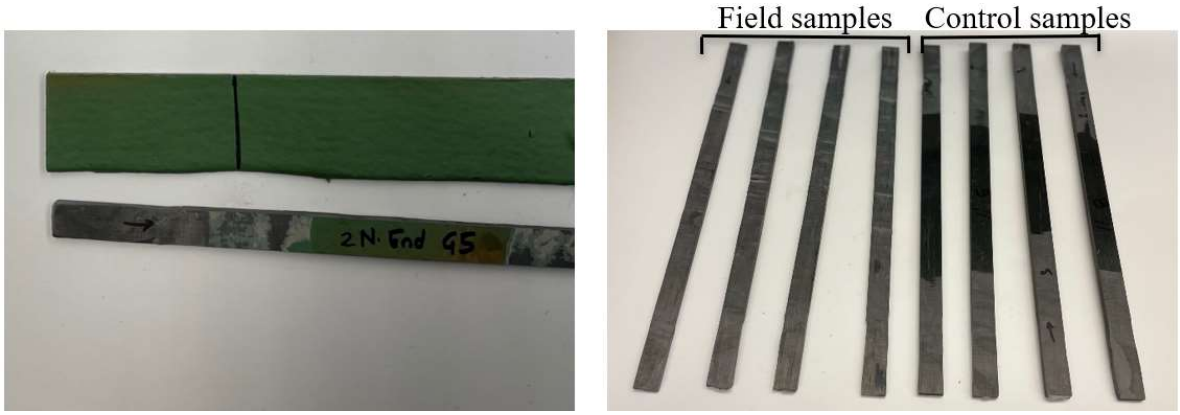

(a) (b)

Figure 72. Tensile and three-point bending test samples: (a) field samples before removal of paint, and b) field samples and control samples.

CFRP coupons, as shown in Figure 72b, were tested on Instron 5985 using an 11-kip static load cell. The samples were loaded to approximately 33 ksi (or 24% of the specified tensile strength) tensile strain at a constant crosshead displacement rate of 0.05 in./min. Multiple demonstration tensile tests were performed on dummy samples to see if the CFRP coupons could be tested until tensile failure. Due to the relatively thick section of the CFRP coupons, a tensile failure could not be achieved by a simple tensile test. The coupons were thus only loaded to 33 ksi, which is well below the elastic limit of the CFRP coupon. To perform the test, both ends of the test samples were clamped, as shown in Figure 73, and a tensile axial load was applied to one end of the specimen, while the other remained stationary. The strain was measured with a two-element 90 deg. tee rosette strain gage with 350 Ω resistance and a gage length of 125 (Vishay Precision Group, Inc.) attached to the CFRP coupons with an adhesive (M-Bond 200), cured at room temperature. Experimental data were collected using StrainSmart V4.31 software and a StrainSmart data acquisition system (Model 5100B) manufactured by Vishay Precision Group, Inc.

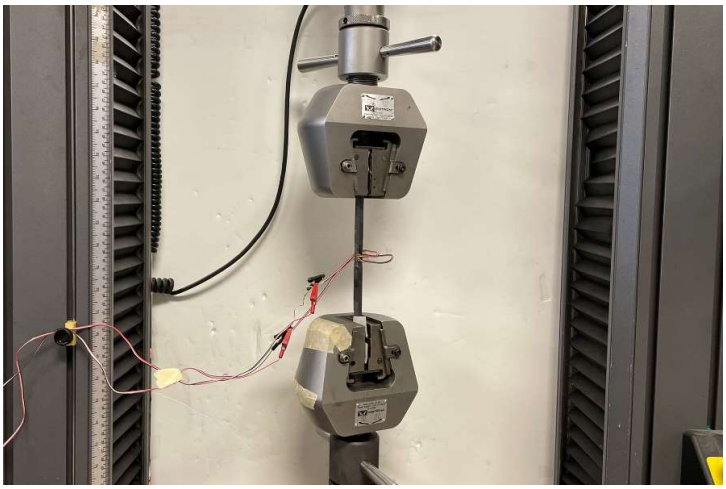

Figure 73. Tensile test setup.

Three-Point Bending Tests

Three-point bending tests were performed on the samples previously tested in tension, as described in Chapter 2. The tests were conducted according to the procedures specified in ASTM D7264 (2015) to determine the flexural stiffness and strength properties by loading the sample to failure. The supported length for the control CFRP sample was 6.75 in. and the field CFRP sample was 5.38 in., consistent with the ASTM-recommended span-to-thickness ratio of 32:1 for control sample, but because of limitation of test support, 33.5:1 was adopted for field sample. All tests were performed on Instron 5567 using a 1-kip static load cell. The rate of crosshead movement adopted was 0.05 in./min, as recommended by the ASTM. To perform the test each sample was placed on two support points and bending force was applied centrally on the sample via crosshead until failure, as shown in Figure 74. The load-displacement curve was plotted using a DCTH2000A type LVDT manufactured by RDPE Group, Inc., mounted at the mid-span of the sample. Experimental data were collected using StrainSmart V4.31 software and a StrainSmart data acquisition system (Model 5100B) manufactured by Vishay Precision Group, Inc.

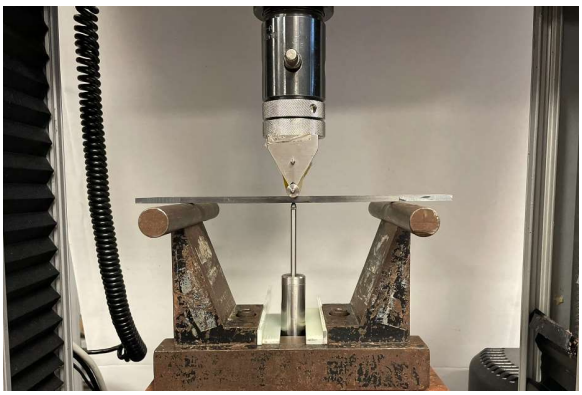

Figure 74. Three-point bending test setup.

EXPERIMENTAL TEST RESULTS

Visual Inspection

The visual inspection of Bridge 1-704 was performed in April 2021. The focus of the inspection was the CFRP, but the overall steel girder and non-composite concrete deck were visually inspected as well. The size of the girder G5, W24×84, as recorded in the as-built drawings provided by DelDOT, was verified during the inspection.

A preliminary visual investigation of the CFRP composite repairs did not indicate the presence of obvious degradation, as shown in Figure 75. However, it was observed that approximately 6×6 in.^{2} of CFRP composite was grit blasted, as shown in Figure 76. According to DelDOT, it was grit blasted during the surface preparation work prior to the application of the paint on the soffit of the girder. The accessible part of the girder (Figure 75b,c) was found painted with graffiti paint. The abutments and concrete deck were inspected periodically throughout the year 2021, and it was observed that the moisture infiltrated the abutment during rainy days, as shown in Figure 77. No signs of ingression of direct rainwater runoff from the roadway were observed on the CFRP composite during the inspection.

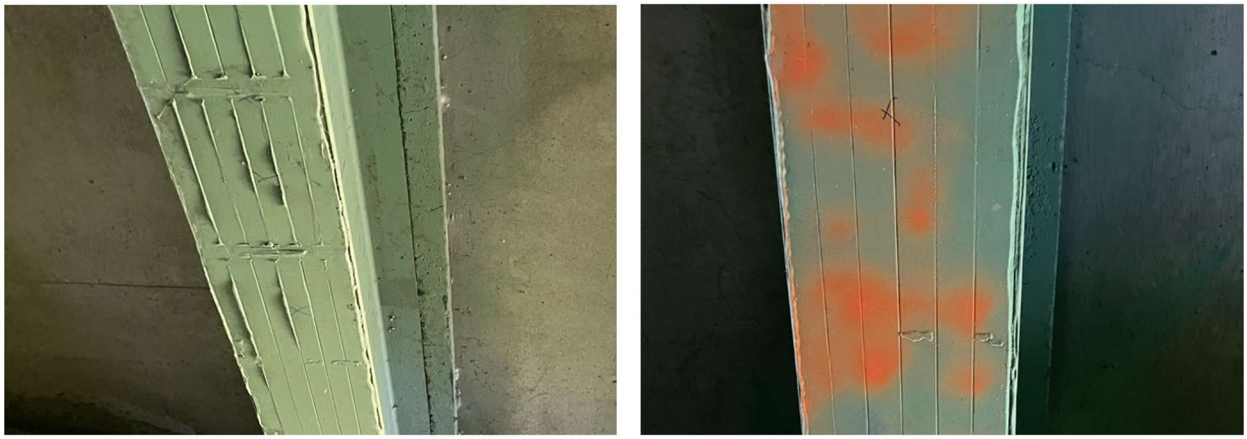

(a) (b)

(c)

Figure 75. Condition of CFRP composite girder repaired in 2000.

Figure 76. Damage to CFRP laminate from grit blasting.

Notes: (a) Stains visible on the concrete retaining wall and abutment; (b) fine sediment aggregates visible on top of concrete abutment.

Figure 77. Infiltration of moisture at the abutment of the bridge.

Structural Health Monitoring of Br 1-704

Diagnostic load tests were performed by Miller (2000) on the girder G5 before and after the installation of CFRP composite using a three-axle dump truck weighing 57.26 kips and 64.24 kips, respectively. The spacing of axle distance of the three-axle dump truck was not available. The hauling permit policy by DelDOT (2018) requires at least 24-ft spacing between the axles for a three-axle vehicle weighing 54 kips, which is greater than the minimum requirement for design truck per AASHTO (2017). After normalizing the results based on the ratio of truck weights, it was observed that the installation of CFRP composite increased the stiffness of the girder G5 by approximately 11%. The effect of CFRP composite on the global stiffness was determined using the method of the transformed section; a strain decrease of 10% was estimated by Miller (2000), which agreed with the results obtained from diagnostic load tests. Miller established that the strain above the threshold strain of 75 με was associated with the truck event from the

diagnostic load tests conducted using a dump truck. Only peak strain events greater than the threshold strain were recorded by Miller, resulting in a total peak strain count of 790 over 14 days.

Unprocessed live-load strain reading at ST355 strain gage and the calculated baseline strain were plotted against time (Figure 78). Baseline corrected peak strain (hereinafter called the "peak strain") was then obtained using the procedure discussed previously, as shown in Figure 79. A trigger threshold of 68 με was used for this particular test based on the assumption that there was no degradation of mechanical properties of CFRP composite and the bond strength. The selected threshold is equivalent to 75 με before installation of CFRP composite; therefore, peak strains below 68 με are not shown in Figure 79. Figure 80 displays the peak strain data count for each 5 με and Figure 81 displays the peak strain data density for each range, where the data obtained from the current study "ST355 (Corrected data)" were compared to those obtained by Miller (2000) before the installation of CFRP composite. The total peak strain count above the threshold strain was equal to 2,505 over 14 days in 2022, which was found to be more than three times greater than Miller's total peak strain count of 790. Figure 81 shows approximately 55% of the overall peak strain counts in 2000 were between 75 and 80 με, which made up only 30% of peak strain counts in 2022.

Given that existing state truck size and weight limit laws were found to be consistent nationwide since 1991 (FHWA, 2015), such a drastic increment in peak strain count (Figure 80) possibly indicates the reduction in global stiffness of the girder. The exact loss in global flexural stiffness of the girder could not be quantified because the diagnostic load tests (i.e., with controlled load magnitude and position) were not performed. The degradation of CFRP composite or the bond strength due to environmental conditioning could have potentially affected the stiffness, but there could have been several other factors affecting the loss in stiffness of the girder. For instance, even though the girders were designed non-compositely, the contribution in stiffness due to the interaction of the steel girder-concrete deck was not evaluated at any stage of the service life of the bridge. In case there was composite action due to the concrete deck, the presence of cracks in concrete, loss of bond, etc. could result in stiffness degradation. Similarly, no studies were conducted to assess the cyclic strength degradation of girder due to dynamic loading, which could lead to a significant increase in peak displacement demands (Veletsos and Newmark, 1960). Overall, it was not possible to quantify the effect of environmental degradation in the reduction of global stiffness of the girder; thus, additional experimental tests need to be performed in the field and laboratory.

No design guidelines or specifications are available to determine the fatigue performance of the CFRP composite and its bond strength with the steel substrate, so past research studies were used for the assessment. The maximum stress in the CFRP composite, obtained from structural health monitoring performed in 2022, was found to be 2.13 ksi (corresponding to 1.6% of tensile strength). In addition, it was estimated that the girder sustained approximately 950,000 cycles by interpolating SHM data between 2000 and 2022. In the previous work by Miller (2000) on the same material, no loss of stiffness or visible damage to the CFRP was reported after 10 million cycles at 5 ksi stress. These findings were consistent with other studies (Broyles 1998; Song 2019), which reported good fatigue performance at stress levels ranging from 13 to 37% of the CFRP tensile strength. In conclusion, the actual stress and number of fatigue cycles that CFRP on bridge Br 1-704 underwent would not be a cause for concern. However, Miller (2000) and other studies did not evaluate the effect of combined environmental conditioning and fatigue on the CFRP and CFRP/steel bond performance; this is a topic deserving further research.

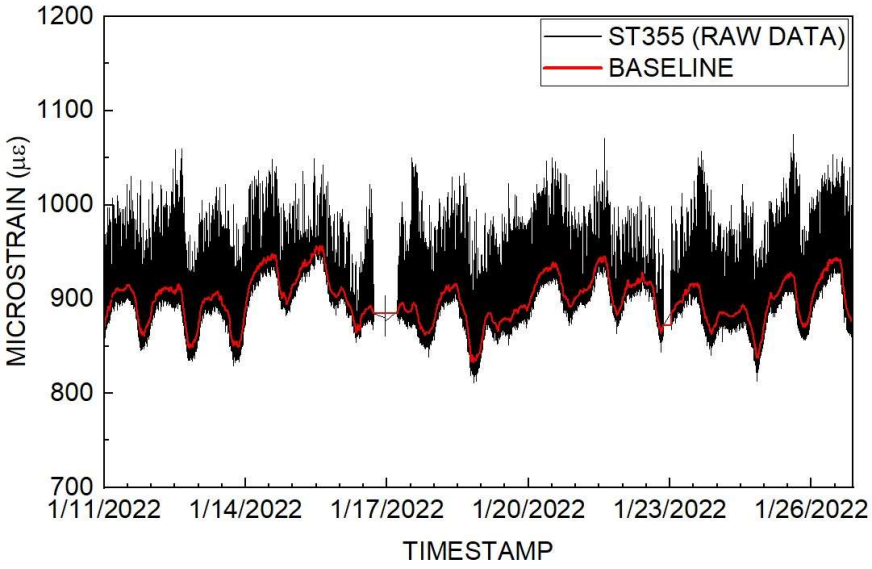

Figure 78.15-day unprocessed strain and baseline strain time history for girder G5.

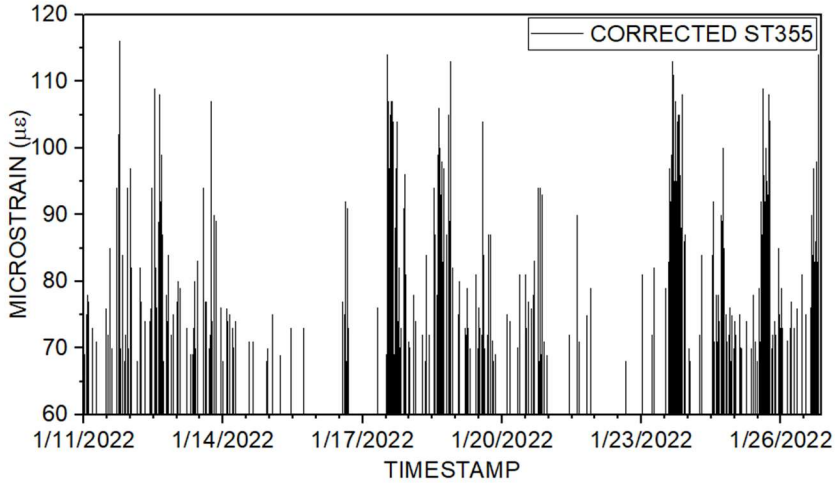

Figure 79. 15-day baseline corrected peak strain time history for girder G5.

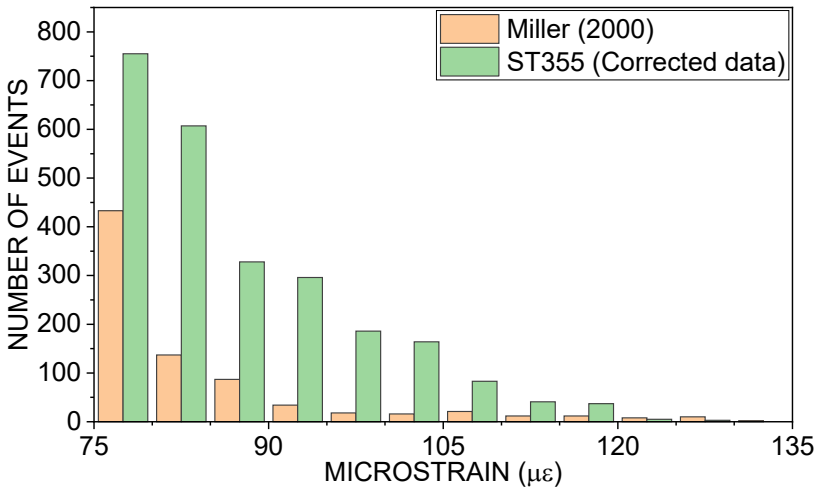

Figure 80. Number of peak live load strain events above threshold at ST355 vs. Miller (2000).

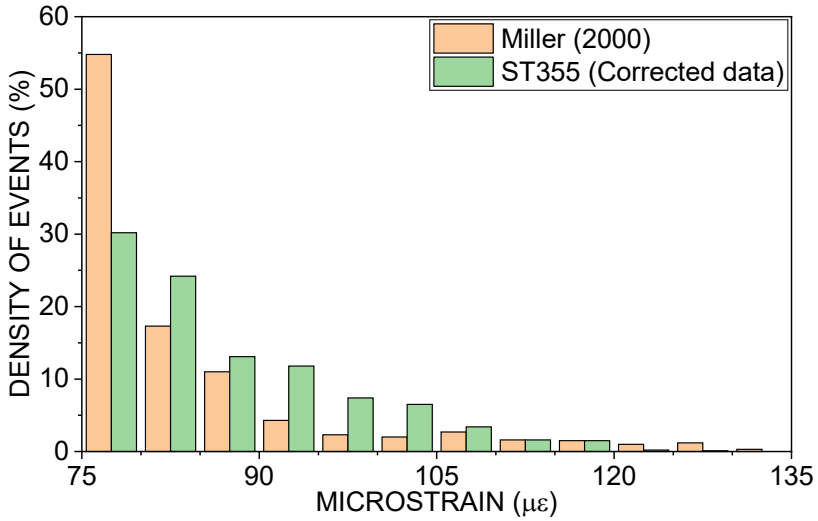

Figure 81. Density of peak live load strain events above threshold at ST355 vs. Miller (2000).

Materials Characterization Experiments

Attenuated Total Reflectance - Fourier Transform Infrared (ATR-FTIR)

ATR-FTIR spectra of the control and field samples with wave numbers ranging from 500 cm^{-1} to 1,900 cm^{-1} are shown in Figure 82. The nomenclature of the sample (e.g., FG5-C/F1) implies the FTIR test of control (C) or field (F) samples from girder G5 and sample number 1. The intensity of peak absorbance close to 1,040 cm^{-1} was chosen as a reference, identified as a C-O stretching of the alcohol group (Visco et al., 2012 and Auad et al., 1997). All other spectra were normalized to the peak at 1,040 cm^{-1} recorded on the FG5-C1 sample for comparison of the peak intensity between different samples and vibration modes associated to various peaks are summarized in Table 3.

Spectra showed only minor spectral changes as a result of environmental exposure to the field conditions for 22 years. Some differences among spectra were observed: (1) intensity of peak absorbance at 700 cm^{-1}, was found present in both control samples FG5-C1 and FG5-C2, but the peak was partially or completely consumed on the field samples; and (2) intensity of peak absorbance at 1,508 cm^{-1} was also found present in both control samples, but the peak was partially or completely consumed on the field samples. The peak band 700 cm^{-1} corresponds to the bending of the aromatic C-H bond in styrene (Jost et al., 2002, and Ziaee et al., 1999). Similarly, the peak band 1,508 cm^{-1} is attributed to the aromatic ring stretching of C=C, aromatic ring per (Auad et al., 1997). The intensities of both peaks at 700 cm^{-1} and 1,508 cm^{-1} were found low and inconsistent in the field samples, which suggests that degradation did not occur or was insignificant.

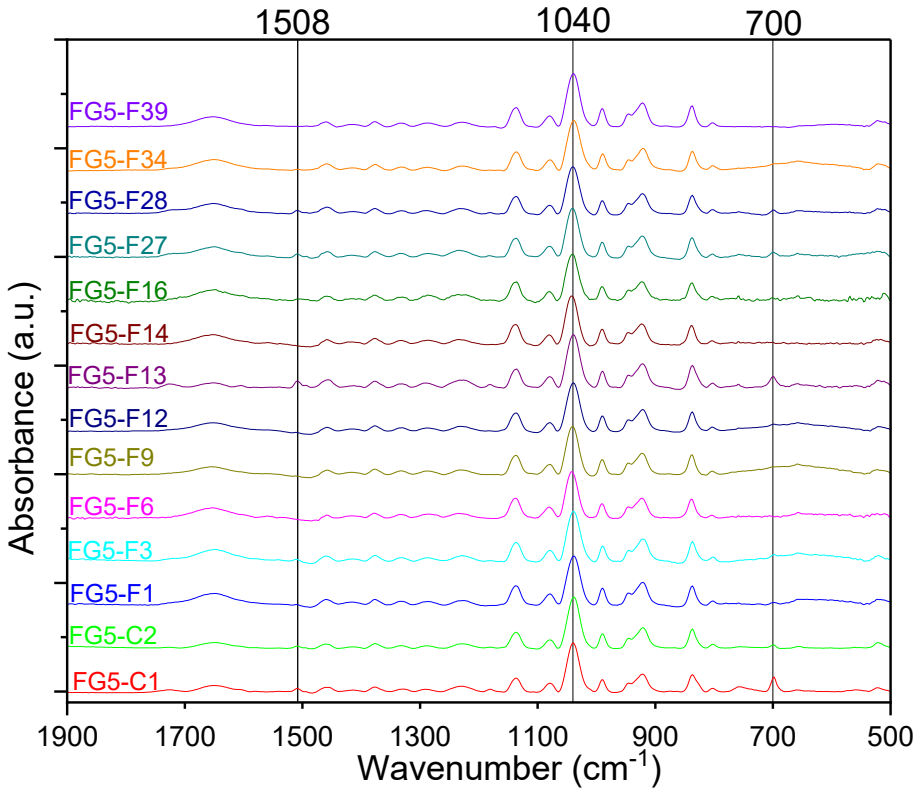

Figure 82. ATR-FTIR spectra of CFRP control and field samples from Br 1-704.

Table 3. ATR-FTIR peak assignment.

FTIR Spectra from Br 1-704	FTIR Band-literature	Vibration Modes
700	700[c,d]	CH2
803	N/A (Not Available)	N/A
838	829[b]	Bending of aromatic C-H bonds
923	947[e]	Out-of-plane bending of C-H bonds
990	N/A	N/A
1,040	1,040[a,b]	C-O stretching vibration of alcohol group
1,078	1,092[e]	In-plane C-H deformations
1,140	1,142[e]	C-O stretching
1,230	1,230[a]	C-O ester stretching vibration
1,332	N/A	N/A
1,378	N/A	N/A
1,461	1,457[b]; 1,450[a]	CH, CH2 and CH3 deformation; CH2
1,508	1,500 to 1,600[a]; 1,508[b]	C=C; aromatic ring stretching of C=C
1,655	1,640[e]	C=C stretching vibration

Source: Visco et al. (2012)[a], Auad et al. (1997)[b], Jost et al. (2002)[c], Ziaee et al. (1999)[d], and McManis (1970)[e]

Dynamic Mechanical Analysis (DMA) of Vinyl Ester Matrix

The storage modulus (E'), loss modulus (E"), and damping factor (tanδ) were plotted as a function of temperature on a linear scale, as shown in Figure 83. The glass transition temperature (T_g) and other alternative temperatures (T_l and T_t) using all three viscoelastic parameters for all the samples were determined per ASTM E1640 (2018). The first tangent was constructed to the storage modulus curve below the transition temperature, and the second tangent was constructed to the storage modulus curve at the inflection point approximately midway through the sigmoidal change associated with the transition. The inflection points, 121 °C (Figure 83a) and 120 °C (Figure 83b), were determined using Origin software for control and field samples, respectively. The temperature at which two tangents were meeting was reported as the T_g of the sample. Similarly, the alternative temperatures, the peak of the loss modulus (T_l), and the peak of tangent delta (T_t) were determined for both control and field samples, as shown in Figure 83.

The nomenclature of the sample (e.g., DG5-C/F1) implies the DMA test of control (C) or field (F) samples from girder G5 and sample number 1. The glass transition temperatures of the control and field samples are shown in Table 4. The T_g of field samples were found lower than the control samples by approximately 9% (Figure 84). Similarly, T_l and T_t of field samples were also found lower compared to control samples by 5% and 3%, respectively.

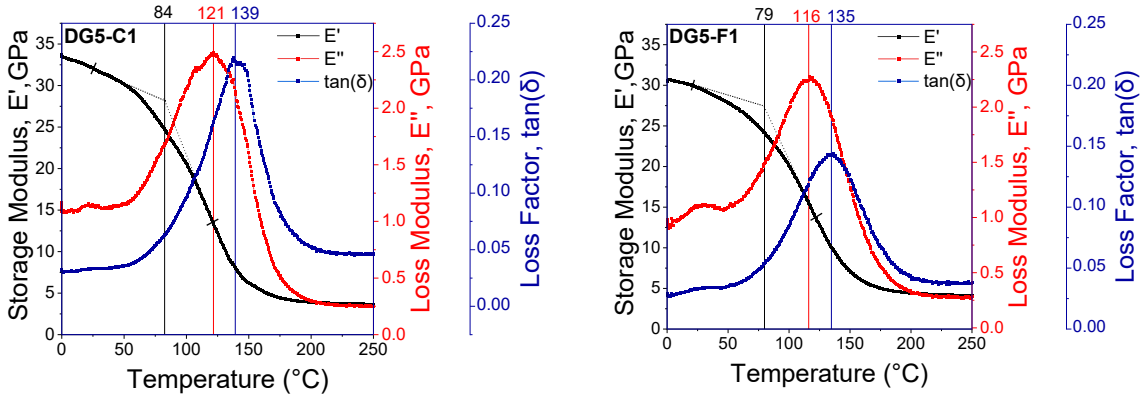

(a) (b)

Figure 83. Representative DMA plots for (a) control and (b) field samples.

AASHTO (2012) recommends minimum T_g of the composite system be greater than the in-service temperature plus 40 °F. The maximum design temperature in Delaware for steel girder bridges with concrete deck per AASHTO (2017) is 43 °C, thus the AASHTO (2012) recommended minimum T_g is approximately equal to 66 °C, which is still lower than the T_g of the field, as shown in Table 4, by approximately 20%. The reduction in T_g of field samples compared to controls can be attributed to the potential ingression of moisture at field conditions. The moisture uptake causes the plasticization and hydrolysis over short-term conditioning and long-term conditioning, respectively, through the breakage of ester linkage, resulting in reduced T_g and softening of vinyl ester, which eventually causes a loss in stiffness and strength of CFRP composite (Chu et al., 2005). In conclusion, some reduction in T_g was observed after 22 years of environmental exposure due to potential ingression of moisture; however, the reduction was not detrimental, as the T_g of the field sample was still found to be greater than the AASHTO (2012) recommended minimum temperature.

Table 4. Glass transition temperature using storage modulus E', loss modulus E", and tanδ.

Label	T_g	T_l	T_t
	Storage Modulus (E')	Loss Modulus, E"	tanδ
DG5-C1	84 °C	121 °C	139 °C
DG5-C2	87 °C	120 °C	138 °C
DG5-C3	90 °C	123 °C	140 °C
Average of Control Samples	87 °C	121 °C	139 °C
DG5-F1	79 °C	116 °C	135 °C
DG5-F2	78 °C	115 °C	134 °C
DG5-F3	81 °C	118 °C	136 °C
Average of Field Samples	79.5 °C	116 °C	135 °C

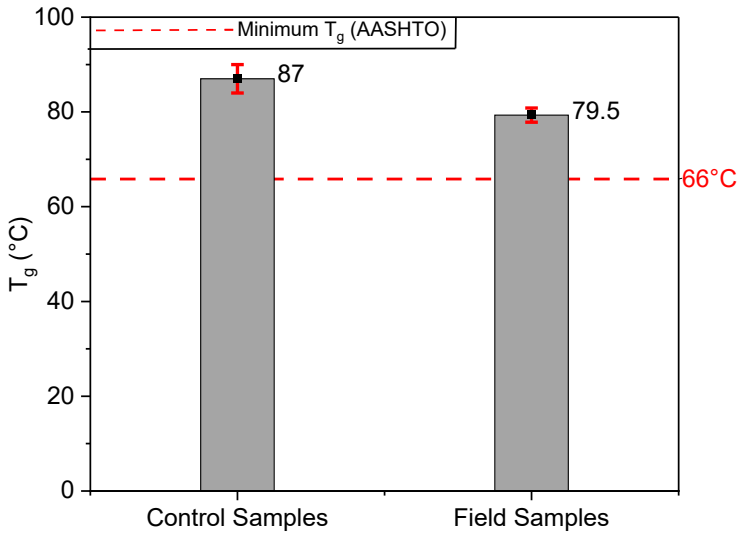

Figure 84. Average glass transition temperature of control and field CFRP samples.

Differential Scanning Calorimetry (DSC) of Structural Adhesives

As shown in Figure 85, the heat flow was plotted as a function of the temperature to determine the T_g of the structural adhesive samples collected from girder G5. The midpoint temperature (T_m) was selected as the T_g for AV8113 structural adhesives, since it is constructed closer to the middle of the temperature range over which the glass transition occurs. The first baseline was constructed to the heat flow curve before the transition temperature, and the linear portion during the phase transition was extrapolated until it intersected the first baseline to determine the T_f per ASTM E1356-08 (2014). The second baseline was then established to the heat flow curve after the transition temperature. The linear portion during the phase transition was again extrapolated to meet the second baseline; the point of intersection is referred to as extrapolated end temperature (T_e). An average midpoint temperature (T_m) for AV8113 was 35.7 ± 2.4 °C, which was found significantly lower than the glass transition temperature (i.e., 90 °C) reported by West (2001).

The extrapolated onset temperature (T_f) was selected as the T_g for MA555 structural adhesives because of the inability to establish the second baseline for determination of midpoint temperature. The first baseline was constructed to the heat flow curve before the transition temperature, and the linear portion during the phase transition was extrapolated until it intersected the first baseline to determine the T_f per ASTM E1356-08. Several endothermic peaks were observed immediately after the phase transition, as shown in Figure 85a. An average extrapolated onset temperature (T_f) for MA555 was 48.1 ± 0.3 °C, which was found to be lower than the glass transition temperature (i.e., 103 °C) reported by West (2001).

The T_g of both structural adhesives were found to be well below the minimum temperature of 66 °C as recommended by AASHTO (2012) and their respective control samples (Figure 86). Some reduction in T_g, similar to vinyl ester, may be due to moisture ingression. The field samples were cured at the field conditions, but the curing information of the control samples was not known. The higher T_g of the control samples could be due to the controlled curing at laboratory conditions. In conclusion, the observed T_g of both structural adhesives were found below the minimum requirement, which is concerning; the T_g of the field sample may have been reduced due to moisture ingression; however, the cure phenomenon of the

control samples was not known, thus the quantification of reduction in T_g due to environmental conditioning was not possible.

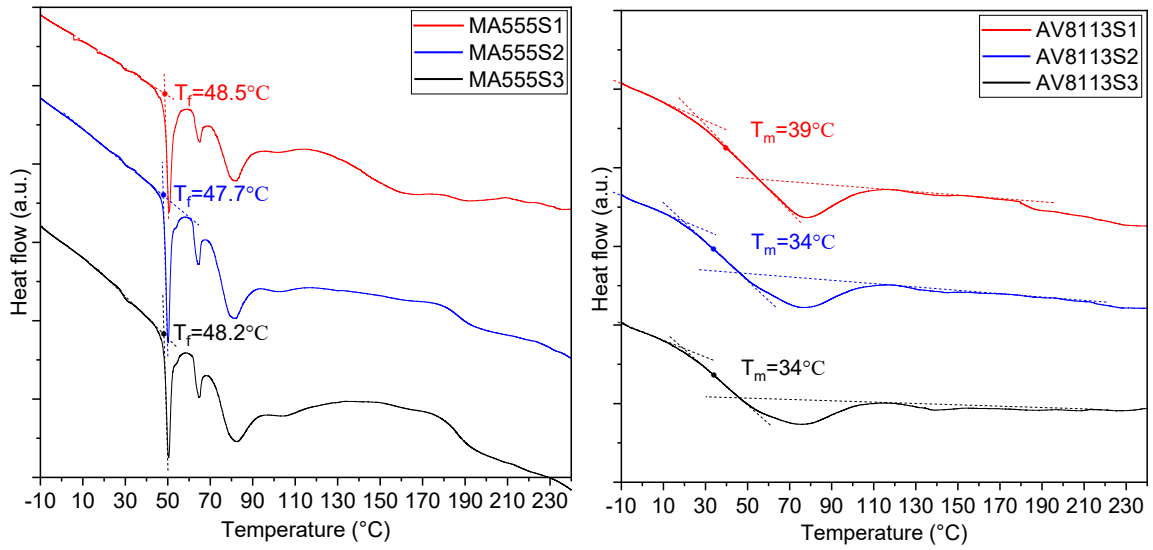

(a) (b)

Figure 85. Glass transition temperature measured on samples from girder G5: (a) MA555 samples and (b) AV813 samples.

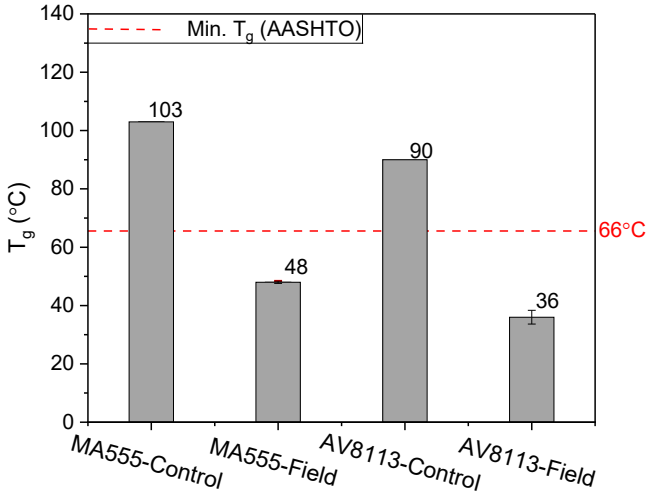

Figure 86. Average glass transition temperature of control and field structural adhesive samples.

Pull-Off Tests

Bond pull-off test results are presented in Table 6, and the photos of observed failure modes are shown in Figure 87. The nomenclature of the sample (e.g., P1) implies the pull-off test at girder G5 and sample number 1. The approximate test locations are shown in Figure 62 and the exact locations are shown in Table 6 with respect to the centerline of the bearing at abutment 2 (Figure 55). A total of 20 tests were performed on the girder, out of which only two samples, P1 and P2, failed in the acceptable mode of failure (Mode C per ASTM D7522, 2021), where the adhesive failure in the adhesive/glass-fabric interface was observed.

An additional two samples, P14 and P15, saw bonding adhesive failure at the loading fixture, which is not an acceptable failure mode per ASTM (2021). The remaining samples did not fail as the capacity of the pull-off tester (1145 psi) was reached.

Due to the unavailability of design guides to address the minimum bond strength of CFRP composite bonded on a steel substrate, test results could only be compared to the bond strength requirement of coatings or paints on a steel substrate by ASTM D4541-22 (2022) and the bond strength requirements of paints and varnishes recommended on a steel substrate by ISO 4624 (2016), as summarized in Table 5. Because of the lack of initial pull-off test data for AV8113 and MA555 structural adhesives during the time of strengthening, quantitative assessment of bond strength degradation was not possible.

Table 5. Summary of bond strength requirements on a steel substrate.

Coating Material	Reference Standard	Min. Bond Strength
Zinc primer	ASTM D4541	400 psi [a,b]
Coatings of aluminum, zinc, and their alloys and composite	ASTM D4541	700 psi (500 psi for zinc) [c]
Coatings of aluminum, zinc, 85/15 (Zn/Al) or 90/10 MMC	ASTM D4541	560 psi [d]
New over-coating paint systems	ASTM D4541	600 psi [e] 250 psi after 100 cycles of exposure
Paints or paint systems	ISO 4624	363 psi (if 0% adhesive failure b/w substrate and first coat, else 726 psi) [f]

Source: NCDOT (2019)[a], TSP-2 AASHTO (2002)[b], IDOT (2017) [c], CDOT (2020)[d], Balaguru et al. (2021)[e], and The EU RO MR Group (2022)[f]

Table 6 shows that the bond strength for two samples, P1 and P2, was significantly below the minimum recommended bond strength value for various coating or paint system (Table 5). A careful observation at those test locations post-testing indicated inadequately saturated glass-fiber fabric and the presence of air bubbles trapped at the adhesive/glass-fiber fabric interface as shown in Figure 87a,b. Such failure at the adhesive/glass-fabric interface indicates issues with surface preparation, poor workmanship, or a combination thereof. The pull-off bond strengths at all the remaining 16 test samples, except P14 and P15, were found to be significant, as high as 1.6 to 4.6 times above the minimum bond strength values shown in Table 5.

Table 6. Pull-off test results for Br 1-704.

Test No.	Distance from North Support (ft. in.)	Adhesive	Bond Strength (psi)	Failure Mode	Interpretation of Failure Mode
P1	2 ft. 9 in.	Plexus MA555	42	Failure Mode C-Adhesive failure at Adhesive/glass-fiber fabric interface	Indicates poor adhesion properties likely resulting from contamination, incomplete cure, environmental degradation, or improper installation.
P2	3 ft. 6 in.		38		
P3	4 ft. 4 in.		>1,145	No failure mode observed, the maximum capacity of the pull-off tester reached	Pull-tests were not successful because of the limited pulling capacity of the pull-off tester.
P4	6 ft. 1 in.				
P5	7 ft.				
P6	8 ft.				
P7	8 ft. 10 in.				
P8	9 ft. 9 in.				
P9	10 ft. 9 in.				
P10	11 ft. 9 in.				
P11	12 ft. 9 in.	Ciba AV8113			
P12	13 ft. 7 in.				
P13	14 ft. 5 in.				
P14	15 ft. 4 in.		514	Failure Mode A-Bonding adhesive failure at loading fixture	Indicates poor adhesion between the bonding adhesive and the puck, which could be due to poor or inadequate surface preparation or treatment, or improper installation.
P15	16 ft. 3 in.		574		
P16	18 ft. 10 in.		>1,145	No failure mode observed, the maximum capacity of the pull-off tester reached	Pull-tests were not successful because of the limited pulling capacity of the pull-off tester.
P17	19 ft. 7 in.				
P18	20 ft. 3 in.				
P19	20 ft. 11 in.				
P20	21 ft. 8 in.				

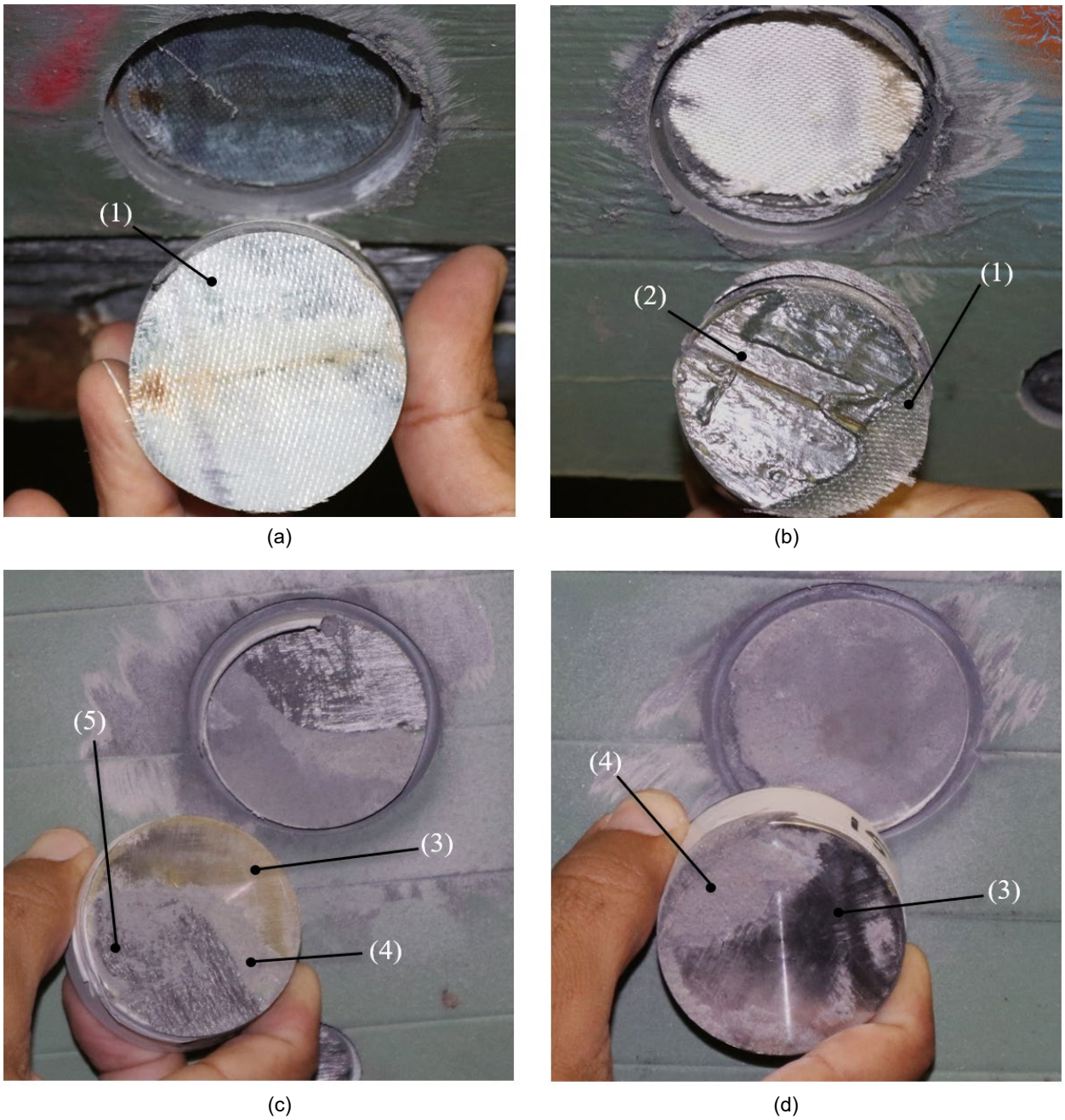

Notes: 1. Glass-fiber fabric observed to be inadequately saturated. 2. Air bubbles trapped at the adhesive/glass-fiber fabric interface. 3. Clean surface of puck visible, no hint of “Sikadur-30” epoxy. 4. Sikadur 30 epoxy residue. 5. Cohesive failure of CFRP composite.

Figure 87. Failure modes observed at different location of G5: (a) mode C at P1, (b) mode C at P2, (c) mode A at P14 , and (d) mode A at P15.

Corrosion of Steel Girder

The final inspection of Bridge 1-704 was performed in July 2022, after the completion of structural health monitoring and sample collection for laboratory tests. The steel surface on the northern end of the girder (Figure 56) was found to have developed corrosion where Plexus PC120 primer was used (Figure 88). Upon

extraction of the sample for laboratory tests, corrosion was observed on the edge of the girder until 6 ft. from the northern end of the CFRP composite, extending about 0.5 in. from the outward edge of the flange. The pull-off tests conducted at this location showed inadequately saturated glass-fiber fabric and entrapped air bubbles at the adhesive/glass-fiber fabric interface (P1 and P2 as shown in Figure 87). No signs of corrosion were observed on the southern half of the girder where Z-6040 silane was used as an adhesion promoter.

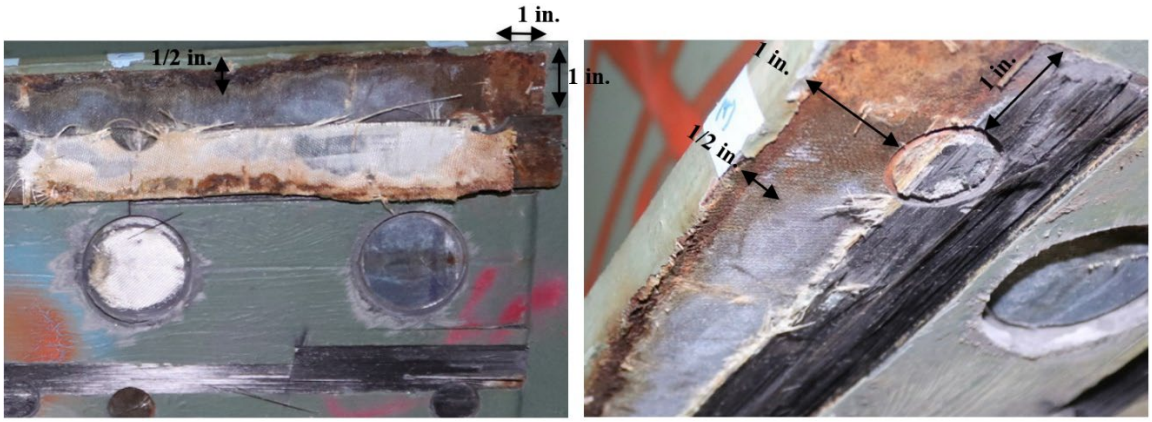

Figure 88. Presence of rust on the northern end of the girder, located 4–10 ft. away from the centerline of abutment 2 (shown in Figure 55).

Out of numerous forms of corrosion that are common in steel infrastructure subjected to environmental exposure, the corrosion observed beneath the CFRP composite is potentially due to galvanic corrosion. Galvanic corrosion is defined as accelerated corrosion of the metal because of electrical contact with another conductive material in a corrosive environment (Hack, 1988). The presence of two conductive materials, an electrical connection between them, and the presence of an electrolyte make the system an electrical circuit known as a galvanic couple.

In the context of this research, the steel girder acts as the anode while the CFRP composite behaves as the cathode. Ingression of moisture along with salt, acid, or a combustion product into the CFRP composite/steel interface may generate an electrolytic solution. Moisture can come from direct rainwater runoff, fog, or even humidity. The chloride concentration on the steel surfaces was not measured before the installation of CFRP composite and during the visual inspection process. Research studies showed that sites within 328 ft of busy roadways are likely to have road salt mist accumulations comparable to moderate to severe coastal conditions and the vertical distance that mists travel depends on the wind speed and the air turbulence, which goes as high as 90 ft depending on the structure's location, spacing, and type (Houska, 2007). The girder is approximately 4 to 6 ft high, which makes the girder susceptible to tiny particles of saltwater or dry salt, eventually forming an electrolyte solution in the presence of moisture and oxygen.

Inadequately saturated glass-fiber fabric observed at the location of corrosion using pull-off tests, potential holes or air voids in the structural adhesive, and inadequate width of glass-fiber fabric likely resulted in an electrical contact between the steel and CFRP composite which, in the presence of electrolyte solution, transformed the connection into a complete galvanic couple, causing corrosion at the steel substrate. West (2001) investigated the potential for galvanic corrosion on the steel surface along the edges of the CFRP composite separated by glass-fiber fabric with similar properties to that of the CFRP system used at Br 1-704 and found that the edges were vulnerable to moisture penetration, which caused surface corrosion at the steel substrate. The corrosion observed beneath the edges of the CFRP composite at Br-1-704 is in

correlation with the findings of West (2001). Overall, the CFRP composite possesses concealing behavior and the traditional visual inspection methods may not be adequate to assess the underlying condition of the steel surface.

Tensile Tests

The tensile modulus for six CFRP coupons is shown in Table 7 and Figure 89. The nomenclature of the coupon (e.g., TG5-C/F1) implies the tensile test of control (C) or field (F) coupons from girder G5 and sample number 1. Tensile modulus, E_{11}, was calculated in the strain range of 0.005 to 0.025% instead of the 0.01 to 0.03% strain range recommended by ASTM D3039/D3039M-08 (2014). Tensile modulus was also calculated using the alternate numerical data method using ASTM E111-17 (2017), per chapter 13.3.2 of ASTMD3039, which was adopted for further analysis.The average tensile modulus of control and field coupons were 15,815±538 ksi and 13,408±820 ksi, respectively, as shown in Table 7. Ammar (1996) performed tensile tests on several 8-in. long x 1.44-in. coupons using Intron 1120 at the University of Delaware to determine the tensile modulus, which yielded a mean value of 16,300±300 ksi. Upon comparison, the average tensile modulus for control and field coupons after 22 years was found to be 3% and 17% less than the tensile modulus determined by Ammar (1996), respectively. The average tensile modulus of control coupons was found to be 15% higher than that of field coupons.

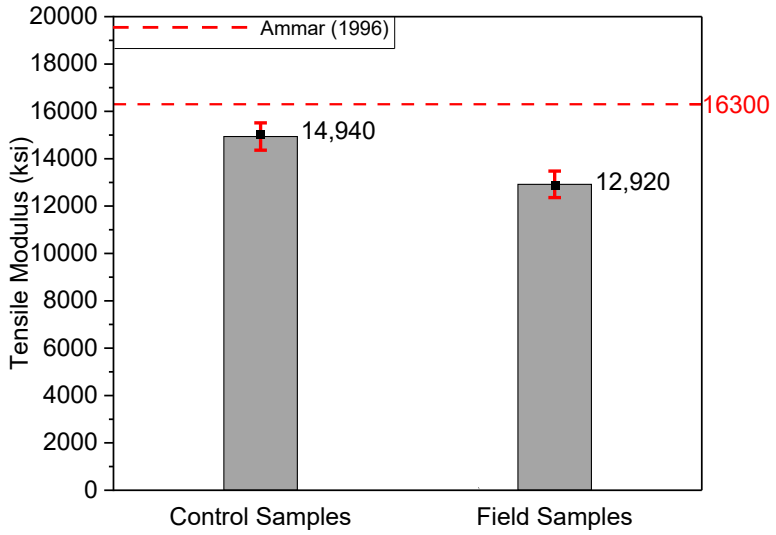

Figure 89. Tensile modulus of field and control coupons after 22 years of service vs. Ammar (1996).

Due to the unavailability of design guides to address the environmental reduction factors of CFRP composite bonded on a steel substrate, the test results could only be compared to the reduction factor requirements recommended by various design guides on a concrete substrate. According to ACI440.2R (2017), the environmental reduction factors, C_E, are applied to determine the design tensile strength and design tensile strain of CFRP composite, which varies between 0.5 and 0.95 depending on the type of fibers and environmental exposure. ACI440.2R recognizes that modulus in some composites may be affected by the environmental exposure, but the guideline does not recommend applying the C_E factor to modulus. Contrary to this, a 17% reduction in the tensile modulus of the field coupons was observed after 22 years of environmental exposure under bridge Br 1-704.

Table 7. Tensile modulus of field and control coupons calculated using ASTM D3039 (ASTM E111): Br 1-704.

Label	Tensile Modulus, ksi	Average, ksi	Standard Deviation	COV	Tensile Modulus, ksi (Ammar, 1996)
TG5-C1	15,584 (16,574)	14,940 (15,815)	577 (538)	3.9% (3.4%)	16,300
TG5-C3	14,468 (15,486)	14,940 (15,815)	577 (538)	3.9% (3.4%)	16,300
TG5-C4	14,769 (15,386)	14,940 (15,815)	577 (538)	3.9% (3.4%)	16,300
TG5-F2	13564 (14,534)	12,920 (13,408)	559 (820)	4.3% (6.1%)	16,300
TG5-F3	12,588 (13,090)	12,920 (13,408)	559 (820)	4.3% (6.1%)	16,300
TG5-F4	12,607 (12,601)	12,920 (13,408)	559 (820)	4.3% (6.1%)	16,300

Contrary to ACI 440.2R, AASHTO (2012) recommends at least 85% retention in tensile strain after exposure to a set of laboratory-accelerated conditionings, which, if applicable to the modulus of elasticity, would have been in line with the reduction observed on the field samples. TR55 (2012), the UK design guide, addresses the potential changes in the modulus of elasticity with time by applying a factor of safety equivalent to a reduction factor of 0.90. Several research studies conducted over the last decade showed the tensile modulus of CFRP composite degraded by up to 26% when exposed to various laboratory-accelerated conditionings for up to 18 months (Alsuhaibani, 2020; Pan et al., 2015; Shi et al., 2022; Al-Jelaway, 2013).

The increment in the number of peak strain events over the 22 years' service life and reduction in T_g of the field CFRP composite are found to be in correlation with the reduction observed in tensile modulus of field samples. The contribution of environmental factors in the reduction in stiffness of the CFRP composite could not be well established because of (1) additional mechanical stresses in the field samples; (2) the manual extraction process from the field involving external force to pry off CFRP composite from the steel substrate; and (3) manipulation of field CFRP samples as part of the specimen preparation procedures. The present data suggest that a knock-down factor of 0.80 may be appropriate for the tensile modulus; however, additional work is required to qualify the effect of environmental factors on the mechanical properties of CFRP composite.

Three-Point Bending Tests

The flexural modulus for eight CFRP coupons is shown in Table 8 and Figure 90. The nomenclature of the coupon (e.g., BG5-C/F1) implies the three-point bending test of control (C) or field (F) coupons from girder G5 and sample number. The maximum strain (ε) at the outer (lower) surface at mid-span was computed using equation 1 from load vs. displacement data, as recommended by ASTM D7264 (2007) as follows:

$$\varepsilon = \frac{6\delta t}{L^2} \tag{1}$$

where δ is the mid-span deflection, L is the support span, and t is the measured thickness of the coupon. Flexural modulus of elasticity, E_f, was then calculated using equation 2 over a strain range of 0.01 to 0.03% per ASTM D7264 as follows:

$$E_f = \frac{3\Delta PL}{2wt^2\Delta\varepsilon} \tag{2}$$

where ΔP is the load change corresponding to the strain range 0.01 to 0.03% ($\Delta\varepsilon$), w is the width of the coupon, L is the support span, and t is the measured thickness of the coupon.

Ammar (1996) performed three-point bending tests on several 5-in. long x 1.44-in. coupons using Intron 1120 at the University of Delaware to determine the flexural strength, which yielded a mean value of 135±4 ksi and also plotted longitudinal stress vs. longitudinal strain until failure. Flexural modulus was calculated from the plot using ASTM D7264, which yielded a mean value of 16,000 ksi, as shown in Figure 90.

The average flexural modulus of control and field coupons were 15,402±557 ksi and 13,560±765 ksi, respectively, as shown in Table 8. Upon comparison, the average flexural modulus of control and field coupons after 22 years was found to be 4% and 15% less than the flexural modulus obtained from Ammar (1996), respectively. The average flexural modulus of control coupons was found to be 14% higher than that of field coupons. The reduction in flexural modulus for both control and field coupons was found consistent with the reduction in tensile modulus.

Similarly, the average flexural strength of control and field coupons were 146±10 ksi and 108±8 ksi, respectively, as shown in Table 8. Upon comparison, the average flexural strength of control coupons after 22 years was found to be 8% higher than the flexural strength obtained from Ammar (1996), while the average flexural strength of field samples was reduced by 25%. After 22 years of service, the flexural strength of field coupons was found to be lower than the design ultimate flexural strength computed using the C_E factor of 0.85 recommended by ACI440.2R (2017). Some reduction in strength, similar to tensile modulus, may be due to specimen extraction/manipulation procedures. However, considering the increment in number of peak strain events over the 22 years' service life and reduction in T_g of the field CFRP composite, it is likely that degradation also occurred. Considering the present data, a C_E factor of 0.75 may be more adequate within the considered service life (22 years) than the 0.85 value currently recommended by ACI 440.2R.

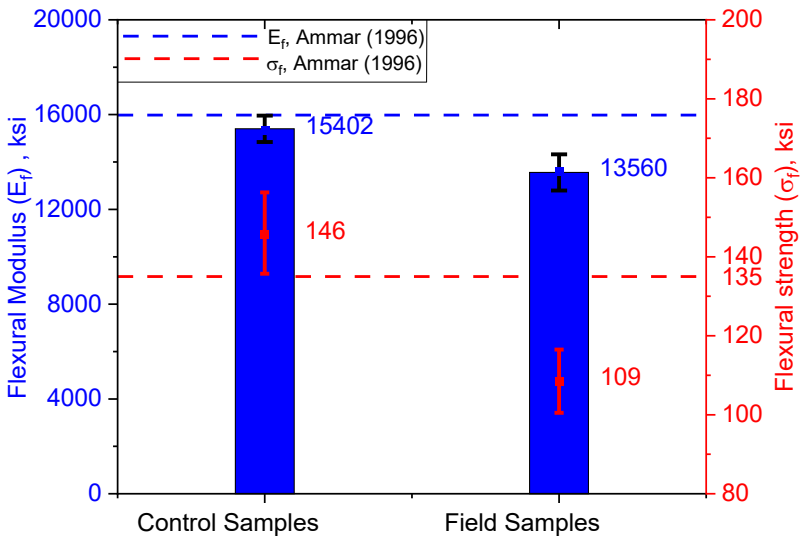

Figure 90. Flexural modulus and flexural strength of field and control coupons vs. Ammar (1996).

Table 8. Flexural modulus of elasticity and flexural strength at failure of coupons - from Bridge 1-704.

04 Label	Flexural Modulus E_f, ksi	Average, ksi	Standard Deviation (COV)	Flexural strength σ_f, ksi	Average, ksi	Standard Deviation (COV)
BG5-C1	15,103	15,402	557 (3.6%)	140	146	10.3 (7%)
BG5-C2	15,581	15,402	557 (3.6%)	160	146	10.3 (7%)
BG5-C3	14,831	15,402	557 (3.6%)	137	146	10.3 (7%)
BG5-C4	16,096	15,402	557 (3.6%)	148	146	10.3 (7%)
BG5-F1	14,346	13,560	765 (5.6%)	103	108.5	8.02 (8.8%)
BG5-F2	12,511	13,560	765 (5.6%)	103	108.5	8.02 (8.8%)
BG5-F3	13,667	13,560	765 (5.6%)	120	108.5	8.02 (8.8%)
BG5-F4	13,715	13,560	765 (5.6%)	108	108.5	8.02 (8.8%)

DISCUSSION

Several tests were conducted in the field and laboratory to assess the influence of environmental factors on the mechanical, thermal, and chemical properties of the CFRP composites. Over the last 22 years, no chemical degradation was observed; however, the thermal and mechanical properties were found to have degraded. Exposure to a humid environment (monthly average RH of 61 to 72%) likely played a significant role in the degradation process. The presence of corrosion beneath the CFRP composite further supports the assertion that moisture was a leading cause of composite degradation. The reduction of T_g, in absence of evidence of chemical degradation, can be accredited to plasticization caused by moisture uptake. In addition to affecting the T_g, plasticization is also linked to reduced elastic modulus and strength of thermosetting polymers, which can have consequences on the macroscale properties of the composite. Furthermore, prior research has indicated that moisture can lead to the weakening or debonding of the fiber-matrix interface. These effects combined could explain the recorded reduction in mechanical properties of CFRP coupons observed in tensile and flexural tests.

The performance of the bond and adhesive between CFRP composite and steel substrate was assessed through acoustic sounding, pull-off bond test, structural health monitoring, and DSC. Acoustic sounding and visual inspection revealed no signs of debonding. The effect of fatigue on the performance of the bond was found to be less concerning, as the number of fatigue cycles and actual stress that the CFRP/steel bond underwent was significantly lower than the test performed by Miller (2000). The lower-bound bond strength in tension for 89% of the pull-off test specimens was found to be 186%, or more than the minimum requirements for zinc coatings on a steel substrate. However, several pull-off tests near the north end of the girder (where corrosion was observed) exhibited low bond strength values ranging from 38 to 42 psi. Interestingly, the T_g of the adhesive near low pull-off bond strength locations was low (average of 36 °C), providing additional evidence that moisture penetration near the CFRP ends was the likely cause of degradation. While structural health monitoring data provide further evidence that the condition of the entire girder has changed over the 22-year period, it cannot be stated with confidence what the main cause of observed changes was. Further research is required to quantify potential degradation (i.e., loss of stiffness) at the girder-to-deck interface, concrete deck, supports, etc.

CHAPTER 4

Foulk Road Bridge

METHODOLOGY

Description Of the Bridge

The State of Delaware has the first externally bonded CFRP repair installed on a publicly owned bridge in the United States in its inventory, the Foulk Road bridge, located in Wilmington, DE. The bridge was originally built in 1965. The bridge superstructure consists of 23 prestressed adjacent box-beam girders supported by concrete abutment walls at each end (Figure 91). The span of the bridge is 54 ft. The bridge was retrofitted in 1994 due to severe longitudinal cracking on the bottom face of box girders. It is believed that these cracks were caused by the lack of transverse reinforcement or due to reinforcement corrosion. To address this issue, unidirectional CFRP composite was externally bonded to the bottom face of the girders, with fiber oriented in the transverse direction to the beam length (Figure 92).

(a) (b)

Figure 91. Foulk Road bridge in Wilmington, DE

Box-Beam Bridge Deterioration

Adjacent box girders are widely used in the United States for short and medium spans up to 100 ft. Girders are placed against each other and connected by grouted shear keys or tie rods. Wearing surface is formed by placing either concrete or asphalt on top of the girders. Typical box-beam geometry with partial-depth shear key, design approach used for Foulk Road bridge, is shown in Figure 93. As shown in the figure, box sections have transverse reinforcement along the top face, but not along the bottom face.

Despite the fact that adjacent box-girder bridges have many advantages (ease of construction, shallow superstructure depth, and high torsional stiffness), issues with durability performance resulted in premature deterioration in many bridges in the United States. After 25 to 30 years in service, several box-beam bridges in Delaware, built in mid 1960s, developed longitudinal cracking on the beam soffit. Investigation of this problem showed that cracking in the grout keys and overlay above the keys is the leading cause of major issues. Cracks in the overlay allow water and deicing chemicals to penetrate into the empty voids and between the shear keys along the full length of the beams. Permeability of concrete allows chlorides and other aggressive agents present in the water to diffuse into concrete and initiate corrosion of reinforcement and prestressing strands, which subsequently cause cracking, spalling, and breaking of prestressing tendons.

Design and construction of girder connections have been recognized as critical to adjacent box-beam bridge durability. Failure of shear keys leads to loss of continuity and differential movement of beams and eventually overloading of individual beams. To prevent differential movement, solutions such as transverse post-tensioning and heavy composite topping were employed.

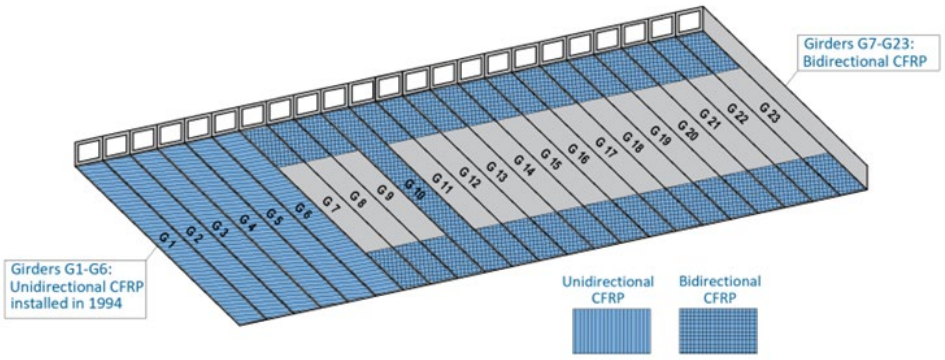

Figure 92. Foulk Road bridge-plan of repaired girders.

FRP Adjacent Box Girders Repairs

To avoid bridge replacement, CFRP was installed on the bottom face of Foulk Road bridge girders in 1994 to extend its service life for 5 to 10 years. The strengthening scheme included bonding unidirectional carbon fiber sheets with fibers oriented perpendicular to the longitudinal axis of the girders to compensate for the missing transverse reinforcement on the bottom face of the girders. The composite system used for girder repairs was Forca Tow Sheets, FTS-C1-20 and FTS-C5-30, manufactured by Tonen Corporation, Japan (Table 9). The Forca Tow Sheet system consists of unidirectional carbon fibers, a two-part epoxy primer to enhance adhesion, a two-part epoxy resin to bond carbon fiber to the concrete surface, and a saturant. The unidirectional carbon fiber prepreg is made of fiber tows fixed to a release-coated paper.

Detailed CFRP installation procedures can be found in the published literature (Finch, 1997). The tow sheet installation procedure involved: (1) application of a two-part epoxy primer; (2) curing the primer coating for 24 hours before installing the Tow sheet; (3) mixing and application of the epoxy adhesive layer; (4) applying Tow prepreg sheet to the concrete surface, and (5) applying a secondary coat of the epoxy resin to impregnate the sheet. Lastly, quality control testing was conducted to determine the presence of voids using acoustic sounding. However, tensile testing to determine the tensile strength of the Tow sheet and the quality of the bond to the concrete were not performed. According to the available literature, protective paint was not applied to the surface of the CFRP.

Six girders were selected for retrofitting based on their condition and accessibility. Girders were numbered as G1 to G6, with the easternmost girder denoted as G1 (Figure 93). Girders G1, G2, G3, G5, and G6 were repaired with one ply of FTS-C1-20, and girder G4 with two plies of FTS-C5-30 (Table 9). The mechanical properties for both types of sheets are given in Table 9 (taken from the manufacturer's technical data sheets). The CFRP applied to G1, G2, G3, G5, and G6 was designed to have tensile strength equivalent to the yield strength of #4 bars spaced at 12 in. on center (yield force 6.3 kips/12 in., assuming steel reinforcement yield strength of 61 ksi, the cross-section area of #4 bar of 0.18 in^2, and safety factor for reinforcement steel of 0.6). After applying a safety factor of three to the tensile strength of the composite, it was determined that the tensile capacity of a 12 in. wide sheet of FTS-C1-20 is 7.65 kips (assuming tensile strength of 550 ksi and 0.004 in. design thickness), which is sufficient to compensate for the tensile strength of the missing reinforcement bars (6.3 kips/12 in.). The CFRP installed on G4 was designed to have the same stiffness (EA, where E is the tensile modulus, A- cross-section area) as the #4 bars, which is 5,680 kips/12 in. EA of C5-30 is 4,210 kN/12 in.; therefore, it was decided to use two plies of this material.

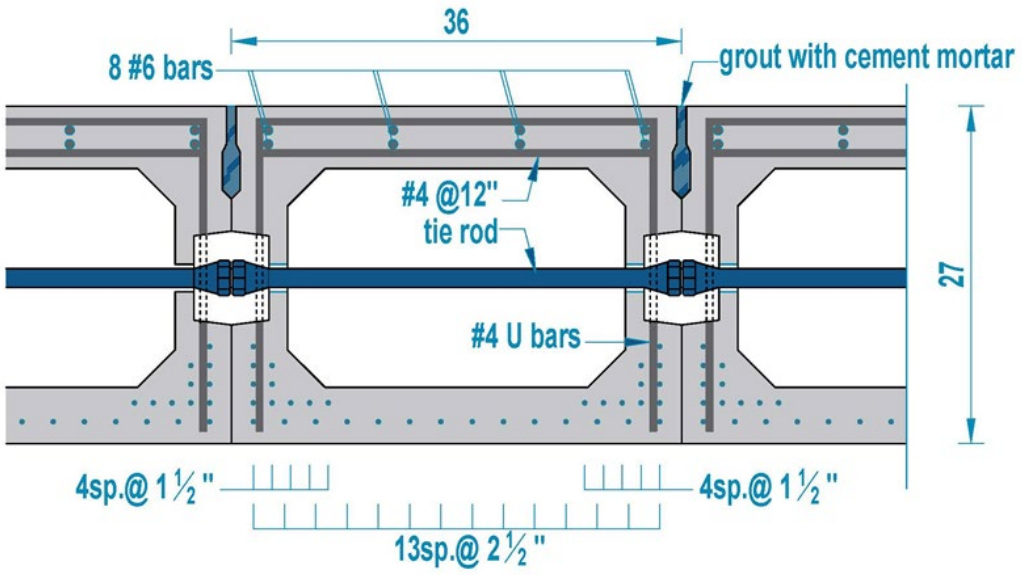

Figure 93. Cross-section of typical girder - Foulk Road bridge.

Table 9. Tow sheet manufacturer's mechanical properties.

Tow Sheet Grade	FTS-C1-20	FTS-C-30
Fiber type	High Tensile Carbon	High Modulus Carbon
Fiber Density (oz/in3)	1.05	1.05
Fiber Areal Weight (oz/yd2)	5.9	7.4
Tow Sheet Width, inches	19.7	19.7
Tensile Strength, lb/inch	2,200	2,800
Tensile Modulus, lb/inch	145,000	350,000
Design Thickness, inches/ply	0.00433	0.00650
Tensile Strength for Design, ksi	505	427
Tensile Modulus for Design, Mpsi	33	54
Ultimate Elongation, %	1.5	0.8

Source: Finch, 1997

Visual Inspection

The bridge was visually inspected to identify and document defects such as cracking in the concrete, corrosion, issues with FRP, and condition of the overlay, joints, and abutment wall.

Material Characterization Experiments

Differential Scanning Calorimetry

Differential scanning calorimetry (DSC) was used to measure the glass transition temperature (T_g) of CFRP material samples collected from four girders (G1, G2, G4, G23). The glass transition is a range of temperatures over which amorphous polymers transition from a glassy to a rubbery state (Michel and Ferrier, 2020). Netzsch DSC 214 Polyma (Selb, Germany) was used for calorimetric measurements. Three replicate samples were taken from 0.8 in. circular CFRP samples that were previously extracted from girders G1, G2, G6, and G23 using a saw with a diamond drill bit. The samples (10 mg to 20 mg) were placed inside aluminum pans, sealed, and then heated from -20 °C to 200 °C at a heating rate of 10 °C/min under a nitrogen atmosphere. Aluminum crucibles were pierced to prevent pressure build-up during the experiment. Mineral oil (Krytox GPL 107 fluorinated synthetic oil, The Chemours Company FC, LLC, Wilmington, DE, US) was applied to the bottom of the pans to improve contact and heat transfer between the sample and the pan. An empty sealed aluminum crucible was used as a reference inside the furnace. Results were analyzed using NETZSCH Proteus TA software to determine the T_g. By selecting the slope of the heat flow/temperature curve before and after the transition, the software automatically calculates T_g according to ASTM E1356 (2008) procedure, which defines T_g as a midpoint of glass transition range. At temperatures above T_g, the mechanical properties of amorphous polymers decrease considerably. For this reason, it is important that T_g of the composite is above the service temperature. To prevent stiffness degradation and loss of load-carrying capacity of CFRP-strengthened members, design specifications/guidelines recommend minimum T_g values. For example, the American Association of State Highway and Transportation Officials (AASHTO-FRPS-1, 2012) recommends that the T_g of the composite, measured using the Dynamic Mechanical Analyzer, be at least 22 °C higher than the design service temperature. ACI 440.2R has a slightly less conservative recommendation and suggests that T_g of the composite be 15 °C above the design service temperature.

Spectroscopy

FTIR spectroscopy is commonly used for the chemical characterization of polymers. When using FTIR, a material is irradiated with infrared light over a range of wavelengths, and absorption is measured as a function of the wavelength. The wavelength of absorption is characteristic of atomic bonds. Resonance interaction between the incident light and a specific vibrational mode results in an FTIR spectrum that can give information on the chemical bonds found in a substance and thus allows its identification. This technique has been used to monitor curing reactions and the degradation of composite by following the concentration of characteristic functional groups (Rezig et al., 2006). The concentration of these functional groups is linearly related to the peak intensity in the FTIR spectra (Min et al., 1993).

FTIR was conducted using a Nicolet Nexus 870 ESP FTIR spectrometer in attenuated total reflection mode (ATR-FTIR). Analyses were carried out with a diamond crystal. Spectra were recorded in the 400-4000 cm^{-1} range at 4 cm^{-1} resolution. All spectra were the average of 64 scans. Background spectra were collected within 60 min of sample spectra collection. "Origin" software was used for baseline correction. To compare peak intensity between different samples, all spectra were normalized to 1,509 cm^{-1} peak recorded on G-2

sample. The value 1,509 cm^{-1} was chosen as a reference based on the literature (Lin et al., 2006; Morsch et al., 2020). ATR-FTIR was performed on the front side of the material samples from five girders (G1, G2, G4, G6, and G23) to investigate if exposure to the environment induced chemical degradation of the CFRP composite. The surface layers of the sample collected from G1 and G23 were sanded, while samples from the other three girders were not.

In Raman spectroscopy, a sample is irradiated with a monochromatic light source (usually a laser). Most of the incident light is scattered off the sample at the same wavelength as that of the laser—a process known as Rayleigh scattering. However, a small amount will scatter from the sample at a wavelength different than the original laser wavelength—this is called Raman scattering. Raman spectroscopy is similar to FTIR; these two vibrational spectroscopy techniques are actually complementary. Vibrations that are strong in an infrared spectrum are usually weak in a Raman spectrum. Likewise, functional group vibrations that give very strong Raman bands usually result in weak infrared signals. For example, hydroxyl- or amine-stretching vibrations and the vibrations of carbonyl groups are usually strong in an FTIR spectrum and are usually weak in a Raman spectrum.

All Raman experiments were carried out on a Kaiser spectrometer equipped with a 785-nm laser. Spectra were recorded in a range of 400-4,000 cm^{-1} at a laser power of 50 mW. Spectra consisting of 10 co-added spectra, each collected with an exposure time of 1 s, were recorded at 4 cm^{-1} spectral resolution. Baseline correction was performed in Origin software, since the fluorescent background and baseline drift appear in the spectra. The background spectra were collected before recording each sample spectra and automatically subtracted. All measurements were taken in the absence of room light to avoid any interference. Baseline correction was performed through subtraction of a linear fit of the baseline from the raw spectrum to remove baseline variation caused by various noises. Spectra were normalized to the phenyl peak height at 1610 cm^{-1} of G1 sample.

Scanning Electron Microscope

A Hitachi TM-3000 scanning electron microscope was used to examine the microstructure of aged CFRP. The SEM specimen preparation procedure involved impregnating a 0.4-in.-long piece of CFRP in epoxy resin. The surface of the impregnated specimen was sanded and polished using silicon carbide polishing paper and aluminum oxide suspension as abrasives. SEM observations were conducted at a 5 kV accelerating voltage.

Tensile Tests

Tensile tests were performed on five tabbed coupons prepared according to procedures specified in ASTM D 3039. Tensile specimens, each 10 in. long and 0.4 in. wide, were cut from a CFRP sample previously peeled from girder G1. Gripping tabs (2 × 0.4 × 0.08 in., made of glass/epoxy composite) were tapered, sandblasted, and bonded to both ends of each specimen using a two-part adhesive. The adhesive was allowed to cure at ambient temperature for 1 week prior to tensile testing.

CFRP coupons were tested on Instron Universal Testing Machine 5900R-4484. Samples were loaded to failure at a constant displacement rate of 0.08 in./min. The strain was measured with strain gages (0.2 in. gage length, 120 Ω resistance) attached to the CFRP coupons with an adhesive, cured at room temperature. Experimental data were collected using a Micro-Measurements data acquisition system.

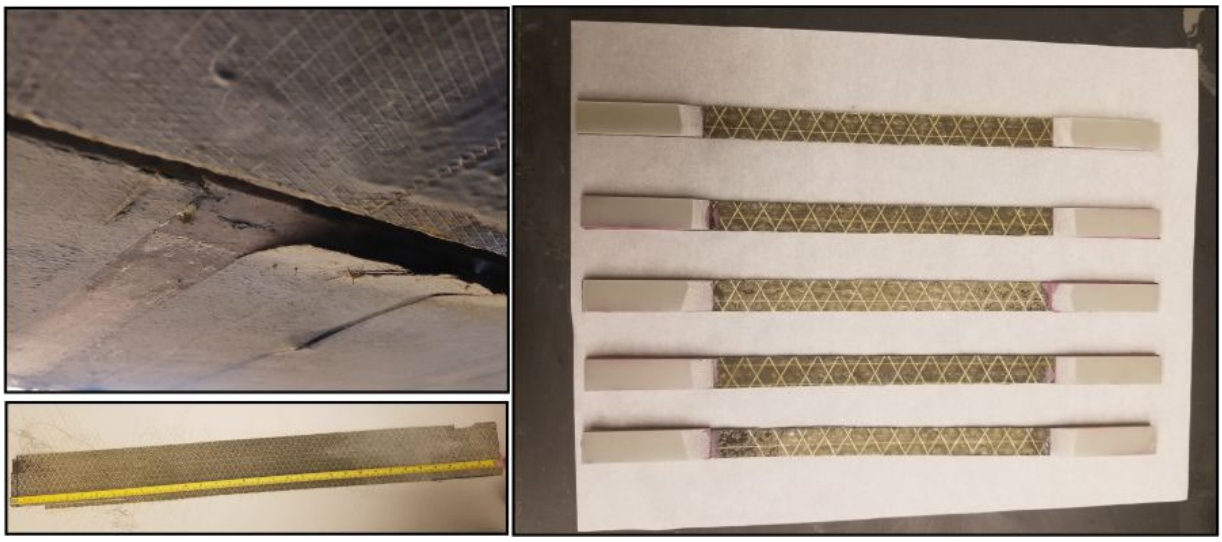

Figure 94. Specimens for tensile testing were prepared using CFRP material extracted from G1.

Pull-Off Tests

Pull-off tests were conducted in the field to evaluate the pull-off strength of the CFRP composite system bonded to a concrete substrate. Three girders were chosen for pull-off tests: G1, G4, and G23, where a total of eight pull-off tests were performed. Three pull-off tests were performed each on G1 and G23 in October 2020, and the remaining two pull-off tests were conducted on G4 in February 2022. Various factors—the number of CFRP plies, exposure to environmental conditions like moisture, and accessibility were considered in the selection of test girders. Girders G1 and G23 were selected as pull-off test locations because they were retrofitted with a single ply of CFRP, were easily accessible, and lastly, had greater exposure to moisture from the water draining from the deck, as indicated by pronounced water stains. G4 was selected, as it was the only girder that was retrofitted with two plies of CFRP. Pull-off tests on each girder were conducted at locations where the CFRP bond seemed visually intact: free of cracks, delamination, and voids, at a sufficient distance from the edges of the girder and the CFRP. A minimum clear spacing of 6 in. between test locations and a minimum clear distance of 4 in. from the edges of the girders or CFRP was maintained at all test locations.

Before attaching an aluminum puck to the girder, the CFRP surface was lightly sanded to remove the paint, surface defects, and irregularities, followed by drilling a circular hole using a 2.25-in. diamond-coated core saw through the CFRP and 0.16 in. into the concrete. A wooden rig with a 2.25-in. hole was anchored into the concrete girder to minimize vibrations and ensure precision during the drilling process. Test pucks were also manually roughened with sandpaper. Both test puck and sanded CFRP surface were then cleaned with acetone. Two-part epoxy adhesive (J-B Weld Quick-Setting Epoxy) was applied to the test puck after mixing part A and part B in the ratio of 3:1 by volume. The puck was then attached to the girder within 15 minutes of epoxy mixing and centered at the previously drilled core. A piece of plywood was placed over the puck and anchored into the concrete girder to keep the puck in place while it cured. After one week of curing, a Proceq DY-216 adhesion tester was used to conduct the test as specified by ASTM D7522 (2021). Load was applied to the puck at a constant loading rate of 1.88 psi/s, as recommended by ASTM D7522. Maximum failure load, failure mode, and photographs of the puck after the test was recorded. The failure mode identified based on the location of the failure interface, as shown in Figure 71, was evaluated according to ASTM D7522 (2021).

EXPERIMENTAL TEST RESULTS

Visual Inspection

The focus of the visual inspection of the bridge was on the CFRP repairs, but the overall condition of the concrete girders was also visually assessed. During the first visit (September 15, 2020), it was noted that all girders were strengthened with CFRP, not only the six girders previously described. Design plans or any other records of the repair of girders G7 through G23 were not found. The wrapping scheme of these girders (G7 through G23) involved CFRP bonded to the soffit of the girders only near the supports (approximately 13 ft). After extracting a CFRP sample from G23, it was determined that the type of composite material installed here was bidirectional CFRP.

During the visual inspection of concrete girders, the team observed concrete spalling, corrosion, and cracking in many girders (Figure 96 and Figure 97). Severe cracks on the bottom of G7 (0.12 in. wide and a 13-ft.-long crack in the middle of the span), G15, and G17 were detected (Figure 96a,b,c). Based on a visual inspection conducted prior to bridge rehabilitation in 1994, the crack on G7 already existed (Finch, 1997). There were multiple patched cracks on the south abutment wall and a large spall below G23 (Figure 95a,b). The abutment is approximately 89 ft long and was built in the 1960s. There are provisions for long concrete structures nowadays to include contraction joints (ACI 224.3R, 1995), but that may not have been the case at the time of construction. The repaired cracks were noted in previous bridge inspection photos and date back as far as 2001.

Debris, motor oil, and efflorescence were observed near the joints (Figure 97d,e,f). Many blisters below the CFRP observed on girders G1-G6 are evidence of severe issues with exposure to water and humidity. When water infiltrates into the voids behind CFRP it can slowly react with components in concrete (sodium, potassium, calcium compounds). Once water is chemically modified by the dissolution of cement components, its solvency for CO_2 is also affected. A small fraction of the CO_2 that dissolves in water reacts rapidly to form carbonic acid. Carbonic acid partially dissociates to form hydrogen, bicarbonate, and carbonate ions ($CO_2 + H_2O \leftrightarrow H_2CO_3 \leftrightarrow H^+ + HCO3^- \leftrightarrow 2H^+ + CO_3^{2-}$). Finally, Ca compounds from cement and dissolved $CO3^{2-}$ react, precipitating CaCO3 (Dow and Glasser, 2003). The presence of calcium carbonate was confirmed by FTIR spectroscopy (Section 0).

Asphalt pavement was also inspected, and the location of longitudinal cracks was recorded. Longitudinal cracks were superimposed (Figure 95c) to the underlying joints to determine if there is a pattern in the development of cracks, since reflective cracking is reported as a common issue in adjacent box-beam girders (M.Ahiborn et al., 2005). As shown in Figure 95c, longitudinal cracks in the asphalt are immediately above or near the shear keys. Cracks in the asphalt allow water and deicing chemicals to infiltrate, leading to corrosion of post-tensioned reinforcement.

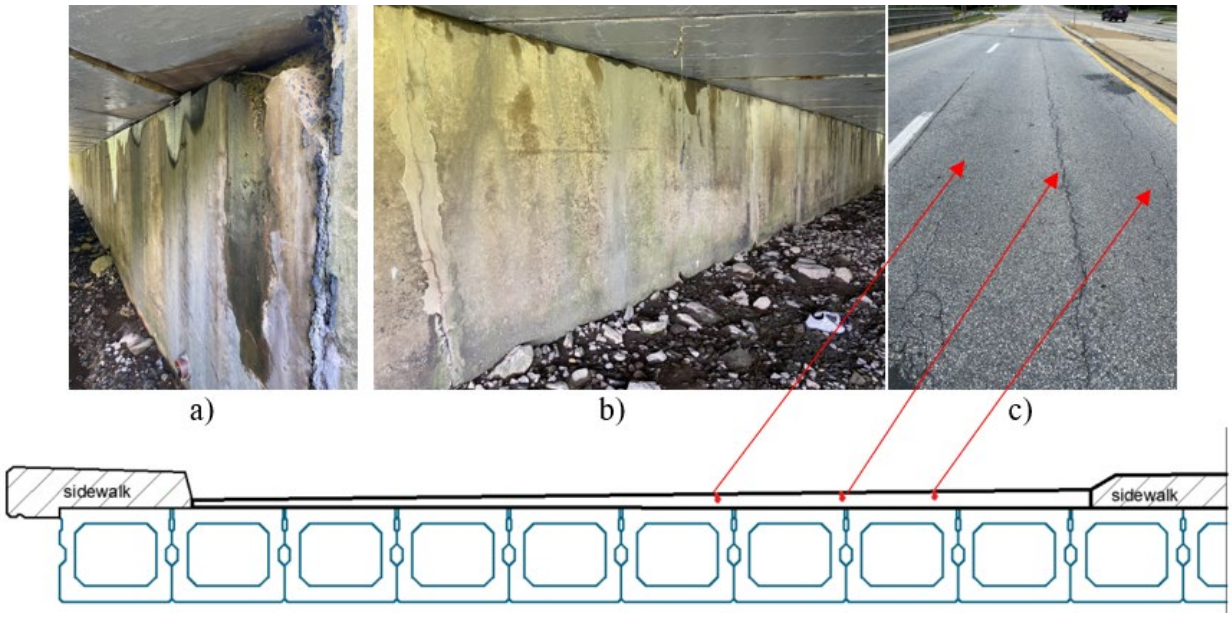

Figure 95. (a) Spalling of the south abutment wall, (b) vertical cracks in the abutment wall, and (c) reflective cracking of the asphalt pavement.

(a) (b) (c)

Figure 96. Longitudinal cracks in G7, G15, and G17.

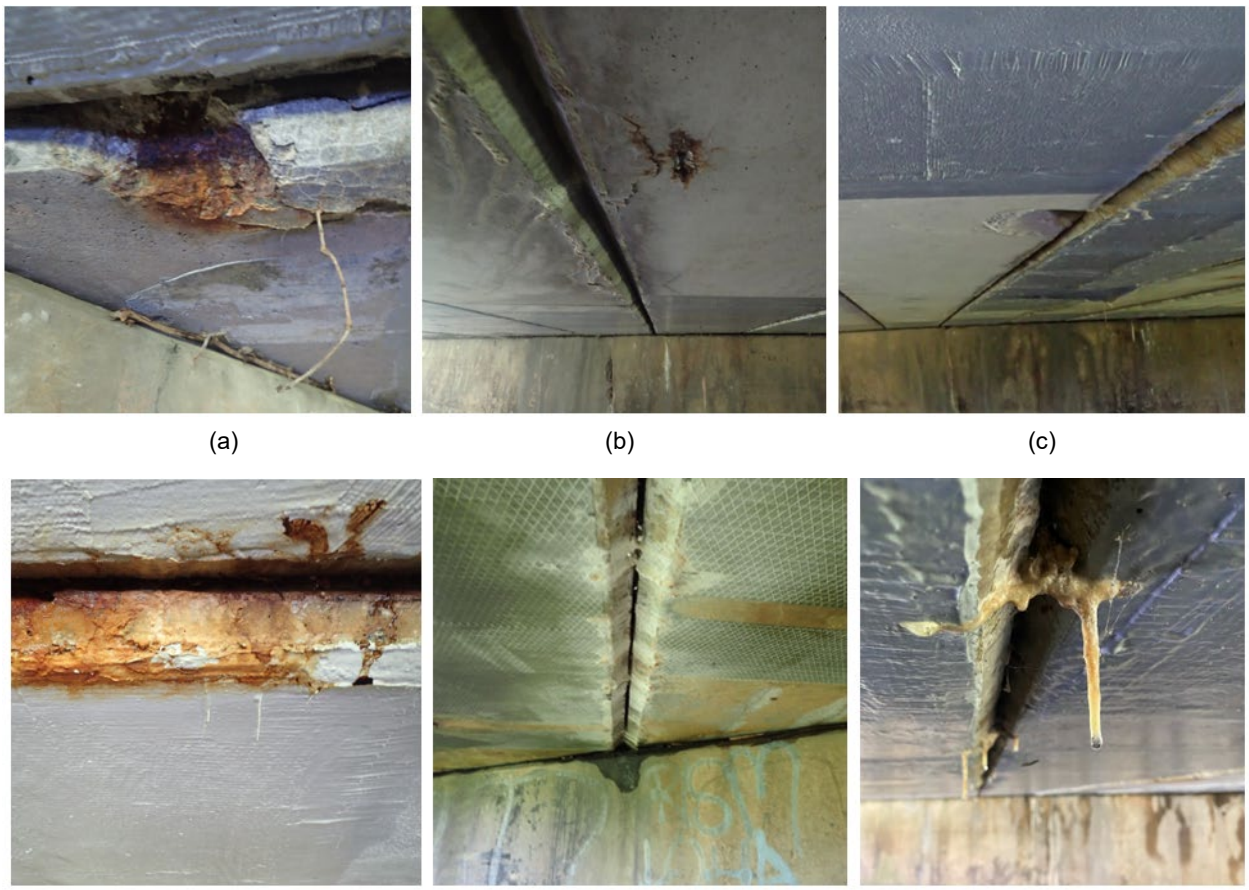

(a) (b) (c)

(d) (e) (f)

Figure 97. Examples of damaged girders and condition of joints: (a,b,c) concrete spalling, (d) motor oil in the joint, and (e,f) efflorescence.

During the second visit (September 21, 2020), all girders were photographed to document existing CFRP damage: discoloration, composite degradation, insufficient saturation, and water staining. CFRP repairs of girders G1 and G2 were in poor condition—there were large water stains, discoloration, insufficient saturation (i.e., dry fibers), and evidence of loosely bonded CFRP that could be effortlessly peeled from the girder (Figure 98d). Similar issues, but with less discoloration and better fiber saturation, were noted on CFRP bonded to G3, G4, G5, and G6. Bidirectional CFRP installed on girders G7 through G23 was visually in better condition than repairs installed in 1994. However, the CFRP of several girders was damaged (on G10, G11, and G15) due to spalling of the concrete substrate (Figure 99).

(a) (b) (c)

(d) (e) (f)

Figure 98. Examples of damage of unidirectional CFRP: (a) end peeling, (b) insufficient saturation, (c) blistering, (d) delamination, (e) frayed fiber, and (f) water stains.

(a) (b) (c)

Figure 99. Examples of damage of bidirectional CFRP: (a,b) spalling/CFRP tearing, and (c) bulging below the CFRP indicates the presence of a longitudinal crack.

Material Characterization Experiments

Differential Scanning Calorimetry

The primary objective of DSC experiments was to determine if environmental exposure during 26-year service life had an effect on the $_g$ of the CFRP bridge repairs. Figure 100 shows $_g$ of composite samples from girders G1, G2, G4, and G23. $_g$ of the CFRP installed in 1994 varied between 46 °C and 51 °C. These values were lower than $_g$ of the samples collected from G23 with the $_g$ of 65 °C. The lowest $_g$ was measured on G4. As shown in Figure 98, CFRP on G1 and G2 seemed more deteriorated compared to other girders. It was expected that the $_g$ of composite repairs on G1 and G2 is lower than on G4,since they

seemed more degraded and had more exposure to water, which is related to decreased cross-linking density through polymer chain scission/oxidation/hydrolysis (Lin et al., 2006). Surprisingly, the T_g values were 10% higher in G1 compared to G4. Lower T_g observed in G4 could be attributed to different thermal history. It is possible that exterior girders were more exposed to sunlight. Thermal history directly affects the cross-linking density (i.e., exposure to higher temperatures enhances the epoxy-amine reaction and results in stiffer network and higher T_g).

To determine the effect of environmental exposure during service life on T_g, its initial values are required. According to the available literature, the selection of resins manufactured by Tonen Corporation includes three different types of epoxies suitable for various climate conditions: FR-E3P (standard resin), FR-E3PS (resin summer), and FR-E3PW (resin winter) (Naaman et al., 1997). The resin used on the Foulk Road bridge in 1994 was standard resin FR-E3P (Finch, 1997). A patent filed in 1995 (Saito, 1996), reports a T_g of 50 °C after 7 days curing at room temperature (20 °C) for this type of epoxy.

Assuming that 50 °C was the initial T_g value of the FR-E3P resin, it can be concluded that the reduction in T_g ranged from 0 to 10%. Decrease in T_g of 10% is lower compared to some results reported on artificially/naturally aged epoxy resin. A decrease in T_g in the range of 10%–25% was measured during natural exposure in a tropical environment for no longer than 1 year (Lettieri and Frigione, 2011; Belec et al., 2015). Finally, measured T_g was compared to AASHTO recommendations. Given that maximum design temperature for Delaware is 45 °C, and taking into account AASHTO guidelines (minimum T_g of 45 °C +21 °C) low values like these are deemed inadequate.

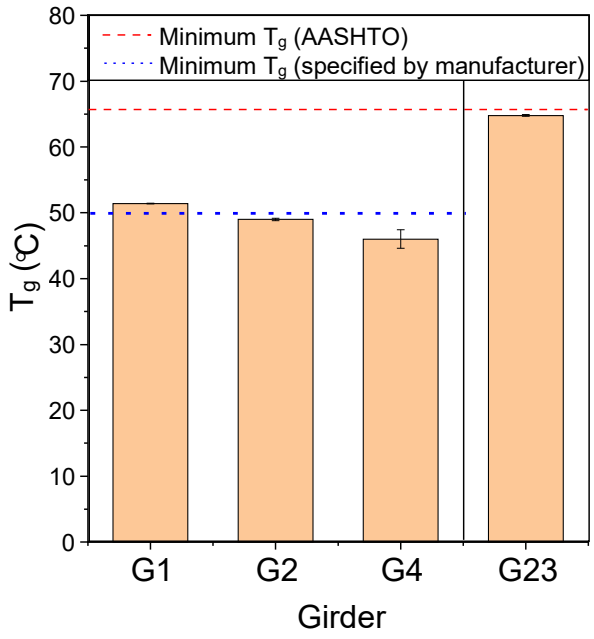

Figure 100. Glass transition temperature measured on samples from girders G1, G2, G4, and G23.

FTIR and Raman Spectroscopy

The degradation process due to typical service conditions including the combined effect of mechanical stress, oxygen, moisture, and temperature variation, is quite complex. Chemical degradation can be

detrimental to the resin and results in reduced glass-transition temperature and microcracking on the micro-level (Xiao and Shanahan, 1998). On the macro-level, the scission of the polymer chains leads to a decrease in tensile and shear strength and elastic modulus (Doblies et al., 2019). Previous research has shown that the changes in the epoxy/amine chemical structure after degradation result mainly from the formation of carbonyl products, growth of amide functions associated with amines, and chain scission reactions (Ernault et al., 2017). Most carbonyl compounds have IR and Raman bands in the 1,550–1,900 region.

ATR-FTIR spectra are shown in Figure 102. Some differences among the spectra were observed: (1) peak at 1,658 cm^{-1} is prominent in some samples; (2) peak at 1,738 cm^{-1} and peak at 874 cm^{-1} is present in the CFRP samples from G1 and G2, but not in the G6 and G23 samples; and (3) a relatively small peak at 1,540 cm^{-1} in the spectra of G2 and G6 samples.

The band at 874 cm^{-1} corresponds to calcium carbonate (Xyla and Koutsoukos, 1989) formed on the concrete surface. As shown in Figure 97, efflorescence was observed on many girders. Efflorescence is typically composed of calcium carbonate formed when leached calcium hydrate (CH) from concrete reacts with carbon dioxide in the atmosphere (Dow and Glasser, 2003).

Almost all FTIR spectra recorded on G1, G2, G4, and G6 show the presence of the peak at 1,656 cm^{-1}, which indicates amine cross-linker-related degradation. The appearance of a band around 1,660 cm^{-1}–1,670 cm^{-1} is reported in amine-cured epoxies (Delor-Jestin et al., 2006; Meiser and Possart, 2011) after thermal aging, hygrothermal cycling (Lin et al., 2006), and UV exposure and outdoor weathering (Belec et al., 2015; Gu et al., 2005), including thermooxidation under mild conditions (70 ℃, 80% RH), Morsch et al., 2020). Researchers suggest that the formation of the 1,657 cm^{-1} band involves a reaction on the phenoxy group and corresponds to quinone methide (Mailhot et al., 2005). According to a different mechanism, 1,658 cm^{-1} is related to amine cross-linker oxidation. As proposed by Morsch et al., 2020, products of imine hydrolysis contribute to the absorbance at 1658 cm^{-1} (primary amine N-H bend).

The peak at 1,738 cm^{-1} was present only in the spectra from G4. This peak was previously reported to correspond to the phenyl formate. The sample from G4 had the lowest T_g, too (Figure 100). It is difficult to state what would be the underlying mechanism of the observed decrease in T_g, but the presence of 1,738 cm^{-1} suggests that the chemical degradation is causing it (possible chain scission reactions in hydroxypropyl ether groups in DGEBA are shown in Figure 101).

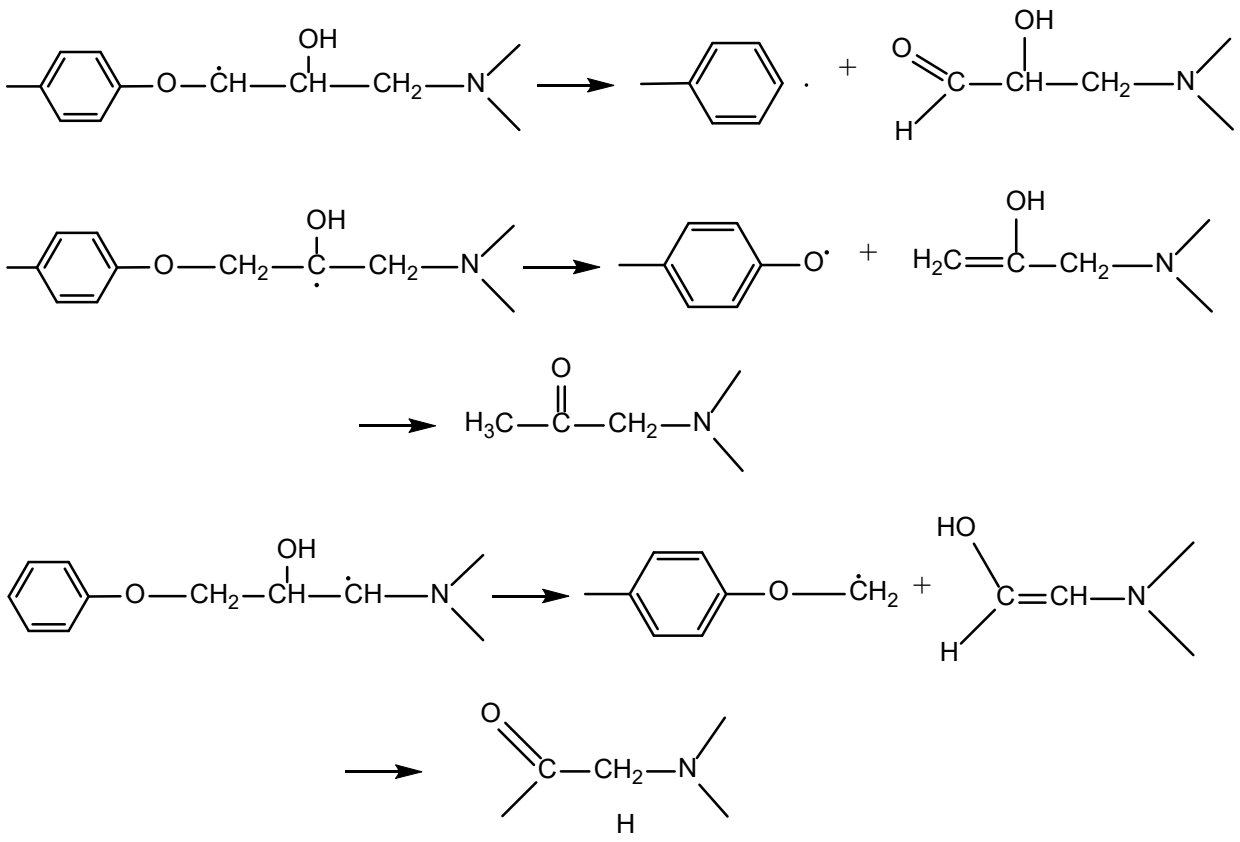

Figure 101. Possible chain scission reactions in DGEBA.

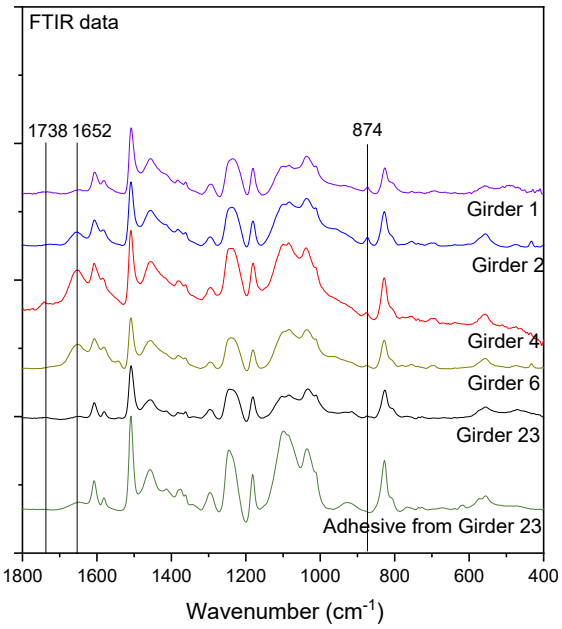

Figure 102. ATR-FTIR spectra of CFRP material samples collected from Foulk Road bridge.

The spectra in the carbonyl range (1,500–1,700) have a poor resolution due to the noise and baseline correction procedures. To provide additional information regarding chemical degradation, Raman spectra were collected. A comparison of Raman spectra recorded on CFRP samples from four different girders are shown in Figure 103. Differences can be noticed at wavenumbers 1,728, 1,525, 1,339, 1,143, 1,000, 744, 680, 585 and 482 cm^{-1}. Published literature on Raman analysis of epoxy was reviewed to serve as a reference for peak assignment (Daimay, 1991; Fu et al., 2020; Rocks et al., 2004; Vaskova and Kresálek, 2011; Younes et al., 1994; Zapata et al., 2013). Two peaks related to degradation are of particular interest: the peak corresponding to the carbonyl group and the peak corresponding to tertiary amides. Tertiary amides are observed in the Raman spectra in the 700–750 cm^{-1} range (Daimay, 1991). The issue with using this peak to monitor the degradation of epoxy/amine is that epoxy ring deformation appears in the Raman spectra at 736 cm^{-1}. Another region of interest is 620–590 related to the skeletal deformation of tertiary amides with R-C(=O)NR2 type of structure. C=O bands are weak in Raman spectra (Daimay, 1991) and they appear at 1,725 cm^{-1}. A 1,725 cm^{-1} peak was observed only in the spectra on G1.

Monitoring variation in peak intensity at 1,324 cm^{-1}, 1,454 cm^{-1}, and 1,150 cm^{-1} is another potentially useful way of monitoring chemical degradation, as these peaks corresponding to C-C functional groups indicate chain scission (Guo et al., 2019). Differences were observed in the Raman spectra from the Foulk Road bridge at 1,447 and 1,142 cm^{-1}, which suggests that degradation occurred.

Table 10. Raman peak assignment.

Raman Spectra from Foulk Road Bridge	Raman Band- Literature	Vibration Modes
482	N/A	
585	N/A	
680	N/A	
744	736, 700–750	C-C stretching vibration
1,000	N/A	
1,108	N/A	
1,142	1,150	C-C stretching, CH bending
1,228	1,231	C-O
1,252	N/A	
1,339	1,324	N/A
1,447	1,454	CH, CH2, CH3
1,728	1,725	C=O (carbonyl)

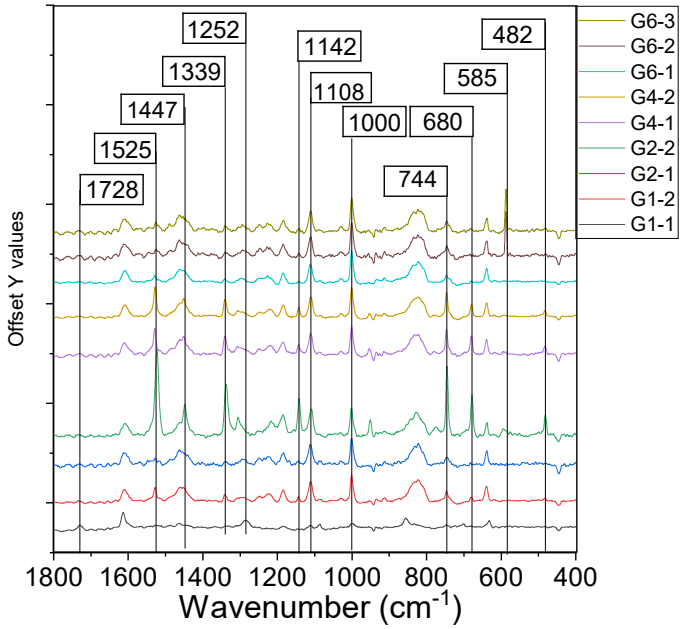

Figure 103. Raman spectra of CFRP samples - Foulk Road bridge.

Scanning Electron Microscopy (SEM)

Figure 104 shows typical SEM images of cross-sections of samples collected from G1, G4, and G23. In the CFRP sample from girder G1 (Figure 104a), matrix cracking was noticed at the fiber/matrix interface. Low magnification images in Figure 104 show the non-uniform distribution of fibers that are about 7 μm in diameter. Cracking along the fiber/matrix interface is one of the most common failure scenarios in composite subjected to static loading or fatigue. This damage mechanism is initiated by the formation of local fiber/matrix debonding, which proceeds until cracks coalesce into one large crack (Pupurs, 2012). This leads to stiffness reduction and eventually results in composite failure (Pupurs, 2012). No evidence of damage was observed in the sample from girder G23 (Figure 104b).

Figure 104c presents a typical SEM image of the sample from girder G4. The image shows two plies of CFRP (~0.5 mm) with a layer of epoxy in between. SEM images show damage in both plies of CFRP but not in the epoxy layer between them. The surface of the exterior ply is the most deteriorated part. Composite damage includes loss of matrix and completely exposed fibers. Synergistic actions of mechanical stress, water diffusion, and temperature are the most likely causes of the composite degradation. The breakdown of resin molecular chains and leaching of broken chains likely increased sensitivity to water uptake, which accelerated resin degradation and fiber-matrix interface.

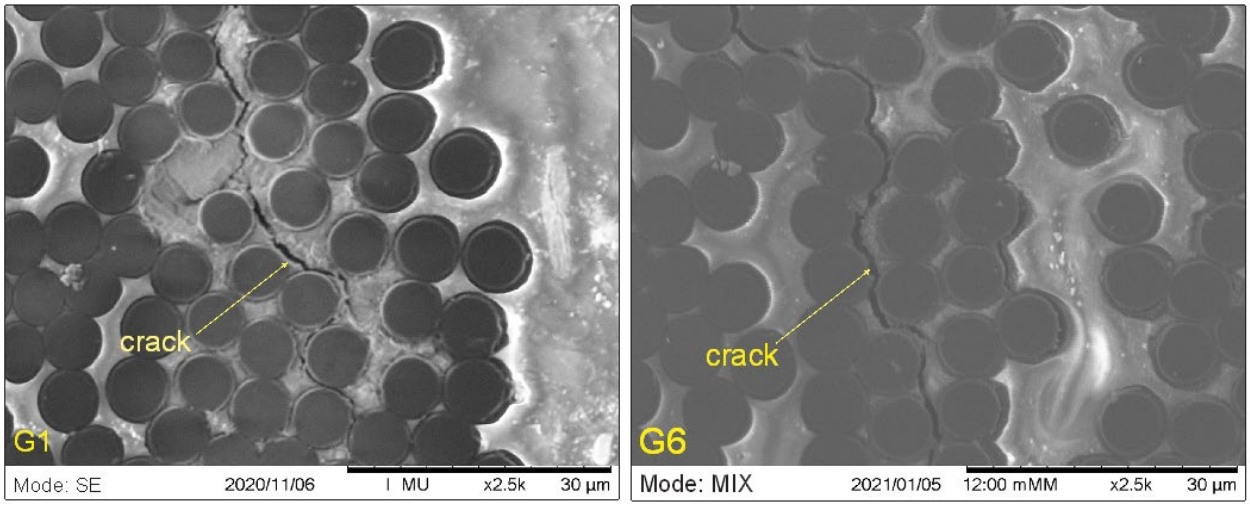

(a) (b)

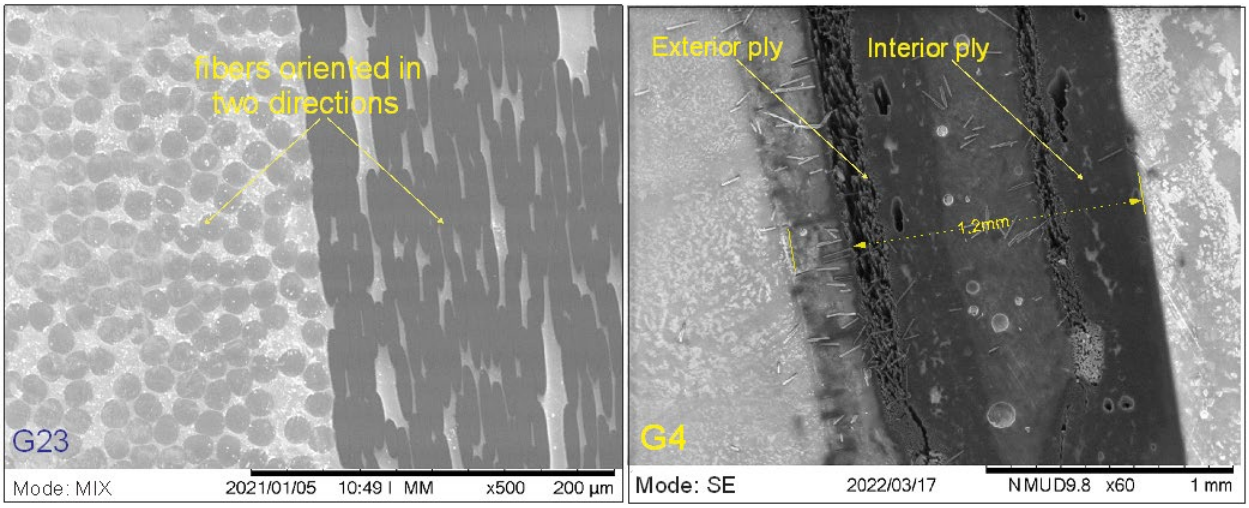

(c) (d)

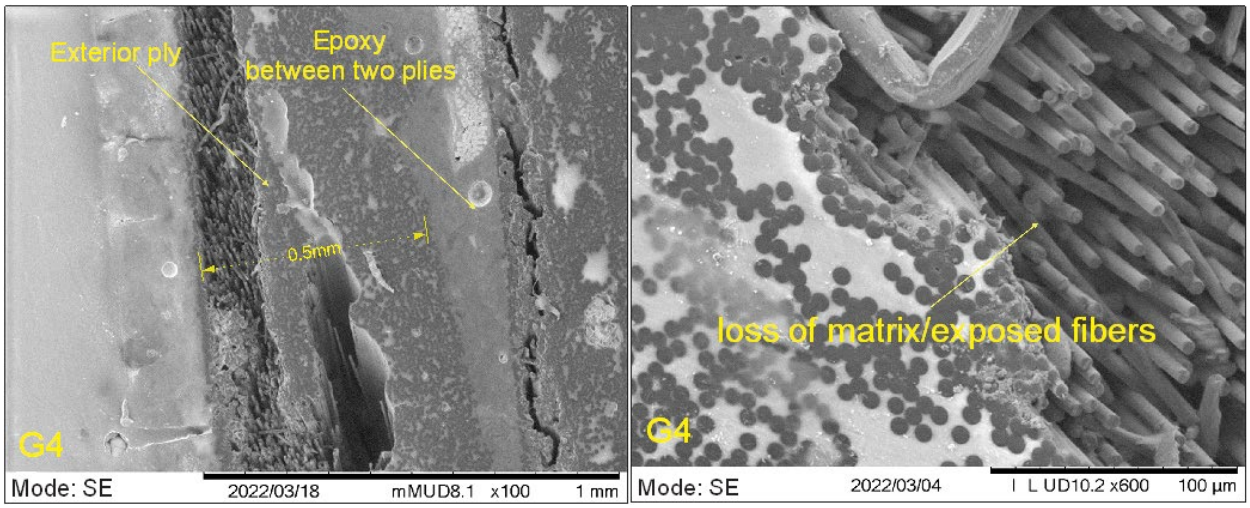

(e) (f)

Figure 104. SEM images of CFRP: (a) cracking at the fiber/matrix interface in G1, (b) cracking in the region of closely spaced fibers in G6, (c) bidirectional CFRP, (d,e) cracking and loss of matrix two-ply CFRP on G4, and (f) high magnification image showing exposed fibers in G4.

Tensile Tests

The tensile strength, modulus, and ultimate strain data for five tested FRP coupons are shown in Table 11. Reported stress, σ, was calculated using nominal thickness $(t*)$ provided by the manufacturer and coupon width (w). Tensile modulus, E, was calculated from the stress-strain curve over the strain range of 0.1% to 0.3%:

$$E = \frac{\Delta\sigma}{\Delta\varepsilon}, \tag{3}$$

where

$\Delta\sigma$ - difference in applied tensile stress between the two strain points

$\Delta\varepsilon$ - difference between the two strain points (0.002)

The average tensile strength was 318 ksi, which is 37% less than the value specified in the materials data sheet—483 ksi. Failure mode can be best described as a staggered failure, with fiber pullout and debonding along the fibers (Figure 105). The load vs. time curve in Figure 106 shows the propagation of the failure where bundles of fiber progressively fail at different locations along the coupon length. As shown in the SEM images, there were many defects in the matrix – cracking and matrix erosion. These defects probably decreased composite strength, since there was not enough resin to ensure uniform distribution of stress between the fibers. According to ACI 440.2R, the environmental reduction factors are applied to CFRP properties and vary between 0.85 and 0.95 depending on the environmental exposure. For CFRP installed on bridges, ACI 440.2R recommends an environmental reduction factor of 0.85. The calculated value of C_E based on strength data in Table 11 was 0.66, which is significantly lower than the value recommended in ACI 440.2R.

Figure 105. Typical failure mode of tensile test coupons.

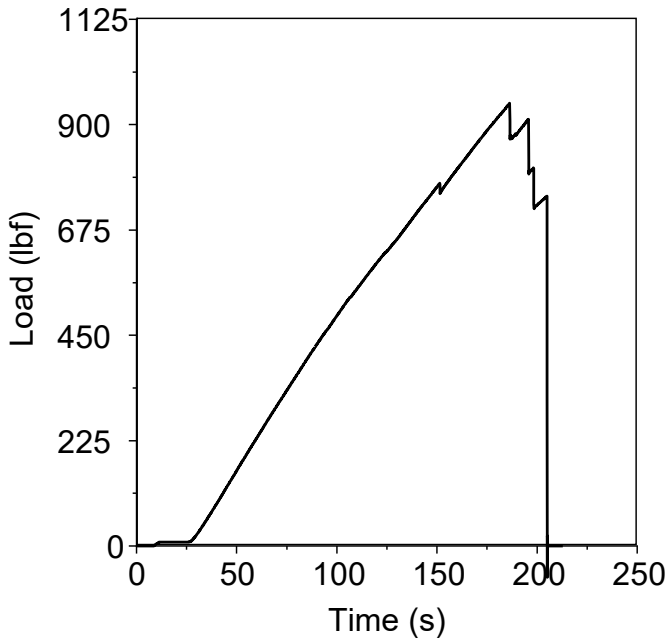

Figure 106. Load vs. time curve (strain gage failed before the coupon failure, so part of the strain data is missing).

Table 11. Tensile properties of aged CFRP.

Sample	Strength, σ (ksi)	Modulus, E (ksi)	ε=σ/E	Specified Strength (ksi)	Specified Modulus (ksi)
1	289	36,260	0.77%	480	33,360
2	340	39,160	0.87%	480	33,360
3	331	38,725	0.86%	480	33,360
4	359	36,110	1.00%	480	33,360
5	280	36,260	0.77%	480	33,360
Average	319	37,290	0.85%	480	33,360
St Dev	36	1,510	0.09%	480	33,360
COV	11.3%	4%	10.7%	480	33,360

Pull-Off Tests

Pull-off test results and interpretation of observed failure modes are presented in Table 12, and the photos of typical failure modes are shown in Figure 107. The nomenclature of the sample (e.g., G1-U/UD/B1) implies the pull-off test at girder G1 with unidirectional CFRP with single ply (U), unidirectional CFRP with double plies (UD), or bidirectional CFRP with single ply (B) and sample number 1. Due to the unavailability of initial pull-off tests data during the time of repair, a quantitative assessment of bond strength degradation was not possible; therefore, the test results were compared to the minimum bond strength of 200 psi recommended by AASHTO-FRPS-1 (2012).

A total of five tests were performed on girders G1 and G4, repaired using unidirectional CFRP in 1994, where the cohesive failure of the CFRP laminate (Mode B per ASTM 2021) was observed on all the samples. It was not possible to determine the actual bond strength at G1 and G4 because the CFRP composite failed in a cohesive mode of failure before reaching the bond failure. The lower-bound bond strength of G1-UX samples was found to be at least 80% greater than the minimum recommended by AASHTO-FRPS-1; however, the bond strength assessment at G4 could not be performed because G4-UDX samples failed prematurely at bond stress much lower than the minimum recommended bond strength (Table 12). The remaining three tests were performed on the girder G23, repaired with bidirectional CFRP, where adhesive failure at the CFRP–concrete interface (Mode E) was observed on all three samples. The average bond strength of G23-BX samples was found to be approximately 62% greater than the minimum recommended value, but the strength of two out of three test samples was below the minimum recommended value by 31% and 3%.

The cohesive failure observed at G1 and G4 can be associated with poor through-thickness properties of CFRP composite, which is generally associated with incomplete wet-out of fibers and environmental degradation. Visual inspection at G1 and G4 indicated the presence of water stains, discoloration, inadequately saturated fibers, and loosely bonded CFRP composite (Figure 98). SEM images at these locations displayed matrix cracking at the fiber/matrix interface, which also explains the 37% tensile reduction observed at G1. Similarly, at these test locations, FTIR spectroscopy analysis and DSC tests indicated the presence of oxidation-related CFRP composite degradation and lower than the minimum recommended T_g value by AASHTO-FRPS-1 (66 °C), respectively. The results from visual inspection, SEM imaging, FTIR spectroscopy, and DSC tests were in good correlation with the failure modes observed at G1 and G4 from pull-off tests, which implies the CFRP repairs were likely affected by environmental degradation or improper workmanship while saturating the fibers during installation.

The visual inspection of G23 did not show any signs of obvious degradation, which was in good correlation with the results obtained from the laboratory tests such as FTIR spectroscopy and SEM imaging. Cohesive failure in CFRP composite was not observed until bond stress reached at least 640 psi, which implies the cohesive strength of CFRP composite was likely less affected by environmental degradation or improper workmanship compared to G1 and G4. The T_g at G23 was also found higher compared to G1 and G4 and approximately equal to the minimum recommended temperature by AASHTO-FRPS-1. G23 repaired with a single-ply bidirectional CFRP composite displayed average bond-strength values greater than the minimum recommended by ACI440.2R. Each of the tests resulted in adhesive failure at CFRP/concrete interface (Mode E), indicating poor adhesion between epoxy and concrete. Two out of three test samples had bond strength less than the minimum recommended value, which can be attributed to environmental degradation, inconsistent surface preparation, or incomplete curing of the epoxy.

Table 12. Pull-off test results- Foulk road bridge.

Label	Bond Strength (psi)	Failure Mode	Failure Mode	Interpretation of Failure Mode
G1-U1	354	B	Cohesive failure in CFRP laminate	Indicates that the perpendicular (tension) force that the CFRP composite can withstand is lower than the tensile strength of concrete and epoxy adhesives, and the bond strength at all interfaces. Such failures are likely due to incomplete wet-out of the fibers or plies comprising the laminate or environmental degradation of the CFRP.
G1-U2	409	B	Cohesive failure in CFRP laminate	
G1-U3	312	B	Cohesive failure in CFRP laminate	
G4-UD1	25	B	Cohesive failure in CFRP laminate	
G4-UD2	0	B	Cohesive failure in CFRP laminate	
G23-B1	138	E	Adhesive failure at CFRP/concrete substrate interface	Indicates poor adhesion properties, likely resulting from improper selection of adhesive for concrete substrate, contamination of adhesive, incomplete or improper cure of adhesive, environmental degradation, or improper installation.
G23-B2	194	E	Adhesive failure at CFRP/concrete substrate interface	
G23-B3	637	E	Adhesive failure at CFRP/concrete substrate interface	

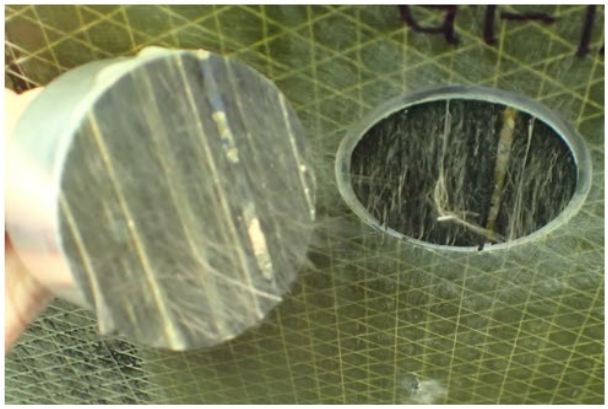

(a)

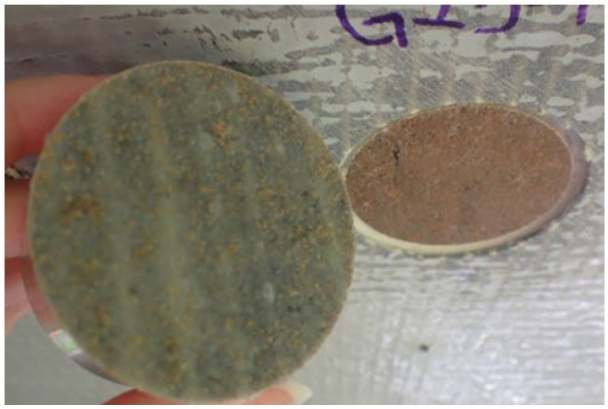

(b)

(c) (d)

Figure 107. Two failure modes observed: (a) mode B on G1-U1, (b) mode E on G23-B1, (c) mode B on G4-UD1, and (d) mode B on G4-UD2.

DISCUSSION

Overall, the condition of the girders and the CFRP on the bridge (G1-G6) was poor. Considering that the CFRP surface was not coated with protective paint, the composite was especially susceptible to degradation. In addition to this, the synergetic effects of stress/moisture on concrete (blistering, discoloration, bubbles/pop-outs, cracks, delamination, efflorescence, steel corrosion) and concrete/epoxy interface were likely aggravated by the continuous CFRP sheets, which prevented concrete from drying. Diffusion of moisture and oxygen through the existing cracks and reaching the steel/concrete interface would have increased the corrosion activity. According to the available literature (Finch, 1995), all major cracks were sealed with epoxy, and exposed reinforcement bars or corrosion were not observed at the time of CFRP installation. However, no treatment of the hairline cracks (0.1 mm) was mentioned. During the visual inspection in October 2020, severe corrosion (and exposed reinforcement) was observed on multiple girders (Figure 99), suggesting that CFRP installation did not prevent girder deterioration. Over the last 20 years, design guidelines and construction procedures were developed to improve bridge repair techniques. Davalos et al. (2011) recommend complete cover replacement using polymer-modified concrete with corrosion inhibitors before installing the CFRP. In the case of box girders, this would only partially solve the issue, considering that water penetrates into the voids from the deck and then migrates toward the CFRP composite/concrete interface. In a situation like this, a good design solution would be installing CFRP strips instead of continuous sheets to facilitate water migration.

Exposure to a high-humidity environment probably had a major contribution to CFRP deterioration. Besides physical degradation (swelling, crack propagation, decrease in T_g), fragmentation of the polymer network through hydrolysis is a possibility. Previous research related to the chemical modification of epoxy/amine polymer network on the molecular level due to moisture is scarce. Although stable, the ether bonds are considered to be the most vulnerable to hydrolysis in the epoxy/amine network. The possibility of C-O bond hydrolysis was recently studied using an MD simulation (Karuth et al., 2022). It was shown that C-O-C bond hydrolysis is possible due to the formation of nucleophiles from water dissociation (water dissociates to form OH^- and H^+ ions). The authors observed that the epoxy cured with aliphatic amines is more susceptible to hydrolytic degradation compared to epoxy cured with aromatic amine, since ether bonds are more accessible to water molecules, which aggregate around polar groups (Karuth et al., 2022).

Reflective cracking of the bridge asphalt pavement infers differential movement between beams. The purpose of transverse post-tensioning is to tie all the beams in the system together, so they act jointly. If the stiffness in the transfer direction is not sufficient, the bridge system may no longer behave as designed and overloading of individual girders may occur. Stresses developed as a result of this load would involve additional longitudinal tensile and shear stresses. Considering that installed CFRP reinforcement was supposed to resist thermal stresses and expansion due to freeze-thaw cycling, these additional mechanical stresses (and reduced flexural capacity of the girders due to corroded reinforcement) may have accelerated degradation. In macromolecules (such as epoxy), free radicals can be formed by chemical bond rupture during mechanical treatment. Dilara and Briassoulis (2000) state: "While small molecules are generally free to change positions and accommodate the applied stress, the local high stresses that lead to the rupture of chemical bonds are produced in macromolecules because they possess lower mobility." Damage observed in the SEM image (Figure 104d,e) in the interior ply may be attributed to the mechanisms briefly described above. Fragmentation of polymer chains due to mechanical stress in the presence of water resulted in the loss of matrix and completely exposed fibers (Figure 104d,e).

CHAPTER 5

Analysis of Literature Database

INTRODUCTION

A literature review was performed to assess the effect of various environmental conditioning and laboratory-accelerated conditioning on the durability of the CFRP composite externally bonded to the concrete substrate. A database of 60 previous studies was compiled, normalized, and analyzed. The report presents findings from a detailed statistical analysis of data collected from previous studies and makes recommendations with respect to the design of externally bonded CFRP composite for durability. The evaluated studies performed various shear and pull-off bond tests to assess the degradation of CFRP/concrete adhesive bonds on small-scale concrete specimens and reinforced concrete beams under environmental conditioning and laboratory-accelerated conditioning.

METHODOLOGY

The analysis conducted compared the bond strength retention, R_b, value of concrete specimens externally bonded to CFRP composite tested in numerous academic papers. The R_b value measures the respective strength of test specimens after undergoing various environmental or laboratory-accelerated conditioning with respect to the test specimens in a controlled laboratory environment. On some studies, the temperature and relative humidity information of the control environment were not available. In such cases, the temperature and RH were assumed to be 23 ℃ and 50%, respectively.

The bond strength retention, R_b,was found using Equation 4, where ACP bond strength is the bond strength of the CFRP bonded specimen after undergoing conditioning, and control strength is the bond strength of a control CFRP bonded specimen that did not undergo conditioning. Bond strength was computed based on the force needed to fail the specimen.

$$R_b = \frac{ACP\ Bond\ Strength}{Control\ Strength} \tag{4}$$

The data collected from 60 studies were classified into various categories depending on the test method utilized. Some of the common test methods utilized in the literatures were: (1) direct tension test or pull-off bond test; (2) beam test in three-point bending; (3) beam test in four-point bending; (4) single-lap shear test; (5) double-lap shear test; and (6) tensile tests of the CFRP composite coupons. These test methods were narrowed down to two categories (as shown in Figure 108) based on the type of force applied. Beam tests, single-lab shear test, and double-lap shear test were categorized as “Category A: Shear tests” because both tests involved shearing force at the CFRP composite/concrete interface. The direct tension test or pull-off bond test were categorized as “Category B: Pull-off tests.” The data collected were further classified into sub-categories based on their exposure conditions. Environmental conditioning was categorized as

"Field" and laboratory-accelerated conditioning was categorized as freeze-thaw, heat cycle, hygrothermal, UV exposure, and wet-dry cycles, as shown in Table 13. Tensile test data were not considered for evaluation because of inadequate datapoints available for different exposure conditions.

Table 13. Exposure conditions and their description.

Exposure Conditions	Nomenclature	Description
Freeze-thaw	FT	The specimen undergoes cycles of a specified freezing and thawing temperature.
Heat cycle	HC	The specimen undergoes cycles of a specified high temperature and lab conditions in a dry environment.
Hygrothermal	HYG	The specimen is immersed in a medium for a specified amount of time. Immersion mediums studied were alkaline (ALK), chloride (Chl), chloride deicer (ChlD), fresh or distilled water (F/D), saltwater (S), or no medium (none).
Ultra-violet exposure	UV	The specimen is exposed to UV light for a specified period of time.
Wet-dry cycle	WD	The specimen undergoes cycles of immersion in medium and dry typically lab conditions.
Field conditions	Field	The specimen is subject to environmental conditioning in the outdoor environment. Specimens were further classified under field conditions by the specific climate they were exposed to. Specimens were a mix of both small-scale concrete specimens placed in outdoor environment and operational bridge sections.

A series of histograms were made to gain a general understanding of the data's distribution for each test category and exposure condition (for example, category A: shear tests, HYG exposure condition). Figure 108 shows a breakdown of the various categories and sub-categories of data that were collected from the database, and the number of data points associated with each one. A total of 966 category A data points, and 464 category B data points were collected from the past studies (Figure 108). In the case of category A, hygrothermal exposure condition (HYG) was further classified into various media of immersion like alkaline, chloride, chloride deicer, filtered or distilled water, saltwater, and no medium. The media of immersion filtered or distilled water and saltwater were further divided into two temperature groups, less than or equal to 30 ℃ (<= 30) and greater than 30 ℃ (> 30).

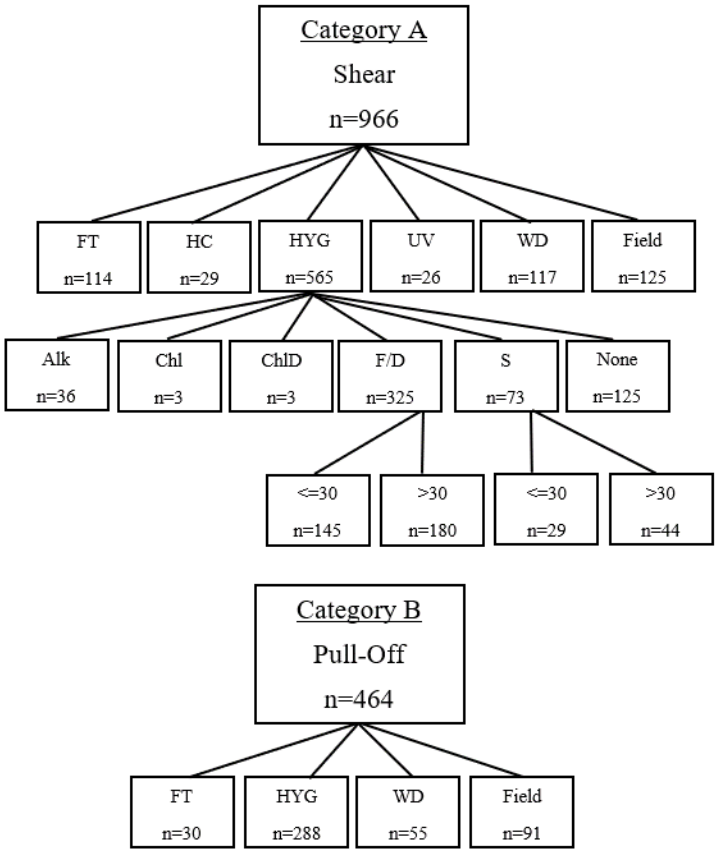

Figure 108. Breakdown of data collected from existing studies.

Analysis of variance (ANOVA), a hypothesis-testing technique, was used to determine whether the differences in means between groups are statistically significant (Girden, 1992). That is accomplished by comparing the variation of data within the groups to variation of data between groups. Mathematically, ANOVA is the ratio of the mean square of treatment (MSTR) to the mean square of error (MSE). The null hypothesis in ANOVA is that population means are equal. If the MSTR is much larger than the MSE or if a significant P-value limit is not reached (usually 0.05), null hypothesis is rejected.

To confirm that ANOVA assumptions (i.e., normal distribution of data and equal variance) were satisfied, the Kolmogorov-Smirnov test (Chakravart, Laha, and Roy, 1967) and Levene's test (Levene, 1960) were performed to determine if the data were normally distributed and if the variance between the groups was approximately equal, respectively. Following ANOVA, for cases where statistical significance was identified, a post-hoc t-test was performed to identify the specific groups between which a statistically significant difference exists.

TEST RESULTS AND DISCUSSION

Histograms were created for each exposure condition under each test category to gain a preliminary understanding of the effect of each exposure condition on bond strength retention (R_b). Figure 109 shows the histogram with the R_b value plotted against frequency for hygrothermal exposure conditions for both test categories. A summary of the data extracted from all the histograms for each exposure condition can be found in Table 14. Exposure conditions with fewer datapoints (FT, HC, UV, WD, and Field) did not

show an evenly distributed bell curve effect, where the frequencies were in the range as high as 16%. It was observed that datapoints category A and category B for hygrothermal (HYG) exposure conditions created an evenly distributed bell curve effect with frequencies ranging from 0–6% (Figure 109). Category A-HYG had 565 datapoints and category B-HYG had 279 datapoints, for which statistical significance was tested.

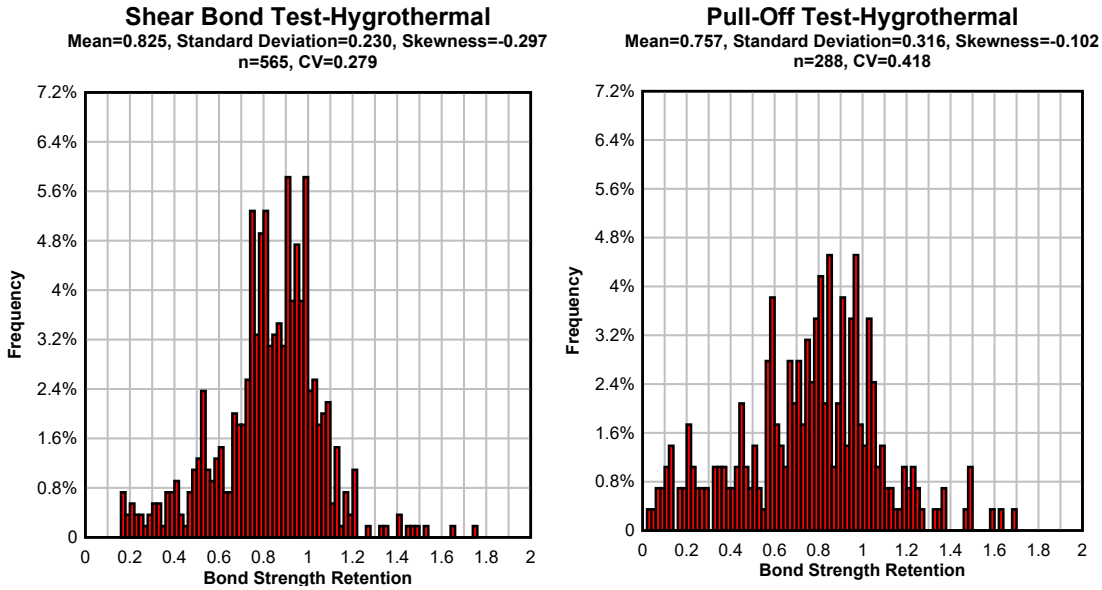

(a) (b)

Figure 109. Histogram showing R_b vs. frequency for hygrothermal exposure condition: (a) Category A: Shear tests, and (b) Category B: Pull-off tests.

Table 14. Summary of data.

Test Type		Exposure Conditions					
		FT	HC	HYG	UV	WD	Field
Category A: Shear Tests	N	114	29	565	26	117	125
Category A: Shear Tests	Mean	0.873	1.033	0.825	0.93	0.914	0.982
Category A: Shear Tests	St. Dev.	0.218	0.128	0.23	0.16	0.260	0.229
Category A: Shear Tests	Skewness	0.376	0.026	0.297	0.57	-1.14	-0.65
Category A: Shear Tests	COV	0.25.	0.124	0.279	0.172	0.284	0.233
Category B: Pull-Off Tests	N	30	-	288	-	55	91
Category B: Pull-Off Tests	Mean	1.064	-	0.757	-	0.864	0.877
Category B: Pull-Off Tests	St. Dev.	0.302	-	0.316	-	0.446	0.433
Category B: Pull-Off Tests	Skewness	0.62	-	-0.10	-	0.868	0.436
Category B: Pull-Off Tests	COV	0.284	-	0.418	-	0.516	0.494

Effect of Exposure Conditions and Test Methods on the Bond Strength

A series of statistical techniques were conducted to determine if there was a significant difference between various exposure conditions of category A test. When testing category A data points, all exposure conditions passed the Kolmogorov-Smirnov test except for HC and UV exposure conditions. That means all the datapoints for FT, HYG, WD, and Field exposure conditions were found to be normally distributed. All the datapoints related to HC and UV exposure condition were removed, and the remaining exposure categories were further evaluated for variance using Levene's test. All the datapoints for FT, HYG, WD, and Field exposure conditions also passed Levene's test and proved to be statistically significant when run through ANOVA-Single Factor.

Similar tests were performed to determine if there was a significant difference between various exposure conditions of category B test. It was observed that all exposure conditions passed the Kolmogorov-Smirnov test except for FT exposure condition. Upon further evaluation for variation, it was determined that all the exposure conditions failed the Levene's test. Additional tests were performed to determine if there was a significant difference between category A and category B tests. The Kolmogorov-Smirnov test and Levene's test were performed for category A vs. category B tests for each exposure condition. Each exposure condition passed the Kolmogorov-Smirnov test but failed the Levene's test. The variation between category A and category B tests, as well as among category B tests across exposure conditions, indicates that the category B datapoints could not be used to accurately measure the durability of externally bonded system.

After confirming there was statistical significance between FT, HYG, WD, and Field exposure conditions of category A test data, the post-hoc t-test was performed to determine which groups contained statistical significance from each other. Table 15 shows the results from the post-hoc t-test, where the values displayed in bold font indicate there is a statistically significant difference between the tested groups. It was found that FT vs. Field, HYG vs. WD, and HYG vs. Field contained a statistically significant difference.

Table 15. Results of the post-hoc t-test comparing shear bond test exposure conditions.

	FT	HYG	WD	Field
FT		0.025	0.098	**0.0001**
HYG	-		**0.0001**	**9.87 E -12**
WD	-	-		0.016
Field	-	-	-	

Note: Bold font in the table indicates statistically significant difference between tested groups.

All the laboratory-accelerated conditionings were grouped together as an "accelerated" exposure category and environmental conditioning was referred to as "Field" exposure category. Then, bond strength retention (R_b) for shear tests (category A) and pull-off tests (category B) were plotted, as shown in Figure 110. It was observed that the R_b values for category A datapoints and category B datapoints do not differ significantly. Figure 111a and Figure 111b show the R_b values for different exposure conditions for category A and category B tests, respectively. The R_b value was found to be consistent among exposure conditions for both categories. Hygrothermal data showed a decreased R_b compared to other exposure conditions for both categories ranging from 0.75 to 0.80. In the case of wet-dry cycles, the R_b value was

found to be in the range of 0.85 to 0.90. Field exposure showed slightly higher R_b values ranging from 0.88 to 1.

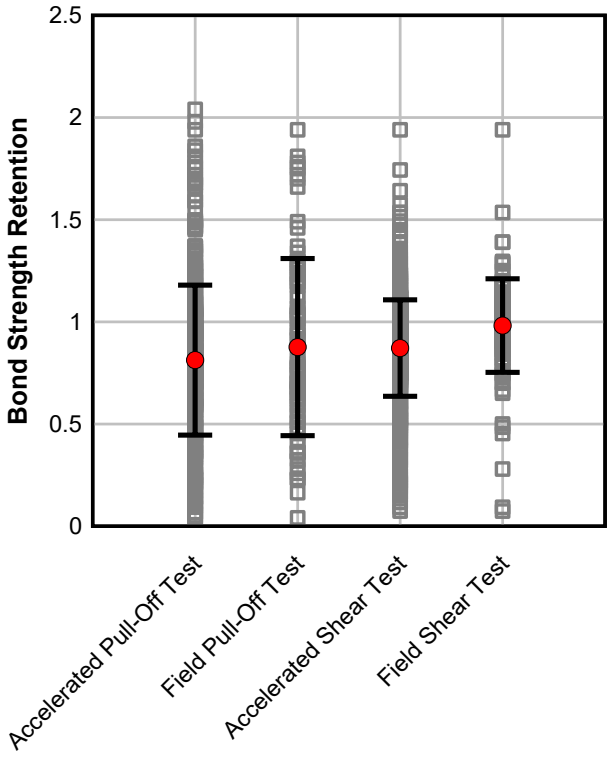

Figure 110. Bond strength retention for pull-off tests (Category B) and shear tests (Category A) for field and laboratory-accelerated conditioning.

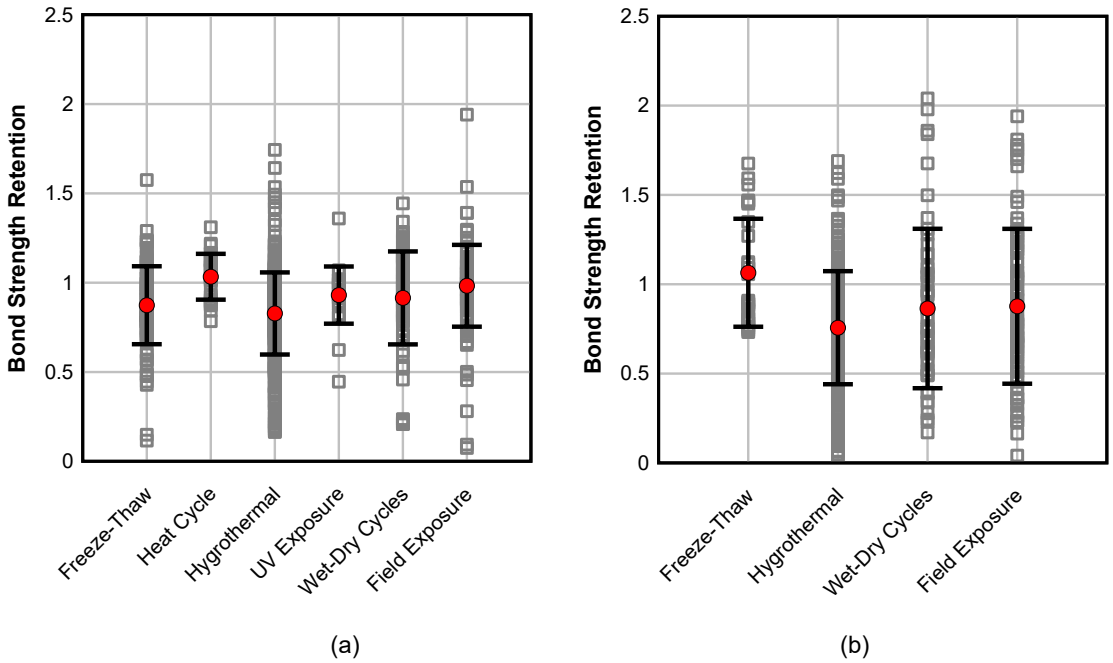

Figure 111. Bond strength retention of different exposure categories: (a) shear tests (category A), and (b) pull-off tests (category B).

Effect of Immersion Medium and Temperature

After determining that there was not a significant difference in bond strength retention when comparing the test method or exposure conditions, the data were further divided into more specific groups based on type of immersion and temperature range. For further analysis, hygrothermal exposure condition was chosen, as abundant datapoints were available compared to other exposure conditions. Specimens conditioned under hygrothermal exposure condition were immersed in immersion mediums like alkali (ALK), chloride (Chl), chloride deicer (ChlD), fresh or distilled water (F/D), saltwater (S), or no medium (none). For the purpose of this analysis, "F/D" and "S" immersion media were considered, as they had the greatest number of datapoints. To assess the effect of the temperature, the data points related to "F/D" and "S" immersion medium were further classified into two temperature groups, > 30 °C and ≤ 30 °C. Thus, four groups were formed, as shown in Table 16.

The Kolmogorov-Smirnov test, Levene's test, and post-hoc t-test were performed to determine if there were statistically significant differences between the four groups. Table 17 shows the results from the post-hoc t-test, in which values displayed in bold font indicate there is a statistically significant difference between the tested groups. Both fresh or distilled (F/D) water and saltwater (S) show a statistically significant difference between the two temperature groups, > 30 °C and ≤ 30 °C. From this it can be understood that the type of immersion medium has influence on bond strength retention (R_b).

Table 16. Groups of datasets for evaluation of the effect of immersion medium and temperature on bond strength.

Group Nomenclature	Immersion Medium	Test Temperature
F/D ≤ 30	Fresh water or distilled water	≤ 30 °C
F/D >30	Fresh water or distilled water	> 30 °C
S ≤ 30	Saltwater	≤ 30 °C
S >30	Saltwater	> 30 °C

To further understand the influence of immersion medium, the four groups (Table 16) were plotted against the R_b value, as shown in Figure 112. It was observed that there was clear decrement in the R_b value as the temperature increases above 30 °C for both fresh/distilled water and saltwater media. The decrement was found to be approximately 25% for fresh/distilled water and approximately 23% for saltwater. The R_b values were found to be consistent for each temperature group, > 30 and ≤ 30 °C, subjected to different immersion media, which concludes that temperature has more effect on bond strength retention than the immersion medium.

Table 17. Results of the post-hoc t-test comparing test data related to immersion medium fresh/distilled (F/D) water and saltwater (S) subjected to temperature > 30 ℃ and ≤ 30 ℃.

	F/D<=30	F/D>30	S<=30	S>30
F/D<=30		**1.41E-11**	0.348	**4.85E-05**
F/D>30	-		**6.94E-05**	0.331
S<=30	-	-		**0.005**
S>30	-	-	-	

Note: Bold font in the table indicates statistically significant difference between tested groups.

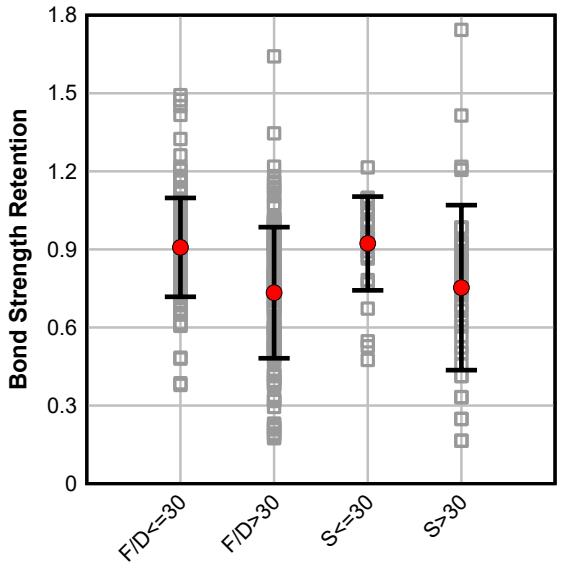

Figure 112. Bond strength retention for immersion medium fresh/distilled (F/D) water and saltwater (S) subjected to temperature > 30 ℃ and ≤ 30 ℃.

C H A P T E R 6

Conclusions

BRIDGE BR 1-704

A series of experimental tests in the laboratory and field were conducted to assess the durability performance of CFRP-strengthened steel girder of bridge Br 1-704 (Newark, Delaware) after 22 years of service. The field experimental campaign consisted of visual inspection, acoustic sounding of CFRP, structural health monitoring (for 14 days), and pull-off bond tests. Collected field samples were then tested in the laboratory; the testing included thermal analysis methods such as DSC and DMA, ATR-FTIR spectroscopy, tensile tests, and three-point bending tests of the field and control samples. Based on the evidence from these experiments, the following conclusions were made:

- CFRP composite possesses concealing behavior; the conventional visual inspection and acoustic sounding did not reveal any form of degradation, but upon collection of samples, corrosion was observed on the steel substrate along the edges of the CFRP composite, likely due to ingression of moisture and poor workmanship. Implementation of quality control procedures during the installation and routine inspection/maintenance during the service life may offset the poor workmanship issues. In addition, moisture penetration could likely be limited by adequate detailing (e.g., adhesive fillet around the CFRP perimeter).

- Average T_g of field CFRP composite samples was 79 ℃, which was lower than the control group by 9% and higher than the minimum temperature requirement of AASHTO (2012) by 20%. Similarly, the average T_g of MA555 and AV8113 structural adhesives were 48 ℃ and 36 ℃, respectively. These values were up to 60% lower than the T_g reported by the manufacturer and up to 45% lower than the minimum temperature requirement of AASHTO (2012).

- The flexural/tensile modulus and flexural strength of the field CFRP coupons after 22-year service life were approximately 15% and 25% lower than the control group (kept in standard laboratory conditions), respectively. Based on the findings from this study, a C_E factor of 0.75 and 0.80 is recommended for the determination of flexural strength and flexural/tensile modulus, respectively.

- ATR-FTIR spectroscopy did not detect any significant differences between control and field samples after 22 years of environmental exposure, indicating that likely no notable chemical degradation occurred under field conditions.

- The bond strength in tension for 89% of the pull-off test specimens was greater than 1,145 psi, which is 186% greater than the minimum strength requirements for zinc coating per TSP-2 AASHTO (2002). However, two test specimens near the north end of the girder exhibited very low

strength with an average of 40 psi, which is likely due to poor workmanship during the installation, as dry glass-fiber fabrics and entrapped air voids were observed at the CFRP/steel interface.

Limitations of the Research and Future Work

Some potential areas of future work are summarized below:

1. The interface between the fiber and matrix of the CFRP composite was not evaluated. Scanning electron microscopy tests will be performed to evaluate the composite microstructure for evidence of matrix cracking and/or fiber-matrix debonding.

2. Lack of control structural adhesive specimens or their test reports/procedure made a meaningful comparison to the current test results difficult.

3. The diagnostic load tests were not performed after 22 years of service. Had it been conducted, the effect of the CFRP composite retrofit on global flexural stiffness before installation of CFRP composite, immediately after installation of CFRP composite, and after 22 years of installation of CFRP composite, could be assessed more reliably.

4. The tests performed by Miller (2000) on two large-scale girders to assess the fatigue durability of the CFRP composite did not consider the effect of environmental conditioning, so proper evaluation of bond strength for fatigue after 22 years of service was not possible. Both of these two girders, with a history of 10 million fatigue cycles and sustained loading for 22 years, are currently located outside of the Structural Engineering Laboratory at the University of Delaware. Future testing on these girders will provide more insights into the durability of the CFRP composite system.

FOULK ROAD BRIDGE

An evaluation of CFRP repairs installed on the Foulk Road bridge (Wilmington, DE) was conducted to provide information on the durability performance of CFRP after being in service for 26 years. The condition of the repairs was assessed through visual inspection, pull-off bond tests, and laboratory testing of material samples collected from the bridge. Laboratory testing included thermal analysis, spectroscopy, and microscopic observations to determine potential physical and chemical degradation due to long-term environmental exposure. Based on the field and laboratory evaluation of Foulk Road bridge CFRP composite repairs, the following conclusions may be made:

- The presence of CFRP damage, debonding, discoloration, insufficient matrix saturation, and water stains was recorded on repairs installed in 1994 on girders G1 through G6. CFRP repairs of girders G7 through G23 appear to be in visually good condition. Damage to CFRP on a few girders was observed mostly at the locations of major concrete girder deterioration, which does not seem to be prevented by CFRP strengthening. Based on the condition of the girders, it can be inferred that installing CFRP as a replacement for transverse reinforcement did not prevent the deterioration of the girders.

- Pull-off tests on G1, repaired in 1994, indicated lower-bound bond strength at least 80% higher than the minimum recommended by AASHTO-FRPS-1. Bond performance of double-ply unidirectional CFRP on G4 could not be determined, as the composite failed cohesively at pull-off stress less than 25 psi. Undesired failure mode at the CFRP–concrete interface was observed on

girder G23, repaired with newer bidirectional CFRP, but the average bond strength was greater than the minimum AASHTO recommendation by 62%.

- T_g of the CFRP installed in 1994 varied between 46 °C and 51 °C. These values were up to 10% lower than the T_g reported by the resin manufacturer.

- Spectroscopy analysis revealed the presence of a peak at 1,658 cm^{-1} that could be related to amine cross-linker oxidation.

- Matrix cracking at the fiber/matrix interface was observed in all CFRP sample repairs installed in 1994. Matrix erosion and exposed fibers were present in the two-ply composite on G4. No signs of degradation were noticed in the bidirectional CFRP sample.

- The tensile strength of the CFRP coupons was 44% lower than the strength specified in the manufacturer data sheet after 26 years of service life.

DATA ANALYSIS – LABORATORY-ACCELERATED CONDITIONINGS

The data analysis was performed using data extracted from 60 past studies that assessed the durability of CFRP composite/concrete bond strength when subjected to a variety of field conditioning and accelerated conditioning protocols environments. Data were first divided into two categories, based on the test method—shear tests and pull-off tests—and then further divided into sub-categories based on exposure conditions, immersion medium, and the conditioning temperature. The bond strength retention (R_b) value for each test sample was determined by dividing the strength of laboratory or field-conditioned samples by the average control strength. ANOVA was used to determine whether the differences in the mean R_b between categories/sub-categories were statistically significant, which was later confirmed using the Kolmogorov-Smirnov test and Levene's test. A post-hoc t-test was then performed to identify sub-categories between which statistically significant differences exist. Based on the statistical data analysis, the following conclusions were made:

- Statistical significance for test data related to freeze/thaw, heat cycle, UV, and cyclic wet/dry exposures could not be established because of the smaller sample sizes in the existing studies. The histogram plotted for these exposure conditions showed non-normal distribution. Additional research should be performed to expand the experimental database for the above exposure conditions.

- From shear test data, it was observed that hygrothermal, wet-dry cycles, and field exposure resulted in the mean R_b value of 0.80, 0.90, and 1, respectively. Similarly, the pull-off test data showed the lowest R_b value of 0.75 for hygrothermal exposure, 0.85 for wet-dry cycles, and 0.88 for field exposure. Based on the 60 studies, the R_b values from ACP are conservative, suggesting opportunities to refine ACPs. However, the effects of exposure time, material properties of the CFRP composite, the strength of concrete, etc. on the on R_b needs to be further assessed to properly establish a relationship between the field performance and ACPs.

- The average R_b value after hygrothermal immersion in freshwater or saltwater at 30 °C or higher temperature was found to be approximately 24% lower when conditioned below 30 °C, which indicates that the conditioning temperature has a significant effect on R_b. The immersion medium had no statistically significant influence on the R_b value.

Appendix

FATIGUE ANALYSIS OF STEEL GIRDER (AASHTO, 2017)

AASHTO LRFD (2017) requires fatigue evaluation of a structural element when the maximum tensile live-load stress due to the Fatigue I load combination exceeds the unfactored permanent compressive stress. Due to the absence of permanent compressive stress in the bottom flange of the girder and the presence of tensile live-load stress (shown in Figure 79), fatigue evaluation is required by AASHTO (2017). The maximum live-load strain recorded at the bottom flange of the girder G5 at location "ST355" during the recent structural health monitoring was found to be 127.7 με, as shown in Figure 80, which translates to a tensile stress at the bottom of the flange of the steel girder (Δf_{steel}) of 3.7 ksi. The infinite life resistance of the steel girder was determined using the Fatigue I load combination and Equation 5, which was obtained from AASHTO LRFD (2017) Article C6.6.1.2.2. During the investigation of the Fatigue I load combination, the CAFT value or threshold resistance for category detail A (i.e., 24 ksi) was found to be greater than or equal to the factored live-load stress (i.e., 6.48 ksi), so further evaluation using the Fatigue II load combination is not required. According to AASHTO (2017) Table 6.6.1.2.3-1, detail category A includes base metal with no changes in geometry and rolled or clean surfaces. The factored fatigue stress in the steel girder is very low compared to the threshold, thus it has infinite fatigue life.

$$\eta\gamma(\Delta f) \leq \phi(\Delta F)_n \tag{5}$$

$$6.48\ ksi \leq 24\ ksi$$

Where for fatigue limit state, $\eta = \phi = 1$

$$\gamma = 1.75$$

$$(\Delta F)_n = (\Delta F)_{TH}$$

$$CAFT\ value = (\Delta F)_{TH} = 24\ ksi$$

$$(\Delta f_{steel}) = \varepsilon \times E_{steel} = 127.7 \times 10^{-6} \times 29000 = 3.7\ ksi$$

FATIGUE ANALYSIS OF CFRP COMPOSITE (AASHTO, 2012 & 2017)

AASHTO (2012), which is a guideline for CFRP composite bonded to concrete bridges, recommends that structural members be designed for the Fatigue I limit-state load combination. Chapter 3.3.1 recommends limiting the fatigue strain in the CFRP composite to less than 4,950 με, which is significantly higher than the maximum fatigue strain (130 με) observed during the structural health monitoring of the bridge.

$$\left(\varepsilon_{cfrp}\right) \leq \eta\varepsilon_{cfrp}^{ut} = 0.55 \times 9000 = 4950 \leq 5000\ \mu\varepsilon$$

$$\left(\Delta f_{cfrp}\right) = \varepsilon \times E_{cfrp} = 130 \times 10^{-6} \times (9{,}400 \sim 16{,}400) = 1.22\sim2.13\ ksi$$

where ε_{cfrp} = strain in CFRP (in./in.); ε_{cfrp}^{ut} = characteristics value of the tensile failure strain of CFRP (in./in.); Δf_{cfrp} = tensile stress at CFRP (ksi); E_{cfrp} = tensile modulus of CFRP in the direction of structural action (ksi); and η = strain limitation coefficient that is less than unity.

The S-N curve for the CFRP/steel bond and CFRP composite itself was not known, so it was not possible to determine the infinite or finite fatigue life. In the absence of the S-N curve, the category E' detail was chosen. According to AASHTO (2017), category A has the highest fatigue life while category E' has the lowest fatigue life and thus is identified as the worst fatigue grouping. The infinite life resistance of the CFRP was determined using the Fatigue I load combination using and 5, which was obtained from AASHTO LRFD (2017) Article C6.6.1.2.2. During the investigation of the Fatigue I load combination, the CAFT value or threshold resistance for category detail E' (i.e. 2.6 ksi) was found to be greater than or equal to the service live-load stress (i.e. 2.13 ksi), so further evaluation using the Fatigue II load combination is not required.

References

AASHTO-FRPS-1, 2012. Guide specifications for design of bonded FRP systems for repair and strengthening of concrete bridge elements (Washington DC), 1st Edition.

AASHTO LRFD Bridge Design Specifications, 8th Edition, AASHTO, 2017

AC125 ICC-ES (2007) Acceptance Criteria for Concrete and Reinforced and Unreinforced Masonry Strengthening Using Fiber-Reinforced Polymer (FRP) Composite Systems. International Code Council (ICC)- Evaluation Service, Whittier, CA.

ACI, A. (2004). 440.3 R-04: Guide Test Methods for Fiber-Reinforced Polymers (FRPs) for Reinforcing or Strengthening Concrete Structures. *American Concrete Institute, Farmington Hills, USA*.

ACI Committee 440 (2015) 440.9R-15 Guide to accelerated conditioning protocols for durability assessment of internal and external fiber-reinforced polymer FRP reinforcement (American Concrete Institute, Farmington Hills, MI).

ACI Committee 440 (2017) 440.2R-17 Guide for the design and construction of externally bonded FRP systems for strengthening concrete structures (American Concrete Institute, Farmington Hills, MI).

Agarwal, B. D., L. J. Broutman, and K. Chandrashekhara. 2006. *Analysis and Performance of Fiber Composite*. 3rd ed. Hoboken, NJ: John Wiley and Sons, Inc.

Alsuhaibani, E. (2020). DURABILITY AND PREDICTION OF LONG-TERM PERFORMANCE OF CARBON FIBER REINFORCED POLYMER (CFRP) LAMINATES UNDER ENVIRONMENTAL CONDITIONS (Doctoral dissertation).

Alfar, A., Rostary, F., Budelmann, H., & Hadid, T. A. (2006). Durability of reinforced concrete members strengthened with CFRP plates and subjected to moisture and salts. *Technische Universität Braunschweig*.

Al Azzawi, M., Hopkins, P., Mullins, G., & Sen, R. (2018). FRP–Concrete bond after 12-year exposure in tidal waters. *Journal of Composite for Construction*, *22*(5), 04018031.

Al-Jelawy, H. (2013). Experimental and numerical investigations on bond durability of CFRP strengthened concrete members subjected to environmental exposure.

Al-Lami, K., Colombi, P., & D'Antino, T. (2020). Influence of hygrothermal ageing on the mechanical properties of CFRP-concrete joints and of their components. *Composite Structures*, *238*, 111947.

Al-Mahmoud, F., Mechling, J. M., & Shaban, M. (2014). Bond strength of different strengthening systems–Concrete elements under freeze–thaw cycles and saltwater immersion exposure. *Construction and Building Materials*, *70*, 399-409.

Al Nuaimi, N., Sohail, M. G., Hawileh, R., Abdalla, J. A., & Douier, K. (2021). Durability of reinforced concrete beams externally strengthened with CFRP laminates under harsh climatic conditions. *Journal of Composites for Construction*, *25*(2), 04021005.

Al-Tamimi, A. K., Hawileh, R. A., Abdalla, J. A., Rasheed, H. A., & Al-Mahaidi, R. (2015). Durability of the bond between CFRP plates and concrete exposed to harsh environments. *Journal of Materials in Civil Engineering*, *27*(9), 04014252.

Allen, D. G. (2011). *Evaluating the long-term durability of fiber reinforced polymers via field assessments of reinforced concrete structures* (Doctoral dissertation, Colorado State University).

Allen, D. G., & Atadero, R. A. (2012). Evaluating the long-term durability of externally bonded FRP via field assessments. *Journal of Composites for Construction*, *16*(6), 737-746.

Ammar, N. (1996). *Rehabilitation of steel bridge girders with graphite pultrusion*. University of Delaware.

"ASCE Report Card," 2021. [Online]. Available: http://www.infrastructurereportcard.org/. [Accessed 05 13 2022].

"ASCE Report Card," 2017. [Online]. Available: http://www.infrastructurereportcard.org/. [Accessed 05 13 2022].

ASTM. Committee C-9 on Concrete and Concrete Aggregates. (2013). *Standard Test Method for Tensile Strength of Concrete Surfaces and the Bond Strength Or Tensile Strength of Concrete Repair and Overlay Materials by Direct Tension (pull-off Method).* ASTM International.

ASTM, S. (2014). E1356-08. *Standard Test Method for Assignment of the Glass Transition Temperatures by Differential Scanning Calorimetry, American Society of Testing and Materials, Philadelphia, USA.*

ASTM (2015) D7264/D7264M-07 Standard Test Method for Flexural Properties of Polymer Matrix Composite Materials (ASTM International, West Conshohocken, PA).

ASTM E111-17,. (2017). Standard Test Method for Young's Modulus, Tangent Modulus, and Chord Modulus. *ASTM International*, 1-7.

ASTM (2017) D3039/D3039M-17 Standard Test Method for Tensile Properties of Polymer Matrix Composite Materials (ASTM International, West Conshohocken, PA). https://doi.org/https://doi.org/10.1520/D3039_D3039M17

ASTM International. (2018). E1640-18 Standard Test Method for Assignment of the Glass Transition Temperature By Dynamic Mechanical Analysis.

ASTM D7522/D7522M, 2021 Edition, January 1, 2021 - *Standard Test Method for Pull-Off Strength for FRP Laminate Systems Bonded to Concrete or Masonry Substrates.*

American Society for Testing and Materials (ASTM). (2022). Standard test method for pull-off strength of coatings using portable adhesion testers. ASTM D4541. Philadelphia: ASTM.

Attanayake U, Aktan H. Reflective Cracking between Precast Prestressed Box Girders 2017:1–2.

Au, C., & Büyüköztürk, O. (2006). Peel and shear fracture characterization of debonding in FRP plated concrete affected by moisture. *Journal of Composites for Construction*, *10*(1), 35-47.

Auad, M. L., Aranguren, M., & Borrajo, J. (1997). Epoxy-based divinyl ester resin/styrene copolymers: Composition dependence of the mechanical and thermal properties. *Journal of Applied Polymer Science,* 66(6), 1059-1066.

Balaguru, P., Roy, S., & Yagnik, H. (2021). *Implementation of a Protocol for Acceptance of New Over-Coating Systems for Steel Surfaces* (No. FHWA-NJ-2021-003). Rutgers University. Center for Advanced Infrastructure and Transportation.

Banna, M. H., Shirokoff, J., & Molgaard, J. (2011). Effects of two aqueous acidic solutions on polyester and bisphenol A epoxy vinyl ester resins. *Materials Science and Engineering: A*, *528*(4-5), 2137-2142.

Banthia, N., Abdolrahimzadeh, A., Demers, M., Mufti, A., & Sheikh, S. (2010). Durability of FRP-concrete bond in FRP-strengthened bridges. *Concrete international*, *32*(8), 45-51.

Belec, L., Nguyen, T. H., Nguyen, D. L., and Chailan, J. F., 2015. Comparative effects of humid tropical weathering and artificial ageing on a model composite properties from nano- to macro-scale. *Composite Part A: Applied Science and Manufacturing*, **68**, 235–241.

Borrie, D., Al-Saadi, S., Zhao, X. L., Raman, R. S., & Bai, Y. (2021). Effects of CNT modified adhesives and silane chemical pre-treatment on CFRP/steel bond behaviour and durability. *Construction and Building Materials*, 273, 121803.

Bridge Diagnostic Inc (2019), *ST350- Strain Transducer operations manual*, Louisville, Colorado

Broyles, N. S., Verghese, K. N. E., Davis, S. V., Li, H., Davis, R. M., Lesko, J. J., & Riffle, J. S. (1998). Fatigue performance of carbon fibre/vinyl ester composite: the effect of two dissimilar polymeric sizing agents. *Polymer*, 39(15), 3417-3424.

Cabral-Fonseca, S., Correia, J. R., Rodrigues, M. P., & Branco, F. A. (2012). Artificial accelerated ageing of GFRP pultruded profiles made of polyester and vinylester resins: characterisation of physical–chemical and mechanical damage. *Strain*, *48*(2), 162-173.

Campbell Scientific Inc (2001), *CR5000 measurement and control system operator's manual,* Logan, Utah.

CTDOT, "Replacement of bridge 04562 spring street over the Quinnipiac River," 2020 [Online]. Available: https://biznet.ct.gov/SCP_Documents/Bids/55357/Project_131-206_Addendum_1.pdf [Accessed 10 31 2022]

Chajes, M., Rollins, T., Dai, H., & Murphy, T. (2019). *Report on Techniques for Bridge Strengthening: Main Report* (No. FHWA-HIF-18-041). United States. Federal Highway Administration. Office of Infrastructure.

Chakravarti, Laha, and Roy, (1967). *Handbook of Methods of Applied Statistics, Volume I*, John Wiley and Sons, pp. 392-394.

Choi, S., Gartner, A. L., Etten, N. V., Hamilton, H. R., & Douglas, E. P. (2012). Durability of concrete beams externally reinforced with CFRP composites exposed to various environments. *Journal of Composites for Construction*, *16*(1), 10-20.

Chotickai, P., & Somana, S. (2018). Performance of CFRP-strengthened concrete beams after exposure to wet/dry cycles. *Journal of Composite for Construction*, *22*(6), 04018053.

Chu, Wellington, and Vistasp M. Karbhari. "Effect of water sorption on performance of pultruded E-glass/vinylester composites." *Journal of materials in civil engineering* 17.1 (2005): 63-71.

Cromwell, J. R., Harries, K. A., & Shahrooz, B. M. (2011). Environmental durability of externally bonded FRP materials intended for repair of concrete structures. *Construction and Building Materials*, *25*(5), 2528-2539.

Cruz, R., Correia, L., Dushimimana, A., Cabral-Fonseca, S., & Sena-Cruz, J. (2021). Durability of epoxy adhesives and carbon fibre reinforced polymer laminates used in strengthening systems: Accelerated ageing versus natural ageing. *Materials*, *14*(6), 1533.

CS TR55, 2012 Edition (2012). TR55 Design guidance for strengthening concrete structures using fibre composite materials.

Dai, J. G., Yokota, H., Iwanami, M., & Kato, E. (2010). Experimental investigation of the influence of moisture on the bond behavior of FRP to concrete interfaces. *Journal of Composites for Construction*, *14*(6), 834-844.

Daimay, L.-V., 1991. The Handbook of Infrared and Raman characteristic frequencies of organic molecules. Academic Press, INC.

Darby, A., Ibell, T., & Clarke, J. (2004). TR55 Design guidance for strengthening concrete structures using fibre composite materials.

Davalos, J. F., Parish, G. C., Chen, A., and Ray, I., 2011. Effect of anchoring schemes for beams aged by accelerated corrosion and strengthened with carbon fibre-reinforced polymer. *Structure and Infrastructure Engineering*, **9**(3), 229–241. DOI: 10.1080/15732479.2010.542166

Davey, S. W. (2004). *A foundational investigation of vinyl ester/cenosphere composite materials for civil and structural engineering* (Doctoral dissertation, University of Southern Queensland).

DelDOT, "2405 Oversize/Overweight Hauling Permit Policy and Procedures Manual," 2018 [Online]. Available: https://regulations.delaware.gov/register/january2018/final/21%20DE%20Reg%20585%2001-01-18.htm [Accessed 11 10 2022]

Delor-Jestin, F., Drouin, D., Cheval, P. Y., and Lacoste, J., 2006. Thermal and photochemical ageing of epoxy resin - Influence of curing agents. *Polymer Degradation and Stability*, **91**(6), 1247–1255.

Dilara, P. A., and Briassoulis, D., 2000. Degradation and Stabilization of Low-density Polyethylene Films used as Greenhouse Covering Materials. *J. agric. Engng Res*, **76**, 309–321. DOI: 10.1006/jaer.1999.0513

DIN, E. (2016). 4624: 2016-08 Paints and Varnishes—Pull-off Test for Adhesion (ISO 4624: 2016). *European Committee for Standardization: Brussels, Belgium*.

Doblies, A., Boll, B., & Fiedler, B. (2019). Prediction of thermal exposure and mechanical behavior of epoxy resin using artificial neural networks and Fourier transform infrared spectroscopy. *Polymers*, *11*(2), 363.

Douglas, E. P., Hamilton III, H. R., & Nino, J. (2014). *Highly accelerated lifetime for externally applied bond critical fiber-reinforced polymer (FRP) infrastructure materials* (No. BDK75-977-45). University of Florida.

Dow, C., and Glasser, F. P., 2003. Calcium carbonate efflorescence on Portland cement and building materials. *Cement and Concrete Research*, **33**, 147–154.

Dukes, J., Goodwin, D. , Sattar, S. and Sung, L. (2022), An Overview of Research Needs Concerning the Performance of Fiber Reinforced (FR) Composite Retrofit Systems for Buildings and Infrastructure, ACI Special Publication, [Online], https://tsapps.nist.gov/publications [Accessed 07 30 2022]

Ernault, E., Richaud, E., and Fayolle, B., 2017. Thermal-oxidation of epoxy/amine followed by glass transition temperature changes. *Polymer Degradation and Stability*, **138**, 82–90. Elsevier Ltd. DOI: 10.1016/j.polymdegradstab.2017.02.013

Etxebarria, I., Prieto-Taboada, N., Lama, E., Arana, G., Rodríguez-Laso, M. D., & Madariaga, J. M. (2021). Graffiti Characterization Prior to Intervention in the Punta Begoña Galleries (Getxo, North of Spain): Raman and XRF Spectroscopy in the Service of Restoration. *Applied Sciences*, *11*(18), 8640.

Fafach, D., Shing, B., Chang, S., & Xi, Y. (2004). *Evaluation of the FRP-retrofitted arches in the Castlewood Canyon Bridge* (No. CDOT-DTD-R-2005-01).

Fazli, H., Yassin, A. M., Shafiq, N., & Teo, W. (2018). Pull-off testing as an interfacial bond strength assessment of CFRP-concrete interface exposed to a marine environment. *International Journal of Adhesion and Adhesives*, *84*, 335-342.

Finch, W., 1997. Investigation of bonding advanced composite materials toconcrete with an application in bridge rehabilitation. *PhD Dissertation*.

FHWA. "Compilation of Existing State Truck Size and Weight Limit Laws," 2015. [Online]. Available: https://ops.fhwa.dot.gov/freight/policy/rpt_congress/truck_sw_laws/index.htm#ex6 [Accessed 05 18 2022].

FHWA, " Deficient Bridges by Highway System," 2017. [Online]. Available: http://www.fhwa.dot.gov/. [Accessed 07 13 2022].

Frigione, M., Lettieri, M., & Mecchi, A. M. (2006). Environmental effects on epoxy adhesives employed for restoration of historical buildings. *Journal of materials in civil engineering*, *18*(5), 715-722.

Frigione, M., Caló, E., Maffezzoli, A., Acierno, D., Carfagna, C., & Ambrogi, V. (2006). Preformed microspherical inclusions for rheological control and physical property modification of epoxy resins. *Journal of applied polymer science*, *100*(1), 748-757.

Frigione, M., & Rodríguez-Prieto, A. (2021). Can Accelerated Aging Procedures Predict the Long Term Behavior of Polymers Exposed to Different Environments?. *Polymers*, *13*(16), 2688.

Fu, X., Yi, D., Tan, C., and Wang, B., 2020. Micromechanics analysis of carbon fiber/epoxy microdroplet composite under UV light irradiation by micro-Raman spectroscopy. *Polymer Composite*, **41**(6), 2154–2168. DOI: 10.1002/pc.25528

Gamage, J. C. P. H., Al-Mahaidi, R., & Wong, M. B. (2009). Durability of CFRP-strengthened concrete members under extreme temperature and humidity. *Australian Journal of Structural Engineering*, *9*(2), 111-118.

Garcez, M., Meneghetti, L., & da Silva Filho, L. C. (2008). Structural performance of RC beams poststrengthened with carbon, aramid, and glass FRP systems. *Journal of Composite for Construction*, 12(5), 522-530.

Girden, E. R. (1992). *ANOVA*: Repeated measures. Sage.

Google Maps. (2022). *Newark, Delaware.* [Online]. Available: http://www.google.com/maps/place/Newark,+DE/@39.6540661,-75.7541927 [Accessed 08 13 2022].

Gu, X., Nguyen, T., Oudina, M., Martin, D., Kidah, B., Jasmin, J., Rezig, A., et al., 2005. Microstructure and morphology of amine-cured epoxy coatings before and after outdoor exposures - An AFM study. *Journal of Coatings Technology and Research*, **2**(7), 547–556.

Guo, X., Lin, Z., Wang, Y., He, Z., Wang, M., and Jin, G., 2019. In-line monitoring the degradation of polypropylene under multiple extrusions based on Raman spectroscopy. *Polymers*, **11**(10), 1–11. DOI: 10.3390/polym11101698

Guo, X., Shu, S., Wang, Y., Huang, P., Lin, J., & Guo, Y. (2020). Effect of subtropical natural exposure on the bond behavior of FRP-concrete interface. *Polymers*, *12*(4), 967.

Hack, H. P. (Ed.). (1988). *Galvanic corrosion* (Vol. 978). ASTM International.

Hamilton, H. R., Brown, J., Tatar, J., Lisek, M., & Brenkus, N. R. (2017). Durability evaluation of Florida's fiber-reinforced polymer (FRP) composite reinforcement for concrete structures. *Florida Department of Transportation*.

Hammami, A., & Al-Ghuilani, N. (2004). Durability and environmental degradation of glass-vinylester composites. *Polymer composites*, *25*(6), 609-616.

Hassan, S. A., Gholami, M., Ismail, Y. S., & Sam, A. R. M. (2015). Characteristics of concrete/CFRP bonding system under natural tropical climate. *Construction and Building Materials*, *77*, 297-306.

Herzog, B., Gardner, D. J., Lopez-Anido, R., & Goodell, B. (2005). Glass-transition temperature based on dynamic mechanical thermal analysis techniques as an indicator of the adhesive performance of vinyl ester resin. *Journal of applied polymer science, 97(6),* 2221-2229.

Houska, C. (2007). Deicing salt–recognizing the corrosion threat. *International Molybdenum Association, Pittsburgh, TMR Consulting*, 1-10.

IDOT, "Metallizing of Structural Steel," 2017 [Online]. Available: https://idot.illinois.gov/Assets/uploads/files/Doing-Business/Manuals-Guides-&-Handbooks/Highways/Bridges/Bridge-Special-Provisions/GBSP82.pdf [Accessed 10 31 2022]

Jost, N., & Karger-Kocsis, J. (2002). On the curing of a vinylester–urethane hybrid resin. *Polymer*, *43*(4), 1383-1389.

Karuth, A., Alesadi, A., Vashisth, A., Xia, W., and Rasulev, B., 2022. Reactive Molecular Dynamics Study of Hygrothermal Degradation of Crosslinked Epoxy Polymers. *ACS Applied Polymer Materials*, **4**, 4411–4423. DOI: 10.1021/acsapm.2c00383

Lai, W. L., Kou, S. C., Poon, C. S., Tsang, W. F., & Lee, K. K. (2013). A durability study of externally bonded FRP-concrete beams via full-field infrared thermography (IRT) and quasi-static shear test. *Construction and Building Materials*, *40*, 481-491.

Levene, H. (1960). In *Contributions to Probability and Statistics: Essays in Honor of Harold Hotelling*, I. Olkin et al. eds., Stanford University Press, pp. 278-292.

Lin, Y. C., Chen, X., Zhang, H. J., and Wang, Z. P., 2006. Effects of hygrothermal aging on epoxy-based anisotropic conductive film. *Materials Letters*, **60**(24), 2958–2963.

Liu, S., Pan, Y., Li, H., & Xian, G. (2019). Durability of the bond between CFRP and concrete exposed to thermal cycles. *Materials*, *12*(3), 515.

Long, M., Djelal, C., Kesteloot, S., Bigourdan, B., Le Gac, P. Y., & Szulc, J. (2012). Durability of CFRP concrete bonding in a marine environment. In *Proc. Eur. Conf. Compos. Mater*.

Lu, P., Phares, B. M., Greimann, L., & Wipf, T. J. (2010). Bridge Structural Health–Monitoring System Using Statistical Control Chart Analysis. *Transportation research record*, 2172(1), 123-131.

Mailhot, B., Morlat-Thérias, S., Ouahioune, M., and Gardette, J. L., 2005. Study of the degradation of an epoxy/amine resin, 1 photo- and thermo-chemical mechanisms. *Macromolecular Chemistry and Physics*, **206**(5), 575–584.

Mallick, P. K. 2007. *Fiber-reinforced Composite Materials, Manufacturing, and Design.* 3rd ed. Boca Raton, FL: CRC Press, Taylor and Francis Group.

Mata, O. R., & Atadero, R. A. (2014). Evaluation of pull-off tests as a FRP–concrete bond testing method in the laboratory and field. *Practice Periodical on Structural Design and Construction*, *19*(2), 04014001.

McManis, G. E. (1970). Infrared absorption spectra of vinyl esters of carboxylic acids. *Applied Spectroscopy*, 24(5), 495-498.

Menard, K. P., & Menard, N. R. (2020). *Dynamic mechanical analysis*. CRC press.

Meier, U. (2005). Design and rehabilitation of concrete structures using advanced composite materials. In *PRE CONGRESSO-LATINO-AMERICANO DE PATOLOGIA DA CONSTRUÇÃO*. Porto Alegre: PRECONPAT.

Meiser, A., and Possart, W., 2011. Epoxy-metal interphases: Chemical and mechanical aging. *Journal of Adhesion*, **87**(4), 313–330.

Mertz, D. R., & Gillespie Jr, J. W. (1996). *Rehabilitation of steel bridge girders through the application of advanced composite materials* (No. NCHRP-IDEA Project 011).

Mertz, D. R. (2003). *Application of fiber reinforced polymer composite to the highway infrastructure* (Vol. 503). Transportation Research Board.

Mikami, C., Wu, H. C., & Elarbi, A. (2015). Effect of hot temperature on pull-off strength of FRP bonded concrete. *Construction and Building Materials*, *91*, 180-186.

Milev, S., Goodwin Jr, D. G., Sattar, S., & Tatar, J. (2022). Materials characterization of FRP composite seismic retrofits after long-term service in a subarctic Alaskan environment. *Construction and Building Materials*, *340*, 127810.

Miller, T. C. (2000). "The Rehabilitation of Steel Bridges Girders Using Advanced Composite Materials," Master's Thesis, University of Delaware, Newark, DE.

Miller, T. C., Chajes, M. J., Mertz, D. R., & Hastings, J. N. (2001). Strengthening of a steel bridge girder using CFRP plates. *Journal of bridge engineering*, *6*(6), 514-522.

Min, B. G., Stachurski, Z. H., Hodgkin, J. H., and Heath, G. R., 1993. Quantitative analysis of the cure reaction of DGEBA/DDS epoxy resins without and with thermoplastic polysulfone modifier using near infra-red spectroscopy. *Polymer*, **34**(17), 3620–3627. DOI: 10.1016/0032-3861(93)90046-D

Mitchell, M. M. (2008). Freeze-thaw durability of reinforced concrete deck girders strengthened for shear with surface-bonded carbon fiber-reinforced polymer.

Mohammadi, M., Mostofinejad, D., & Barghian, M. (2017). Effects of surface preparation method on FRP-concrete bond strength under alkaline conditions. *J. Compos. Constr*, *21*(4), 04017010.

Morsch, S., Liu, Y., Lyon, S. B., Gibbon, S. R., Gabriele, B., Malanin, M., and Eichhorn, K. J., 2020. Examining the early stages of thermal oxidative degradation in epoxy-amine resins. *Polymer Degradation and Stability*, **176**, 109147.

Naaman, A., Park, S. Y., Lopez, M., and Stankiewicz, P., 1997. RC-1355 - Glued-On Fiber Reinforced Plastic (FRP) Sheets for Repair and Rehabilitation.

National Academies of Sciences, Engineering, and Medicine, "Use of Fiber-Reinforced Polymers in Highway Infrastructure," 2017.

North Carolina Department of Transportation (NCDOT), "Structural steel shop coating program," 2019. [Online]. Available: https://connect.ncdot.gov/resources/Materials/MaterialsResources/. [Accessed 10 31 2022].

Pack, J. R. (2003). *Environmental durability evaluation of externally bonded composites* (Doctoral dissertation, University of Cincinnati).

Pallempati, H., Beneberu, E., Yazdani, N., & Patel, S. (2016). Condition assessment of fiber-reinforced polymer strengthening of concrete bridge components. *Journal of Performance of Constructed* Facilities, *30*(6), 04016052.

Pan, Y., Xian, G., & Silva, M. A. (2015). Effects of water immersion on the bond behavior between CFRP plates and concrete substrate. *Construction and* Building *Materials*, *101*, 326-337.

Pan, Y., Xian, G., & Li, H. (2018). Effects of freeze-thaw cycles on the behavior of the bond between CFRP plates and concrete substrates. *Journal of Composite for Construction*, *22*(3), 04018011.

Phares, B., Jayathilaka, S., Deng, Y. J., Greimann, L., & Wipf, T. J. (2020). Development of a Structural Health Monitoring System to Evaluate Structural Capacity and Estimate Remaining Service Life for Bridges.

Powers, D. A. (2009). *Interaction of water with epoxy* (No. SAND2009-4405). Sandia National Laboratories (SNL), Albuquerque, NM, and Livermore, CA (United States).

Pupurs, A., 2012. Micro-Crack Initiation and Propagation in Fiber Reinforced Composite. (DOCTORAL THESIS, Ed.).

Rajagopalan, G., Immordino, K. M., and Gillespie, J. W., Jr. (1996). ''Adhesive selection methodology for rehabilitation of steel bridges with composite materials.'' Proc., Am. Soc. for Compos. 11th Tech. Conf., Technomic Publishing Co., Lancaster, Pa., 222

Rezig, A., Nguyen, T., Martin, D., Sung, L., Gu, X., Jasmin, J., and Martin, J. W., 2006. Relationship between chemical degradation and thickness loss of an amine-cured epoxy coating exposed to different UV environments. *Journal of Coatings Technology and Research*, **3**(3), 173–184.

Rocks, J., Rintoul, L., Vohwinkel, F., and George, G., 2004. The kinetics and mechanism of cure of an amino-glycidyl epoxy resin by a co-anhydride as studied by FT-Raman spectroscopy. *Polymer*, **45**(20), 6799–6811.

Saito, M., 1996. European patent specification.

Sen, R., Shahawy, M., Sukumar, S., & Rosas, J. (1999). Durability of carbon fiber reinforced polymer (CFRP) pretensioned elements under tidal/thermal cycles. *Structural Journal*, *96*(3), 450-457.

Siavashi, S., Eamon, C. D., Makkawy, A. A., & Wu, H. C. (2019). Long-term durability of FRP bond in the midwest United States for externally strengthened bridge components. *Journal of Composite for Construction*, *23*(2), 05019001.

Shrestha, J., Ueda, T., & Zhang, D. (2015). Durability of FRP concrete bonds and its constituent properties under the influence of moisture conditions. *Journal of materials in civil engineering*, *27*(2), A4014009.

Shrestha, J., Zhang, D., & Ueda, T. (2016). Durability performances of carbon fiber–reinforced polymer and concrete-bonded systems under moisture conditions. *Journal of composite for construction*, *20*(5), 04016023.

Shi, Z., Zou, C., Zhou, F., & Zhao, J. (2022). Analysis of the Mechanical Properties and Damage Mechanism of Carbon Fiber/Epoxy Composite under UV Aging. *Materials*, 15(8), 2919.

Shin, Y. S., & Lee, C. (2003). Flexural behavior of reinforced concrete beams strengthened with carbon fiber-reinforced polymer laminates at different levels of sustaining load. *ACI Structural Journal*, *100*(2), 231-239

Sohail, M. G., Al Nuaimi, N., Hawileh, R. A., Abdalla, J. A., & Douier, K. (2021). Durability of plain concrete prism strengthened with galvanized steel mesh and CFRP laminates under harsh environmental conditions. *Construction and Building Materials*, *286*, 122904.

Song, S., Zang, H., Duan, N., & Jiang, J. (2019). Experimental research and analysis on fatigue life of carbon fiber reinforced polymer (CFRP) tendons. *Materials*, 12(20), 3383.

Sopal, G. J. (2008). Environmental durability of reinforced concrete deck girders strengthened with surface-bonded carbon fiber-reinforced polymer.

Sukanto, H., Raharjo, W. W., Ariawan, D., Triyono, J., & Kaavesina, M. (2021). Epoxy resins thermosetting for mechanical engineering. *Open Engineering*, *11*(1), 797-814.

Tatar, J., & Hamilton, H. R. (2016). Comparison of laboratory and field environmental conditioning on FRP-concrete bond durability. *Construction and building materials*, *122*, 525-536.

Tatar, J., & Hamilton, H. R. (2016). Bond durability factor for externally bonded CFRP systems in concrete structures. *Journal of Composites for Construction*, *20*(1), 04015027.

Tatar, J., & Hamilton, H. R. (2016). Implementation of bond durability in the design of flexural members with externally bonded FRP. *Journal of Composites for Construction*, *20*(3), 04015072.

Tatar, J., Wagner, D., & Hamilton, H. R. (2016). Structural Testing and Dissection of Carbon Fiber-Reinforced Polymer-Repaired Bridge Girders Taken Out of Service. *ACI Structural Journal*, *113*(6).

Tatar, J., & Brenkus, N. R. (2021). Performance of FRP-Strengthened Reinforced Concrete Bridge Girders after 12 Years of Service in Coastal Florida. *Journal of Composites for Construction*, *25*(4), 04021028.

Tatar, J., Sattar, S., Goodwin, D., Milev, S., Ahmed, S., Dukes, J., & Segura, C. (2021). Performance of externally bonded fiber-reinforced polymer retrofits in the 2018 Cook Inlet Earthquake in Anchorage, Alaska. *Earthquake Spectra*, *37*(4), 2342-2371.

Tian, W., & Hodgkin, J. (2010). Long-term aging in a commercial aerospace composite sample: Chemical and physical changes. *Journal of Applied Polymer Science*, *115*(5), 2981-2985.

The EU RO MR Group, "Corrosion-resistant paints," 2022 [Online]. Available: https://content.euromr.org/storage/uploads/TR_Corrosion-resistant_paints_(final).pdf [Accessed 10 31 2022]

TSP-2 AASHTO, "Guide Specification for Coating Systems with Inorganic Zinc-Rich Primer," 2002. [Online]. Available: https://www.tsp2.org [Accessed 10 31 2022].

Vaskova, H., and Kresálek, V., 2011. Quasi real-time monitoring of epoxy resin crosslinking via Raman microscopy. *International Journal of Mathematical Models and Methods in Applied Sciences*, **5**(7), 1197–1204.

Veletsos, A. S., & Newmark, N. M. (1960, July). Effect of inelastic behavior on the response of simple systems to earthquake motions. Department of Civil Engineering, University of Illinois.

Visco, A. M., Brancato, V., & Campo, N. (2012). Degradation effects in polyester and vinyl ester resins induced by accelerated aging in seawater. *Journal of Composite Materials*, 46(17), 2025-2040.

W. Finch , *INVESTIGATION OF BONDING ADVANCED COMPOSITE MATERIALS TO CONCRETE WITH AN APPLICATION IN BRIDGE REHABILITATION,* Newark, DE: University of Delaware, 1997.

Wang, W., J. Dai, and K. Harries. 2013. "Performance Evaluation of RC Beams Strengthened with an Externally Bonded FRP System under Simulated Vehicle Loads." *Journal of Bridge Engineering* 18, no. 1.

West, T. D. (2001). *Enhancements to the bond between advanced composite materials and steel for bridge rehabilitation* (Doctoral dissertation, University of Delaware).

Wipf, T. J., Phares, B. M., Greimann, L. F., Wood, D. L., & Doornink, J. D. (2007). *Evaluation of steel bridges (Volume I): monitoring the structural condition of fracture-critical bridges using fiber optic technology* (No. IHRB Project TR-493).

Xiao, G. Z., and Shanahan, M. E. R., 1998. Irreversible effects of hygrothermal aging on DGEBA/DDA epoxy resin. *Journal of Applied Polymer Science*, **69**(2), 363–369.

Xie, Z., Xie, J., Guo, Y., & Huang, Y. (2018). Durability of CFRP-wrapped concrete exposed to hydrothermal environment. *International Journal of Civil Engineering*, *16*(5), 527-541.

Xyla, A. G., and Koutsoukos, P. G., 1989. Quantitative analysis of calcium carbonate polymorphs by infrared spectroscopy. *Journal of the Chemical Society, Faraday Transaction 1*, **85**(10), 3165–3172.

Younes, M., Wartewig, S., Lellinger, D., Strehmel, B., and Strehmel, V., 1994. The curing of epoxy resins as studied by various methods. *Polymer*, **35**(24), 5269–5278.

Zapata, L. E., Portela, G., Suárez, O. M., and Carrasquillo, O., 2013. Rheological performance and compressive strength of superplasticized cementitious mixtures with micro/nano-SiO2 additions. *Construction and Building Materials*, **41**, 708–716. DOI: 10.1016/j.conbuildmat.2012.12.025

Ziaee, S., & Palmese, G. R. (1999). Effects of temperature on cure kinetics and mechanical properties of vinyl–ester resins. *Journal of Polymer Science Part B: Polymer Physics*, *37*(7), 725-744.

Yun, Y., & Wu, Y. F. (2011). Durability of CFRP–concrete joints under freeze–thaw cycling. *Cold Regions Science and Technology*, *65*(3), 401-412.

Zhang, F., Dai, J. G., Wang, Z., Wang, M., Leng, Y., & Xu, Q. (2021). Bond durability of epoxy and cement-bonded CFRP reinforcement to concrete interfaces subject to water immersion. *Materials and Structures*, *54*(2), 1-12.

Zheng, X. H., Huang, P. Y., Guo, X. Y., & Huang, J. L. (2016). Experimental study on bond behavior of FRP-concrete interface in hygrothermal environment. *International Journal of Polymer Science*, *2016*.